Harry Schmidt

Thermal and Nonthermal Properties of Closed Bipartite Quantum Systems

Universität Stuttgart
2007

Thermal and Nonthermal Properties of Closed Bipartite Quantum Systems

Von der Fakultät Mathematik und Physik
der Universität Stuttgart zur Erlangung der Würde
eines Doktors der Naturwissenschaften (Dr. rer. nat.)
genehmigte Abhandlung

Vorgelegt von

Harry Schmidt

aus Ludwigsburg

Hauptberichter: Prof. Dr. G. Mahler
Mitberichter: Prof. Dr. U. Seifert

Tag der mündlichen Prüfung: 6. August 2007

Institut für Theoretische Physik
der Universität Stuttgart

2007

Contents

1. Introduction

Controlling small quantum systems in experiment has become an important field of research in recent years. Particularly the field of quantum information processing and quantum computation has attracted a lot of attention. Often the Hamiltonian of a single or very few low level systems has to be designed and manipulated precisely. However, while quantum systems can easily be treated as isolated from the world in theory, no single quantum particle (or node of a quantum network) is ever totally decoupled from the rest of the universe in reality. Usually, the system is embedded into a large and uncontrollable bigger system (environment) that leads to deviations of the small system from the desired behavior.

This coupling of small "central" quantum mechanical systems to a larger quantum environment typically leads to decoherence and dissipation [1–5]. After some time, the smaller system reaches an almost stationary state (an equilibrium state), even if the total system is in a pure state evolving under completely unitary Schrödinger dynamics [6]. The equilibrium usually exhibits several thermodynamic properties.

This relaxation poses a severe problem for the controlled manipulation and scalability of these systems. The understanding of the relaxation and the stationary state is important in order to create, examine, and manipulate nonequilibrium states in experiment. Of particular interest are systems for quantum information processing [7], which are almost always far from equilibrium, but also quantum thermodynamic processes and machines [8]. In the latter case, the deviation from the equilibrium will be smaller, but several different equilibrium states are necessary to observe and control such processes.

Since the quantum environments typically are huge systems, it is usually impossible to use a closed description for the whole system. The behavior of the central system is often addressed by a reduced description where the action of environment enters as a fluctuating force (Langevin equations) or is eliminated from the description via a Born-Markov assumption, a bath or reservoir approximation, leading to a master equation for the small system. When using a reduced description of the small system, the environment

often is modeled by a bath of harmonic oscillators [9]. Of particular interest is the spin-boson model, where a single spin-1/2 particle is coupled to a sea of harmonic oscillators.

However, at low temperatures the influence of the environment is dominated by localized modes like defects or nuclear and paramagnetic spins. The basic principles regarding dynamical and statistical properties of spin systems were already examined several decades ago [10,11]. In recent years there has been considerable interest in the entanglement within these systems in energy eigenstates as well as in thermal states. The entanglement of spin chains has been addressed [12–14]. But more complex geometrical structures have been examined as well like spin-stars (Fig. 4.2) and ring-stars (Fig. 4.4). An important field of interest were stationary properties like quantum phase transitions [15–18].

Dynamical properties like relaxation were addressed as well, using spin systems as environmental models [19–22]. Examples for physical systems of interest are the coupling of a central spin to effectively independent environmental spins and the relaxation of magnetic systems. Corresponding to the spin-boson model, the spin-spinbath model was introduced.

Usually, the coupling between the environmental spins is neglected and the environment is eliminated to get a reduced description for the central system alone. Often, the spinbath is replaced by a randomly varying magnetic field. However, Breuer *et al.* were able to solve a specific spin-star model explicitely. The solution was then compared to several different approximation methods [23]. The authors could explicitely demonstrate the failure of markovian and nonmarkovian master equations for the considered system.

In the present text the behavior of a central spin-1/2 system coupled to an environment that typically consists of many spins will be examined. The environmental spins may interact with each other and it will be shown that this interaction has a major impact on the equilibrium state of the central system. No bath approximation will be used; *i.e.*, the total system consisting of the central system and the environment will be treated as closed obeying pure unitary dynamics. That does not mean that the state of the total system has to be pure at all initially. Both pure total states as well as thermal environmental states will be considered.

All environments discussed will be finite. Even for finite systems many thermal properties like relaxation and an equilibrium state can be observed. However, deviations from the behavior of infinite baths or reservoirs can

be expected and will be seen. In particular, the state after relaxation will not be completely stationary. Finite fluctuations will always remain. Also, contact equilibrium is never fulfilled exactly in finite systems. For some systems the large-particle (thermodynamic) limit can be taken explicitely. In this case the behavior can be compared directly to thermal behavior.

In Chapter 2 the description as well as some of the properties of spin-1/2 particles coupled to larger environments will be presented. If the environment initially is in a thermal state with a given temperature, the central system often approaches a state with the same temperature. It will be shown how this thermal contact equilibrium emerges and what deviations can be expected for finite systems. The terms "canonical" and "thermal" relaxation or behavior will be introduced for finite systems in order to be able to compare possible deviations from these behaviors later. Since random matrices play an important role in the description of complicated large systems, Chapter 3 will give a very brief introduction to random matrix theory as it is needed later in the text. It will be demonstrated that random Hamiltonian systems typically show canonical relaxation.

Chapters 4 to 6 will discuss the time evolution of a single spin-1/2 particle coupled to a (finite) environment of spins. Mainly the quasiequilibrium state reached will be discussed. This state depends strongly on the precise structure of the environment (interacting/noninteracting). This dependence will be examined by numerical methods both for pure and for mixed initial states of the environment.

In Chapter 7 a general method will be presented to characterize the behavior of a single system or a class of systems. The distribution of a particular property of the eigenstates of the total system determines the equilibrium state. The method presented is not only applicable to spin environments, but to a considerably more general class of systems. The method will be applied to certain abstract model systems in Chapter 8. These models show some properties of the spin systems and will give insight to the method presented in Chapter 7.

Chapter 9 again deals with spin systems. The equilibrium behavior observed in Chapter 4 will be examined more closely with the method presented in Chapter 7. The spin systems and their behavior will also be brought into relation with the abstract model systems discussed in Chapter 8.

In Chapter 10 the quantity "relative spectral width" will be introduced. This quantity is also able to help characterize the equilibrium properties of any Hamiltonian system. Unlike the method from Chapter 7, the rela-

tive spectral width will not allow one to make precise predictions. It will rather give indication what to expect. An advantage of this width to the distributions from Chapter 7 is that it is often more readily available.

Finally, Chapter 11 will show why an extension of the method from Chapter 7 to higher dimensional central systems is problematic.

Part of this work has already been published [24, 25].

Part I.

Relaxation and Quasiequilibrium

2. (Thermal) Properties of Two-Level Systems

Since this text will deal with the behavior of two-level central systems coupled to larger environments, some basic properties of these systems will be presented at first. Afterwards, the terms "canonical" and "thermal" behavior will be defined. Later chapters will mainly deal with the deviation from these types of behavior.

2.1. Temperature and Inversion

Let $|0\rangle$ and $|1\rangle$ denote the eigenstates of the local Hamiltonian $\hat{H}$ of a two-level system (TLS)—*e.g.*, a spin-1/2 particle. $\hat{H}$ can always be written in the form

$$\hat{H} = \frac{\delta}{2}\,\hat{\sigma}_z \tag{2.1}$$

with a Zeeman splitting δ. The following form of the Pauli matrices will be used throughout this text [6]:

$$\hat{\sigma}_x = \begin{pmatrix} 0 & 1 \\ 1 & 0 \end{pmatrix}, \quad \hat{\sigma}_y = \begin{pmatrix} 0 & \mathrm{i} \\ -\mathrm{i} & 0 \end{pmatrix}, \quad \hat{\sigma}_z = \begin{pmatrix} -1 & 0 \\ 0 & 1 \end{pmatrix}, \tag{2.2}$$

thus $|0\rangle$ denotes the ground state of the TLS and $|1\rangle$ denotes its excited state. The transition operators are defined by $\hat{\sigma}_x = \hat{\sigma}_+ + \hat{\sigma}_-$ and $\hat{\sigma}_y = \mathrm{i}(\hat{\sigma}_- - \hat{\sigma}_+)$.

The coefficients $\{v_i\}$ of the expansion of the statistical or state operator $\hat{\rho}$ with respect to the Pauli matrices,

$$\hat{\rho} = \frac{1}{2}\hat{1} + \frac{1}{2}\sum_{i=1}^{3} v_i \hat{\sigma}_i,$$

are called the Bloch vector.

If the state[1] of the TLS is mixed in its energy eigenbasis—*i.e.*, its state operator can be written as

$$\hat{\rho} = \rho_{00} \left|0\right\rangle\!\left\langle 0\right| + \rho_{11} \left|1\right\rangle\!\left\langle 1\right| \tag{2.3}$$

($\rho_{00} + \rho_{11} = 1$)—this state can always be interpreted as a canonical (thermal) one and therefore a temperature can be assigned to the TLS. The inverse temperature is then given by

$$\beta = \frac{1}{k_\mathrm{B} T} = \frac{1}{\delta} \ln \frac{\rho_{00}}{\rho_{11}}. \tag{2.4}$$

For convenience, a thermal state of a TLS can also be characterized by its inversion I instead of the temperature,

$$I = \langle \hat{\sigma}_z \rangle = \mathrm{Tr}(\hat{\rho}\, \hat{\sigma}_z) = \rho_{11} - \rho_{00} = -\tanh(\beta\delta/2). \tag{2.5}$$

The inversion is the z component of the Bloch vector of the TLS.

Sometimes also the von Neumann entropy $S = \mathrm{Tr}(\hat{\rho} \ln \hat{\rho})$ and the purity $P = \mathrm{Tr}(\hat{\rho}^2)$ will be used as a characterization. In contrast to the temperature, the inversion, the entropy, and the purity can be calculated for any possible state of the TLS, not only for canonical states.

2.2. Two-Level System Coupled to a Two-Band Environment

Now we consider a "central" two-level system, denoted by S, in resonant contact with a larger environment C consisting of two highly degenerate levels or near-degenerate bands. The environment will be treated fully quantum mechanically. The situation is depicted in Fig. 2.1. Resonant contact means $\delta_\mathrm{S} = \delta_\mathrm{C}$. a and b are used to count the states within each degenerate energy level. The Hamiltonian of the total system is given by

$$\hat{H} = \hat{H}_\mathrm{S} + \hat{H}_\mathrm{C} + \hat{H}_\mathrm{int}, \tag{2.6}$$

where $\hat{H}_\mathrm{S}$ and $\hat{H}_\mathrm{C}$ are the local Hamiltonians of the TLS and its environment, respectively. The interaction part $\hat{H}_\mathrm{int}$ must obey $\langle \hat{H}_\mathrm{int} \rangle \ll \langle \hat{H}_\mathrm{S} \rangle, \langle \hat{H}_\mathrm{C} \rangle$ for the coupling to be weak. We assume canonical coupling, which allows for energy exchange between both parts of the system.

[1] The term "state" will be used both for pure states $|\psi\rangle$ of any system and for generalized states described by a statistical or state operator $\hat{\rho}$.

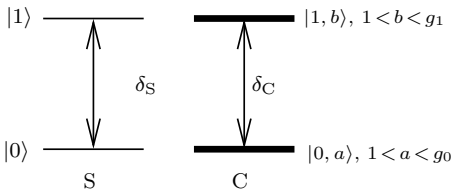

Figure 2.1: A two-level system S in contact with an environment C consisting of two highly degenerate levels with degeneracies g_0, g_1, respectively. The indices a and b are used to count the states within each energy level of the environment.

2.2.1. Decomposition of Hilbert Space for Resonant Coupling

The local Hamiltonians for the system depicted in Fig. 2.1 have the eigenrepresentations

$$\hat{H}_{\rm S} = \frac{\delta_{\rm S}}{2}\,\hat{\sigma}_z, \tag{2.7}$$

$$\hat{H}_{\rm C} = \sum_{a=1}^{g_0}\Big(-\frac{\delta_{\rm C}}{2}+\epsilon_a^{(0)}\Big)\,|0,a\rangle\langle 0,a| + \sum_{b=1}^{g_1}\Big(\frac{\delta_{\rm C}}{2}+\epsilon_b^{(1)}\Big)\,|1,b\rangle\langle 1,b|\,. \tag{2.8}$$

If the energy levels within the environment are truly degenerate, $\epsilon_a^{(0)} = \epsilon_b^{(1)} = 0$ for all a, b. If they are nearly degenerate, we require $\delta_{\rm C} \gg \epsilon_a^{(0)}, \epsilon_b^{(1)}$ for all a, b—*i.e.*, the bandwidths should be significantly smaller than the energy splitting between both bands.

Near resonance ($\delta_{\rm S} \approx \delta_{\rm C}$) the total Hamiltonian consists of three parts that are separated by energy ($|0;0,a\rangle = |0\rangle_{\rm S}\otimes|0,a\rangle_{\rm C}$, *etc.*):

$$\begin{aligned}\hat{H}_{\rm S}+\hat{H}_{\rm C} = &\sum_a\big(-\delta+\epsilon_a^{(0)}\big)\,|0;0,a\rangle\langle 0;0,a| \\ &+\sum_b\big(\delta+\epsilon_b^{(1)}\big)\,|1;1,b\rangle\langle 1;1,b| \\ +\Bigg(&\sum_b\big(-\Delta+\epsilon_b^{(1)}\big)\,|0;1,b\rangle\langle 0;1,b| + \sum_a\big(\Delta+\epsilon_a^{(0)}\big)\,|1;0,a\rangle\langle 1;0,a|\Bigg),\end{aligned} \tag{2.9}$$

where $\Delta = (\delta_S - \delta_C)/2$, $\delta = (\delta_S + \delta_C)/2$.

The interaction between system and environment will be called weak, if it preserves this tripartite structure of the spectrum; *i.e.*, if its energy scale is small compared to the splitting δ between the three parts. In this case the states of each part won't mix much and, therefore, the dynamics of each part can be treated independently.

We are mainly interested in the local dynamics of the central system alone, particularly in the relaxation from non equilibrium to a quasiequilibrium state. In the present system there will be practically no local dynamics of the central system, if the initial state is given by $|0;0,a\rangle$ or $|1;1,b\rangle$ due to energy conservation.[2] Therefore, the Hilbert subspace of interest is spanned by the $g_0 + g_1$ "cross states"

$$\boxed{\left\{|0;1,b\rangle, |1;0,a\rangle\right\} \quad (1 \le a \le g_0, \quad 1 \le b \le g_1).} \tag{2.10}$$

If Δ is sufficiently small, there will be energy exchange between system proper and environment, leading to local dynamics of the TLS. For sufficiently large g_0 and g_1 the central system will typically evolve into some quasiequilibrium state. This will be discussed later in detail.

In the basis (2.10) the total Hamiltonian matrix including the interaction within the Hilbert subspace of interest has the form

$$\left(\begin{array}{ccc|ccc} -\Delta+\epsilon_1^{(1)} & & & & & \\ & \ddots & & & V^\dagger & \\ & & -\Delta+\epsilon_{g_1}^{(1)} & & & \\ \hline & & & \Delta+\epsilon_1^{(0)} & & \\ & V & & & \ddots & \\ & & & & & \Delta+\epsilon_{g_0}^{(0)} \end{array}\right), \tag{2.11}$$

assuming that $\hat{H}_{\rm int}$ does not change the local spectra, $\langle 0;1,b|\,\hat{H}_{\rm int}\,|0;1,b'\rangle = \langle 1;0,a|\,\hat{H}_{\rm int}\,|1;0,a'\rangle = 0$. If $\hat{H}_{\rm int}$ does not meet this condition, the upper left and lower right blocks can be diagonalized individually to arrive at the form (2.11) for the total Hamiltonian.

[2] The environmental state, however, will typically evolve in time. Superpositions of the states $|0\rangle$ and $|1\rangle$ decohere in general.

2.2.2. Dominant Region of Hilbert Space

Now we take $\Delta = 0$; *i.e.*, system and environment are in resonance.

Due to the unitary dynamics of the total system, its energy distribution function $W(E)$ is conserved; $W(E)$ denotes the probability of finding the total system at the energy E. However, for each energy distribution of the total system there are various ways to distribute energy within each partition; *i.e.*, several local energy distribution functions $W(E_s^{\mathrm{S}}, E_k^{\mathrm{C}}) =: W_{sk}$ (here $s, k = 0, 1$) are possible. W_{sk} denotes the combined probability of finding the central system at energy E_s^{S} and the environment at energy E_k^{C}. The probability of finding the total system at the energy E is given by

$$W(E) = \sum_{s,k/E} W_{sk}.$$

Here, $s, k/E$ stands for: all s, k such that $E_s^{\mathrm{S}} + E_k^{\mathrm{C}} = E$.

It can be shown that of all possible local energy distributions $\{W_{sk}\}$ there is one for which the respective region in Hilbert space is far bigger than for any other [26–28]. This region is called the dominant region (index d) of Hilbert space. Most possible states of the system lie within this dominant region; indeed, for sufficiently large systems almost all states lie within this region.

For a total energy $E = \delta$—*i.e.*, for the subspace spanned by the states (2.10)—the dominant distribution is given by

$$W_{01}^{\mathrm{d}} = \frac{g_1}{g_0 + g_1}, \quad W_{10}^{\mathrm{d}} = \frac{g_0}{g_0 + g_1}, \tag{2.12}$$

and obviously $W_{00}^{\mathrm{d}} = W_{11}^{\mathrm{d}} = 0$.

2.2.3. Canonical Equilibrium

Since the dominant region of Hilbert space contains almost all states, almost any trajectory starting outside this region will enter it at some point in time and then almost never leave it again. After the trajectory has entered the dominant region, no more energy will be exchanged between system proper and environment. The local energy distributions will remain constant, given by the dominant distribution. This situation is similar to microcanonical system-environment interaction, prohibiting energy exchange between both parts.

It can be shown that, under microcanonical conditions, almost all states yield almost the same local state of the central system, namely the one with minimal purity (maximal entropy) [26]. Thus, for almost all states of the total system, the central system will be in the minimum purity state with an energy distribution given by (2.12):

$$\boxed{\hat{\rho}_{\mathrm{can}} = \frac{1}{g_0 + g_1}\big(g_1 \left|0\right\rangle\!\left\langle 0\right| + g_0 \left|1\right\rangle\!\left\langle 1\right|\big).} \tag{2.13}$$

This state is the (canonical) equilibrium state of the central system. This state is expected to be the (quasi)attractor state of the central system for almost all initial states of the total system with energy $E = \delta$. It is the final state of a canonical relaxation process. The inversion and inverse temperature of state (2.13) are given by

$$\boxed{\langle \hat{\sigma}_z \rangle_{\mathrm{can}} = \frac{g_0 - g_1}{g_0 + g_1}, \quad \beta_{\mathrm{S}} = \frac{1}{\delta_{\mathrm{S}}} \ln \frac{g_1}{g_0}.} \tag{2.14}$$

Note that this is a spectral property only and does not imply that the environment had been in a thermal state prior to the interaction with the central system; in fact this applies for the total system in a pure state for all time.

Figure 2.2 shows the time evolution of the inversion of the TLS starting from the initial product state $|1; 0, a\rangle$ (central spin excited, environment in lower band). System and environment are in resonance; $g_0 = 91$ and $g_1 = 364$,[3] $\hat{H}_{\mathrm{int}}$ is a random Hermitian matrix, which will be discussed below in detail. The expected equilibrium state is

$$\hat{\rho}_{\mathrm{can}} = \frac{4}{5} \left|0\right\rangle\!\left\langle 0\right| + \frac{1}{5} \left|1\right\rangle\!\left\langle 1\right|$$

with an inversion of $\langle \hat{\sigma}_z \rangle = -0.6$. It can be seen that, after a brief initial relaxation period, the state fluctuates narrowly around the canonical equilibrium state. The fluctuations are due to the system being finite.

2.2.4. Environments with Many Bands

If the environment consists of more than two bands, the results from the previous sections will still apply directly, if all band gaps are equal to the

[3] These values for g_0 and g_1 naturally appear in environments consisting of 14 spin-1/2 particles. Such environments will be used for the examples in Chapter 4.

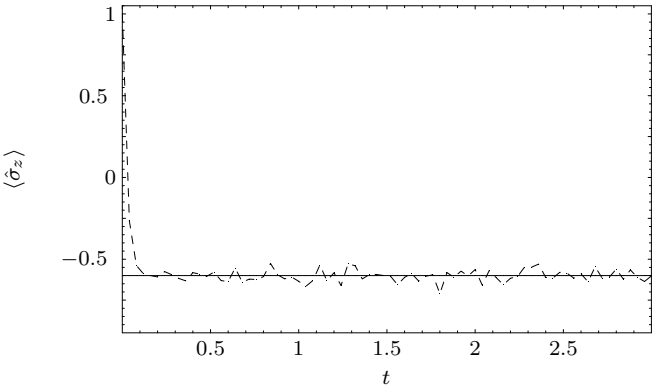

Figure 2.2: Inversion of a central TLS randomly coupled to a two-band environment with degeneracies $g_0 = 91$ and $g_1 = 364$. The solid black line represents the inversion of the canonical equilibrium state. The scaling of time is of little importance since it can easily be changed by altering the interaction strength.

Zeeman splitting of the central TLS and the initial state of the environment is prepared to be pure and wholly lying within one band. In this case, energy conservation restricts the dynamics to two neighboring bands of the environment. The canonical equilibrium state of S may then depend on the exact bands involved; its temperature is approximately given by

$$\beta_{\mathrm{S}} = \frac{\partial \ln g_{\mathrm{C}}(E)}{\partial E},$$

which is a generalization of (2.14).

2.3. Thermal Equilibrium of Larger Systems

Real environmental systems typically consist of more than only two bands, also the environment is usually not in a pure state prior to interaction with the central system. Initially the environment is often in a thermal state with a given (inverse) temperature β_{C}. In this case, a small system brought into contact with this environment is expected to relax towards a thermal state with the same temperature. This behavior will be called

thermal relaxation. In this section it is investigated, if and how canonical relaxation in the sense of Sec. 2.2.3 for subspaces of a huge system can lead to thermal relaxation.

Consider an environment that consists of many bands with respective degeneracies g_0, g_1, g_2 *etc.* and respective energies E_0, E_1, E_2 *etc.*. Its states will be denoted by $|k,l\rangle_{\mathrm{C}}$. The initial thermal state is given by[4]

$$\hat{\rho}_{\mathrm{C}} = \frac{1}{Z}\,\mathrm{e}^{-\beta\hat{H}_{\mathrm{C}}} = \frac{1}{Z}\sum_k \mathrm{e}^{-\beta E_k}\sum_{\ell=1}^{g_k} |k,\ell\rangle\langle k,\ell|_{\mathrm{C}} \tag{2.15}$$

with the partition function

$$Z = \sum_k g_k \mathrm{e}^{-\beta E_k}.$$

A TLS is weakly coupled to this environment, initially in its excited state. The total initial state thus reads

$$\hat{\rho}(0) = \frac{1}{Z}\sum_k \mathrm{e}^{-\beta E_k}\sum_{\ell=1}^{g_k} |1;k,\ell\rangle\langle 1;k,\ell|\,.$$

Due to the weak coupling, the pure total state $\hat{\rho}_{kl}(0) = |1;k,\ell\rangle\langle 1;k,\ell|$ is mainly coupled to the states $|0;k+1,m\rangle\langle 0;k+1,m|$, $1 < m < g_{k+1}$. We are interested in the canonical equilibrium state of the central system alone, reached after some relaxation period. If the total system initially was in the state $\hat{\rho}_{kl}(0)$, this equilibrium state would be given by

$$\hat{\rho}_{kl,\mathrm{can}} = a_k\,|0\rangle\langle 0| + b_k\,|1\rangle\langle 1|\,, \quad a_k = \frac{g_{k+1}}{g_k + g_{k+1}},\ b_k = \frac{g_k}{g_k + g_{k+1}}$$

according to Sec. 2.2.3. Summing up over all environmental bands, canonical relaxation yields the local equilibrium state

$$\begin{aligned}\hat{\rho}_{\mathrm{eq}} &= \frac{1}{Z}\sum_k \mathrm{e}^{-\beta E_k}\sum_{l=1}^{g_k}\big(a_k\,|0\rangle\langle 0| + b_k\,|1\rangle\langle 1|\big)\\ &= \frac{1}{Z}\sum_k g_k \mathrm{e}^{-\beta E_k}\big(a_k\,|0\rangle\langle 0| + b_k\,|1\rangle\langle 1|\big).\end{aligned} \tag{2.16}$$

[4]For notational convenience β is used instead of β_{C} throughout this section. The temperature of the central system will be denoted by β_{S}.

2.3.1. Exponential Degeneracy

If the environmental spectrum is equidistant with an energy splitting δ between the bands, $E_k = \delta k$, and if its degeneracy increases exponentially with energy, $g_k = \mathrm{e}^{\gamma\delta k}$, we get

$$a_k = \frac{1}{1+\mathrm{e}^{\gamma\delta}}, \quad b_k = \frac{1}{1+\mathrm{e}^{-\gamma\delta}}$$

and

$$\hat{\rho}_{\mathrm{eq}} = \frac{1}{Z}\underbrace{\sum_k g_k \mathrm{e}^{-\beta\delta k}}_{Z}\Big(\frac{1}{1+\mathrm{e}^{\gamma\delta}}\,|1\rangle\langle 1| + \frac{1}{1+\mathrm{e}^{-\gamma\delta}}\,|0\rangle\langle 0|\Big).$$

The equilibrium temperature according to (2.4) is then given by

$$\boxed{\beta_{\mathrm{S}} = \gamma \neq \beta.}$$

Here, the TLS would "thermalize" according to the spectrum of the environment, not towards its temperature. This is due to the particular nature of the degeneracy structure. Real environments, however, usually don't have an exponential degeneracy over their whole spectrum.

2.3.2. Environment of Spins

A more "natural" environmental model is given by an array of n spins, which all interact with the central TLS. If all environmental spins are in resonance with the central spin, the degeneracy will be binomial,

$$g_k = \binom{n}{k}.$$

The partition function is then given by

$$Z = \sum_{k=0}^{n}\binom{n}{k}\mathrm{e}^{-\beta\delta k} = \big(1+\mathrm{e}^{-\beta\delta}\big)^n$$

and

$$a_k = \frac{n-k}{n+1}, \quad b_k = \frac{k+1}{n+1}.$$

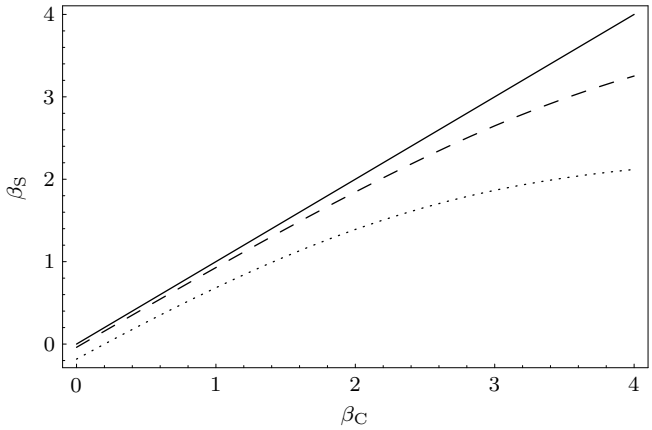

Figure 2.3: Temperature β_S of a central gapped TLS coupled to an environment with a binomial degeneracy structure, $g = \binom{n}{k}$ and an initial temperature β_C; canonical relaxation. Solid line: $\beta_S = \beta_C$ (infinite system), dashed line: $n = 50$, dotted line: $n = 10$.

In equilibrium the excited state population becomes[5]

$$(\hat{\rho}_{\mathrm{eq}})_{11} = Z^{-1} \sum_k \frac{k+1}{n+1} \binom{n}{k} \mathrm{e}^{-\beta\delta k} = \frac{1}{(n+1)Z} \left(n \frac{\mathrm{e}^{-\beta\delta}}{1+\mathrm{e}^{-\beta\delta}} Z + Z \right)$$
$$= \frac{1}{n+1} \left(\frac{n}{1+\mathrm{e}^{\beta\delta}} + 1 \right). \tag{2.17}$$

In the thermodynamic limit for large n this yields

$$\boxed{\hat{\rho}_{\mathrm{eq}} \overset{n\to\infty}{=} \frac{1}{1+\mathrm{e}^{\beta\delta}} |1\rangle\langle 1| + \frac{1}{1+\mathrm{e}^{-\beta\delta}} |0\rangle\langle 0|}$$

with the temperature

$$\boxed{\beta_S = \beta.} \tag{2.18}$$

Thus, for a spin environment weakly coupled to a central spin, we indeed expect the central spin to relax to the temperature of the environment.

[5] See Appendix A for the proof.

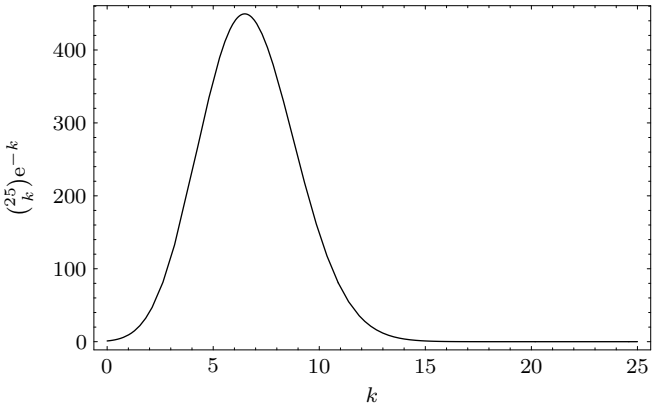

Figure 2.4: $g_k e^{-\beta\delta k}$ for $g_k = \binom{25}{k}$ and $\beta = \delta = 1$.

For a finite environment, deviations from (2.18) are expected, however. Figure 2.3 shows the finite size effects for two different system sizes. Interestingly, for high temperatures (small β), the equilibrium temperature of the central system can even be negative.

2.3.3. More General Degeneracy Structure

If the degeneracy g_k of the environment grows slower than exponentially, which is usually the case for real environments, the term $F_k = g_k e^{-\beta E_k}$ often has a distinct maximum. Figure 2.4 shows this term as a function of k for a binomial degeneracy and an equidistant spectrum. For large environments this maximum often is very narrow. In this case, only a few terms with large $g_k e^{-\beta E_k}$ dominate the sum in (2.16). If the system is sufficiently large and g_k is sufficiently smooth, the maximum of $F_k = g_k e^{-\beta\delta k}$ is given by

$$-\beta\delta g_{k_{\max}} + \left.\frac{\mathrm{d}g_k}{\mathrm{d}k}\right|_{k=k_{\max}} = 0.$$

In the vicinity of $k_{\max}$ we can then write

$$g_{k\approx k_{\max}} \approx \text{const}\, e^{\beta\delta k}.$$

If all terms of the sum in (2.16) are neglected except for those with $k \approx k_{\max}$, the equilibrium temperature of the central spin is given by the result of

Sec. 2.3.1, however, with an effective λ of $\lambda_{\text{eff}} = \beta$ and thus

$$\boxed{\beta_{\text{S}} = \beta.} \tag{2.19}$$

As long as $\beta > 0$, the maximum of F_k will always be in a domain of the environmental spectrum with $g_{k+1} > g_k$.

This leads to the conclusion that the relaxation to a canonical equilibrium state for all subspaces of the total system typically leads to a relaxation to thermal equilibrium for the total system. The result of Sec. 2.3.2 is only a special case of this one.

3. Random Hermitian Matrices

Homogeneously distributed Hermitian matrices play an important role in the modeling of quantum systems when they are highly disordered. They can be used to describe the interaction Hamiltonians of small thermal systems. Often, interactions between different parts of the system are highly complicated and hard or impossible to describe in detail. Random Hermitian matrices are a convenient way to approximate such interactions. The theory of random matrices is well understood [29,30]. Here a brief summary will be presented.

3.1. The Gaussian Unitary Ensemble (GUE)

The elements H_{ii}, $\mathrm{Re}(H_{ij})$, and $\mathrm{Im}(H_{ij})$ of an Hermitian matrix H are independent (for one triangular half) and will be described as random variables to parameterize a random matrix. In order to get an homogeneous distribution, the probability density $P(H)$ has to be invariant under unitary transformations. The distribution function

$$P(H) = C\,\mathrm{e}^{-A\,\mathrm{Tr}\,H^2} \tag{3.1}$$

meets this condition since the trace is invariant under unitary transformations. The parameter A defines the unit of energy and C is determined by normalization. The ensemble of complex Hermitian matrices that are distributed according to (3.1) is called the Gaussian unitary ensemble (GUE).

For a standard deviation $\sigma = \sqrt{2}$, the diagonal elements take the form

$$P_{\mathrm{d}}(H_{ii}) = \frac{1}{2\sqrt{\pi}}\,\mathrm{e}^{-H_{ii}^2/4}. \tag{3.2a}$$

The off-diagonal elements are determined by

$$P_{\mathrm{o}}(\mathrm{Re}\,H_{ij}) = \frac{1}{\sqrt{2\pi}}\,\mathrm{e}^{-(\mathrm{Re}\,H_{ij})^2/2}, \tag{3.2b}$$

$$P_{\mathrm{o}}(\mathrm{Im}\,H_{ij}) = \frac{1}{\sqrt{2\pi}}\,\mathrm{e}^{-(\mathrm{Im}\,H_{ij})^2/2}. \tag{3.2c}$$

3.2. Eigenvector Distributions of the GUE

The distribution of the eigenvectors of random matrices from the GUE will be of importance when analyzing thermal properties of small systems randomly coupled to the environment and will therefore be presented here.

The unit-norm eigenvectors of complex $N \times N$ matrices have N components c_n that are complex in general, $c_n = c'_n + \mathrm{i}c''_n$. The only invariant characteristic of these eigenvectors is the norm itself. The joint probability density for all N complex components is therefore given by

$$P(\{c_n\}) = \text{const}\,\delta\Big(1 - \sum_{n=1}^{N} |c_n|^2\Big). \tag{3.3}$$

This function is uniformly concentrated on the unit sphere in d-dimensional space with $d = 2N$. If we rewrite (3.3) in terms of d variables $x_1, \ldots, x_d$ instead of the c'_n, c''_n, we get (with proper normalization)

$$P^{(d)}(x_1, \ldots, x_d) = \pi^{-d/2}\Gamma\Big(\frac{d}{2}\Big)\,\delta\Big(1 - \sum_{n=1}^{d} x_n^2\Big). \tag{3.4}$$

Integrating out $d - \ell$ variables yields the reduced density

$$\boxed{P^{(d,\ell)}(x_1, \ldots, x_\ell) = \pi^{-\ell/2}\frac{\Gamma(d/2)}{\Gamma((d-\ell)/2)}\Big(1 - \sum_{n=1}^{\ell} x_n^2\Big)^{(d-\ell-2)/2}}. \tag{3.5}$$

The integration is conveniently done in Cartesian coordinates by using a Fourier integral representation of the δ distribution.

Probability densities for functions of the eigenvectors or their components c_n or x_n can be calculated by multiplying $P^{(d,\ell)}$ with an appropriate δ distribution employing the function and integrating over the remaining components. For instance, the population probability density of each entry of an energy eigenstate, $y = |c_1|^2 = x_1^2 + x_2^2$, is given by

$$P(y) = \int \mathrm{d}x_1 \mathrm{d}x_2\, P^{(d,2)}(x_1, x_2)\,\delta(y - x_1^2 - x_2^2), \tag{3.6}$$

integrated over the volume of the unit sphere in ℓ dimensions (here $\ell = 2$; *i.e.*, integrated of the area of the unit circle). Integrals similar to (3.6) will be needed later in this text.

The average level density of the GUE is given by

$$\bar{\rho}(E) = \begin{cases} (2/\pi)\sqrt{1 - \frac{E^2}{\sqrt{8n}}} & \text{for } |E| < 1, \\ 0, & \text{for } |E| > 1, \end{cases} \tag{3.7}$$

for n-dimensional matrices, if the unit of energy is chosen as in Eqs. (3.2). This is known as Wigner's semicircle law.

3.3. Random Coupling and Time Evolution

Here we consider a bipartite system as described in Sec. 2.2: A single spin-1/2 particle coupled to a two-band environment. The transitions are taken to be in resonance and the levels within each environmental band are taken to be exactly degenerate. In this case, $\hat{H}_\mathrm{S} + \hat{H}_\mathrm{C} \propto \hat{1}$ and will therefore be neglected. The interaction will be chosen randomly with the probability density (3.1) of the GUE.

The time evolution of these systems has been studied extensively [31]. An initial pure product between the TLS and the environment typically evolves into the canonical state (2.13) under pure Schrödinger time evolution generated by almost all Hamiltonians chosen randomly as described. Figure 2.2 demonstrates this behavior. Initially, the central system was excited and the environment was in a random state of the lower band

$$|\psi_{\mathrm{S+C}}(0)\rangle = |1\rangle_\mathrm{S} \otimes |0, a\rangle_\mathrm{C}\,. \tag{3.8}$$

The time average of the inversion of the central system for the simulation shown in Fig. 2.2 is given by

$$\langle \bar{\sigma}_z \rangle = \lim_{\tau\to\infty} \frac{1}{\tau} \int_{-\tau/2}^{\tau/2} \mathrm{d}t\ \mathrm{Tr}\big(\hat{\sigma}_z \hat{\rho}_\mathrm{S}(t)\big) = -0.598.$$

This is remarkably close to the canonical value of $\langle \hat{\sigma}_z \rangle_\mathrm{can} = -3/5$.

The fluctuations in the quasiequilibrium regime are due to the finiteness of the environment and will decrease when the system size is increased.

4. Spin Systems and Time Evolution

In Sec. 2.2 we considered a central two-level system weakly coupled to an environment consisting of two highly degenerate bands. It was explained that almost all states of the total system have a certain energy distribution between system proper and environment, determined only by the degeneracies of the environmental bands. In addition, for almost all of these states the entropy of the reduced state for the central system is maximal; *i.e.*, the reduced state is diagonal in the energy eigenbasis of the TLS. The region of Hilbert space spanned by the states with this property was called the dominant region.

Since the dominant region comprises almost the whole Hilbert space, the time evolution of most (or almost all) initial states is expected to enter this region at some point in time and almost never to leave this region. Therefore, a relaxation with respect to the central system is expected, leading to a canonical quasiequilibrium state, in which the central system alone shows none or hardly any time evolution at all. The local state is expected to be given by

$$\hat{\rho}_{\mathrm{can}} = \frac{1}{g_0 + g_1}\left(g_1 \left|0\right\rangle\!\left\langle 0\right| + g_0 \left|1\right\rangle\!\left\langle 1\right|\right) \tag{2.13}$$

after relaxation, independently of the initial state, as long as the total energy of the system is chosen properly.

Section 3.3 and Fig. 2.2 demonstrate that a local relaxation towards the state (2.13) can indeed be observed for interaction Hamiltonians lacking any structure whatsoever—*i.e.*, for those taken randomly from the Gaussian unitary ensemble.

The situation is quite different for structured environments like spin systems. Even though a quasistationary state of the central system still is reached, this state may differ strongly from the canonical equilibrium state and may as well be dependent on the initial state. In this chapter, some model spin environments will be discussed, looking mainly at the stationary state reached by the central system after relaxation.

4.1. The General Model

4.1.1. The Hamiltonian

The environmental Hamiltonian is divided into two parts, one describing the local energy of each spin and the other one the mutual interaction between the spins. The local part consists of a Zeeman splitting for each spin. Therefore, the total environmental Hamiltonian reads

$$\hat{H}_{\mathrm{C}} = \sum_{\nu=1}^{N} \frac{\delta_\nu}{2} \hat{\sigma}_z^\nu + \hat{H}_{\mathrm{CC}}. \tag{4.1}$$

The number of particles in the environment is denoted by N; $\hat{\sigma}_z^\nu$ is the Pauli-z-operator for the ν^{th} particle. As long as the δ_ν's vary narrowly around the Zeeman splitting of the central spin δ_{S} and as long as the interaction $\hat{H}_{\mathrm{CC}}$ is weak relative to the local part, the total Hamiltonian

$$\hat{H} = \frac{\delta_{\mathrm{S}}}{2} \hat{\sigma}_z + \hat{H}_{\mathrm{C}}$$

has the form (2.9) for each neighboring pair of environmental bands. The following analysis will therefore be restricted to only one such pair at a time. If more than one band was populated initially, the total dynamics and quasiequilibrium state can be obtained simply by summing over all bands.

4.1.2. Degeneracy and Canonical Equilibrium

The environment has a degeneracy varying binomially with energy [32],

$$g_k = \binom{N}{k}, \quad E_k = k\delta_{\mathrm{C}},$$

where δ_{C} may be taken as the mean value of the δ_ν's (introducing mutual coupling may shift the energy of those bands slightly). An environment with this structure was briefly discussed in Sec. 2.3.2, where it was shown explicitely that this system shows local thermal relaxation in the thermodynamic limit if the environment is in a thermal state initially.

If only one pair of environmental bands took part in the dynamics due to preparation, the inversion (and temperature) of the canonical equilibrium state

$$\hat{\rho}_{\mathrm{can}} = \frac{1}{g_k + g_{k+1}} \left(g_{k+1} \left|0\right\rangle\!\left\langle 0\right| + g_k \left|1\right\rangle\!\left\langle 1\right| \right) \tag{2.13'}$$

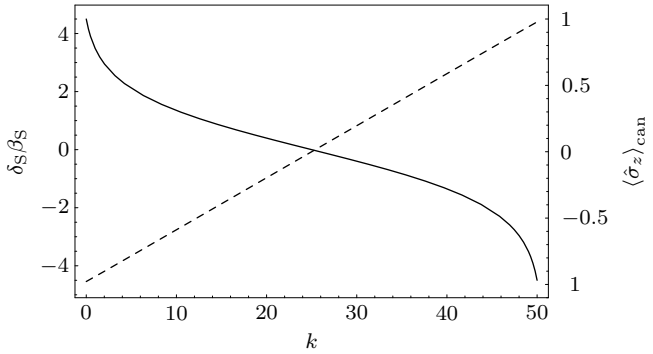

Figure 4.1: Solid line: Inverse canonical equilibrium temperature β_S of the central system depending on the pair of involved bands in the environment, k is the index of the lower lying band. Dashed line: Corresponding population inversion. Shown for $N = 50$ particles.

of the central system would vary depending on which pair of bands is involved. Figure 4.1 shows the inverse equilibrium temperature and inversion of the central system depending on the bands involved. For $\beta < 0$ the population is inverted.

In the following, environments with $N = 14$ spins will be considered, with $k = 2$ particles excited initially. If the central spin initially is excited, the two bands involved will have degeneracies of $g_2 = 91$ and $g_3 = 364$.

4.2. Spin-Star Configuration

At first, intra-environmental interaction is neglected, $\hat{H}_{CC} = 0$. In this case, the total system forms a kind of a "star" as depicted in Fig. 4.2 schematically. The Zeeman splitting of all environmental spins is taken to be in resonance with the central spin.

The most general interaction Hamiltonian for this system is given by

$$\hat{H}_{int} = \sum_{\nu=1}^{N} \sum_{i,j=1}^{3} \gamma_{ij}^{\nu}\, \hat{\sigma}_i \otimes \hat{\sigma}_j^{\nu}. \tag{4.2}$$

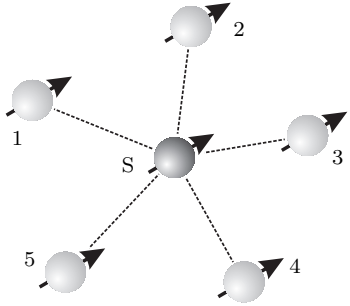

Figure 4.2: Schematics of a spin-star configuration. Typically, the environment consists of a lot more than five spins.

The $\hat{\sigma}_i$'s denote the Pauli operators of the central system, the $\hat{\sigma}_j^\nu$'s denote the Pauli operators of spin ν within the environment. A highly symmetric realization of this class, using only the Heisenberg XY coupling [11], may show dissipation and decoherence with respect to the central spin for a maximally mixed initial state in the environment [23]. This is no longer true, however, if the system initially is in a pure product state such as

$$|\psi_{\mathrm{S+C}}(0)\rangle = |1\rangle_{\mathrm{S}} \otimes |k,m\rangle_{\mathrm{C}}\,, \tag{4.3}$$

which is similar to state (3.8) for an environment with only two bands.

Instead of a highly symmetrical system, a random realization of the Hamiltonian (4.2) is considered; the coefficients γ_{ij}^ν are chosen with a normalized Gaussian distribution. These systems typically have no symmetries. Therefore, no invariant subspaces exist that could a priori prohibit overall relaxation. The precise Hamiltonian used for the following simulations is

$$\hat{H} = \frac{\delta}{2}\hat{\sigma}_z + \frac{\delta}{2}\sum_{\nu=1}^{N}\hat{\sigma}_z^\nu + \alpha\hat{H}_{\mathrm{int}}.$$

For the coupling to be weak, $\alpha \ll \delta$. Time will be scaled by α, since the speed of the relaxation dynamics can be rescaled simply by changing α.

Figure 4.3 shows the time evolution of the local inversion for two different random realizations of (4.2). For both simulations, the precise ratio of $\delta_{\mathrm{S}}/\delta_{\mathrm{C}}$ had to be changed slightly to compensate for the renormalization of the local Hamiltonian of the central TLS by the environment; in particular, $\delta_{\mathrm{S}}/\delta_{\mathrm{C}} = 1.00082$ for the solid curve and $\delta_{\mathrm{S}}/\delta_{\mathrm{C}} = 0.9992$ for the dashed

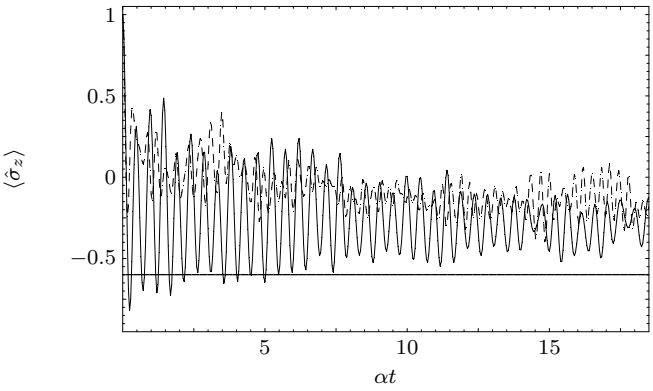

Figure 4.3: Inversion of the central spin for initial state (4.3) ($N = 14$, $k = 2$, $g_2 = 91$, and $g_3 = 364$) for two different random choices of $\hat{H}_{\text{int}}$ for the spin-star configuration. The horizontal black line at $\langle\hat{\sigma}_z\rangle = -0.6$ represents the canonical equilibrium inversion.

curve. Setting $\delta_{\text{S}} = \delta_{\text{C}}$ wouldn't change the results qualitatively, however. The oscillations have a considerably larger amplitude than for a completely random interaction (Sec. 3.3 and Fig. 2.2), because a smaller fraction of Hilbert space is involved in the dynamics. These oscillations will decrease with increasing system size.

More importantly, neither system relaxes towards the canonical equilibrium state with inversion $\langle\hat{\sigma}_z\rangle = -3/5$. The average of the inversion over all times is $\langle\bar{\sigma}_z\rangle = -0.261$ for the solid and $\langle\bar{\sigma}_z\rangle = -0.0976$ for the dashed line. Choosing $\delta_{\text{S}} = \delta_{\text{C}}$ would lead to even bigger deviations from canonical equilibrium.

The two realizations presented in Fig. 4.3 show the typical behavior for this type of model. Similar results hold for other bands of these models. Canonical relaxation is not typical for this class of systems, as will be shown later in more detail. The lack of canonical relaxation within any pair of bands leads to nonthermal relaxation, if the environment is initally in a thermal state. Here, the (quasi)equilibrium temperature of the central system is expected to differ considerably from the temperature of the environment, or, if the total system is finite, from the curves shown in Fig. 2.3. This is demonstrated in Chapter 6.

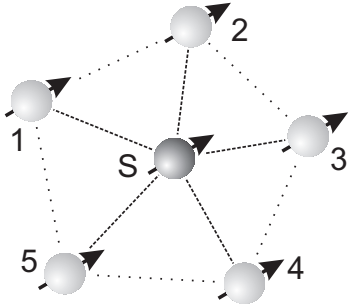

Figure 4.4: Schematics of a ring-star configuration.

4.3. Ring-Star Configuration

Now the spin-star model is extended by introducing mutual interaction between the environmental spins. A simple way to introduce spin-spin coupling within the environment is obtained by next neighbor interaction in form of a spin chain or spin ring. This ring-star configuration is schematically shown in Fig. 4.4. The coupling is introduced in form of a Heisenberg XY interaction,

$$\hat{H}_{\mathrm{CC}} = \frac{J}{2} \sum_{\nu=1}^{N} \left(\hat{\sigma}_x^{\nu} \otimes \hat{\sigma}_x^{\nu+1} + \hat{\sigma}_y^{\nu} \otimes \hat{\sigma}_y^{\nu+1} \right), \tag{4.4}$$

with periodic boundary conditions, $\hat{\sigma}_x^{N+1} = \hat{\sigma}_x^1$. Of particular interest is the dependence of the local quasiequilibrium state on the coupling strength J.

Figure 4.5 compares the time evolution of the spin-star model discussed in Sec. 4.2 (top curve) with two realizations of the ring-star configuration. For all three curves the same $\hat{H}_{\mathrm{int}}$ was used. For the middle curve $\hat{H}_{\mathrm{CC}}$ was added with a coupling strength of $J = 3\alpha/2$ and for the bottom curve with $J = 3\alpha$. The oscillations are reduced with increasing coupling strength, indicating that a larger subspace of Hilbert space is involved. More importantly, the time averaged value of the inversion approaches canonical equilibrium. These averages over all times are $\langle \bar{\sigma}_z \rangle = -0.432$ for weaker and $\langle \bar{\sigma}_z \rangle = -0.591$ for stronger intra-environmental coupling.

The relaxation dynamics and the equilibrium state of the central spin obviously strongly depend on the coupling within the environment. By

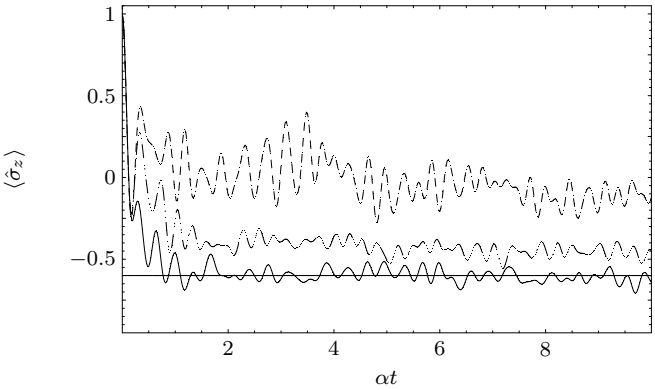

Figure 4.5: Inversion of the central spin for initial state (4.3) ($N = 14$, $k = 2$, $g_2 = 91$, and $g_3 = 364$) with stronger (bottom curve), weaker (middle curve), and without (top curve) intra-environmental interaction. See the text for the respective values of J.

increasing J from zero, the local inversion in quasiequilibrium approaches its canonical value. This is explicitely shown in Fig. 4.6. Other types of interaction—*e.g.*, Heisenberg-type—show similar behavior. Interactions involving $\hat{\sigma}_z$ are somewhat peculiar, though, because they change the effective band splitting in the environment. Therefore, $\delta_\mathrm{S} - \delta_\mathrm{C}$ may have to be adjusted to keep the systems in resonance. (Alternatively, the Zeeman splitting of the central TLS may be considered to be effectively changed by the interaction with the environment; *i.e.*, the local Hamiltonian is renormalized. Such a renormalization occurs naturally when using a reduced description for the system of interest—*e.g.*, by a Markovian master equation [1].)

One may imagine switching on or off the interaction $\hat{H}_\mathrm{CC}$ or tuning its strength dynamically (via "refocusing" pulses [33]). In this way the environment would become adjustable with respect to its effect on the given central spin. This is a phenomenon that in "classical" thermostatistics could hardly have been anticipated. Furthermore, this shows how to control a TLS entirely by a specific modification of its environment.

These systems do not only show dissipation (relaxation of the diagonal elements of $\hat{\rho}_\mathrm{S}$). Additionally, superpositions within S are docehered (the off-diagonal elements relax towards zero); see Fig. 4.7.

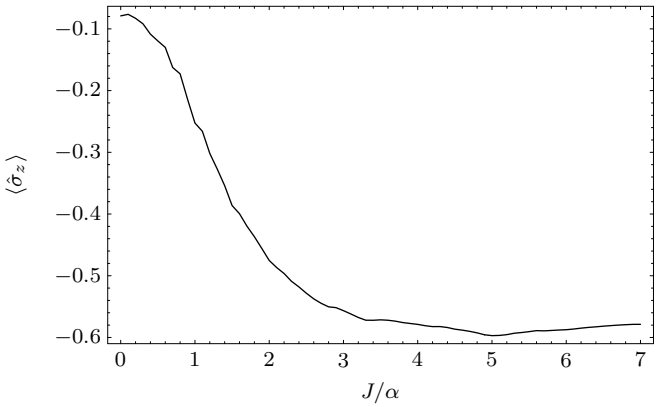

Figure 4.6: Time averaged local inversion for different values of J. Initial state (4.3) ($N = 14$, $k = 2$, $g_2 = 91$, and $g_3 = 364$), $\delta_S = \delta_C$.

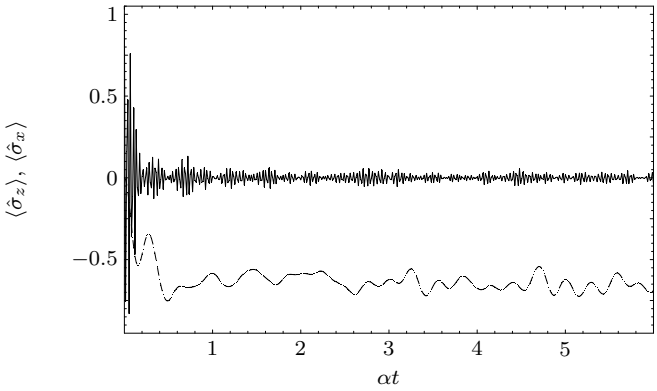

Figure 4.7: x and z components of the Bloch vector of the central spin for an initial superposition $(|0\rangle + |1\rangle)/\sqrt{2}$. Solid line: $\hat{\sigma}_x$, dashed line: $\hat{\sigma}_z$.

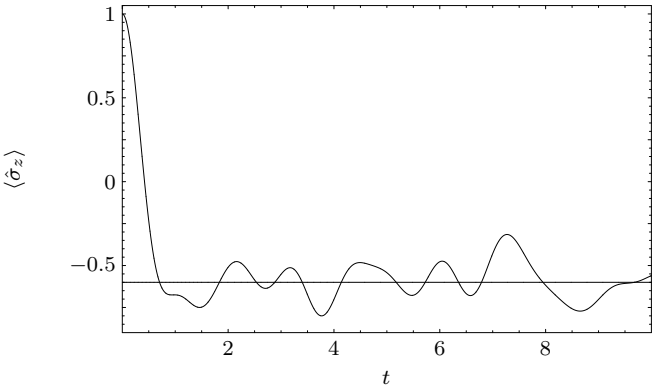

Figure 4.8: Inversion of the first spin of a Heisenberg spin chain for initial state (4.3) ($N = 14$, $k = 2$, $g_2 = 91$, and $g_3 = 364$). The horizontal black line at $\langle\hat{\sigma}_z\rangle = -0.6$ represents the canonical equilibrium inversion.

4.4. Heisenberg Spin Chain

A particular system of interest is the Heisenberg spin chain of $N+1$ particles, which is described by the Hamiltonian

$$\hat{H} = \sum_{\nu=1}^{N} \boldsymbol{\sigma}^{\nu} \cdot \boldsymbol{\sigma}^{\nu+1},$$

where $\boldsymbol{\sigma}^{\nu}$ denotes the vector of the Pauli operators for particle ν. Here, the first spin can be taken as the "central" system and the remaining $\nu = 2, \ldots, N+1$ spins would constitute the environment. This situation differs from those previously discussed, because here the central spin is only coupled to one environmental spin.

Figure 4.8 shows the time evolution of the first spin for a situation comparable to those discussed previously. Relaxation to the canonical equilibrium can be observed nicely. The average value of the inversion over all times is $\langle\bar{\sigma}_z\rangle \approx -0.55$. Not only the first spin of the chain shows canonical relaxation. The time averaged inversion of every spin is close to the canonical equilibrium, after the relaxation the energy is homogeneously distributed over the whole chain.

5. "Thermal Duality:" Relaxation to Negative Temperature States

Consider the spin systems discussed in Chapter 4. If the index k of the initially populated environmental band is larger than $N/2$ (N being the number of spins),

$$\beta_{\mathrm{S}} = \frac{\partial \ln g_{\mathrm{C}}(E)}{\partial E} < 0,$$

and therefore the environment can impart a negative absolute temperature onto the central spin.

We have shown that the environment leads for the considered subsystem to Schrödinger relaxation approaching a quasistationary state with positive temperature (for $k < N/2$). These scenarios may be considered as generic, if simplified, models for what we typically observe in "real life."

The environments with a finite number of states also allow for a different class of relaxation modes: As a typical consequence of a quantum approach to thermodynamics we find relaxation towards negative temperature states when we replace the accessible environment band index k by $N - k$ (the relaxation behavior of the system is fully symmetrical with respect to the transformation $|s\rangle \otimes |k, m\rangle \rightarrow |\bar{s}\rangle \otimes |N - k, m\rangle$, where $\bar{s}$ means logical negation)! Contrary to inversion due to optical pumping, these dual states would be dynamically stable just as their positive temperature counterparts. Again note that the environment is not a heat bath of negative temperature; in fact, it is far from any canonical state.

Since the population of the energy levels of S at $T < 0$ are inverted ($\langle \hat{\sigma}_z \rangle > 0$), negative temperatures are actually "hotter" than positive ones. Spin systems and thermodynamics at $T < 0$ have been considered before [34, 35]. In this regime several statements of thermodynamics, like the second law, have to be reformulated.

Here we show relaxation of S to a state of negative absolute temperature. The situation is essentially the same as discussed in Chapter 4, but now

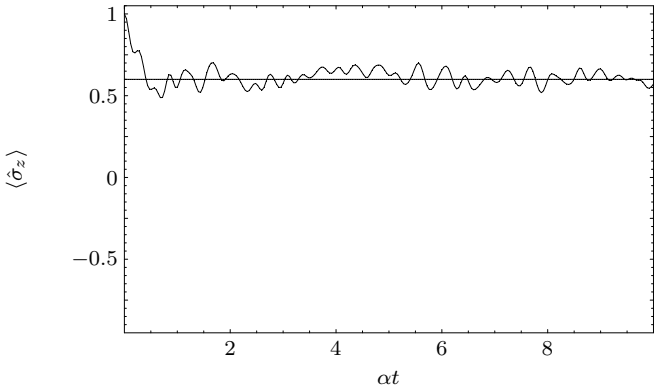

Figure 5.1: Inversion of the central spin for initial state (4.3) ($N = 14$, $k = 11$, $g_{11} = 364$, $g_{12} = 91$). The horizontal black line at $\langle\hat{\sigma}_z\rangle = 0.6$ represents the canonical equilibrium inversion.

we use $|0_S; k, m_C\rangle$ and $|1_S; k', m_C\rangle$ with $k = 12 = N - 2$, $k' = 11 = N - 3$ (instead of $k = 2$, $k' = 3$) as the accessible subspace for the Schrödinger time evolution (see Fig. 4.1).

Fig. 5.1 shows the time evolution of the local inversion for a ring-star geometry of the environment as discussed in Sec. 4.3 and demonstrated in Fig. 4.5. As expected, the time averaged inversion is now close to 0.6 instead of -0.6. Thus, for environments consisting of many spins, the regime $T < 0$ can always be reached for sufficiently high energy in the environment. In this way it is possible to study quantum thermodynamical effects at negative absolute temperature and possibly even heat conduction between embedded subsystems at temperatures of different sign. This "dual" world, though artificial, may contribute to a better understanding of thermal physics based on quantum mechanics.

6. Spin Systems and Thermal Initial States

In Chapter 4 the relaxation of the central system for a pure state of the total system was examined. However, as already noted in Sec. 2.3, a large environment will, typically, not be in a pure state. Instead, large systems may be expected to be in a thermal state with some given temperature,

$$\hat{\rho}_{\mathrm{C}}(0) = \frac{1}{Z}\mathrm{e}^{-\beta\hat{H}_{\mathrm{C}}}. \tag{2.15'}$$

In Sec. 2.3.2 it was shown that for sufficiently large systems, the central system reaches a steady state with the same temperature as of the environment, if the system relaxes canonically for each total pure state. For finite systems, deviations are expected especially for small temperatures (large β); see Fig. 2.3. Since not all of the spin systems discussed in Chapter 4 show canonical relaxation, contact equilibrium (*i.e.*, equal temperatures in equilibrium) will be violated.

Here, the steady state after relaxation will be considered for an initial thermal state in the environment when the central system starts in its excited state. To reduce the numerical complexity, not 14 but only 11 environmental particles are used. Since 11 (as well as 14) is far from infinity, sizable deviations from contact equilibrium are expected anyway. However, if the systems do not relax canonically, the final temperature should deviate even further from the (initial) temperature of the environment.[1]

To get the equilibrium temperature of the central system, the time averaged state was calculated for each pair of bands separately. These states were summed up according to Eq. (2.16). This has been done for a number of different random realizations of the spin-star and spin-ring models.

Figure 6.1 shows the averages of the local equilibrium temperatures over all realizations for the spin-star and the ring-star model (solid curves). The intra-environmental coupling for the ring-star was chosen to be of similar

[1] If the environment is infinite, its state doesn't change during the time evolution. For finite systems, however, the environmental state is not stationary.

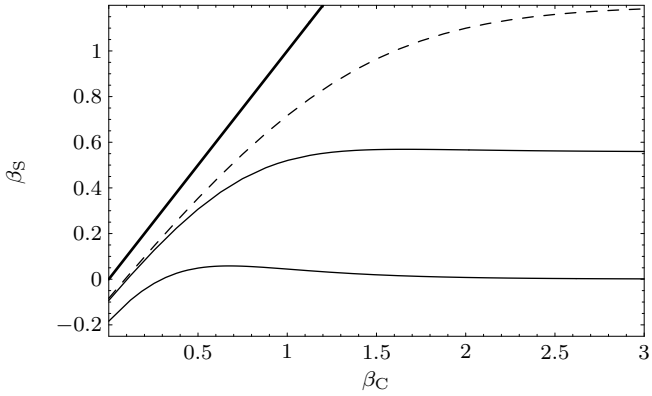

Figure 6.1: Equilibrium temperature of the spin-star (bottom solid curve) and the ring-star (upper solid curve) model classes, averaged over many realizations of both classes. The dashed line represents the canonical equilibrium temperature for a finite environment of 11 spins. The thick black line indicates contact equilibrium, $\beta_S = \beta_C$.

strength as the bottom curve in Fig. 4.5. For large temperatures (small β), the mean equilibrium temperature of the ring-star models is close to the canonical equilibrium temperature (dashed curve). The mean temperature of the spin-ring systems, however, is far from the canonical value. This result is the translation of the results from Chapter 4 for pure total states. The spin-star models violate contact equilibrium on average.

For small temperatures (large β), the deviation from the canonical state is large on average for both system classes. This is to be expected, since only the lowest band of the environment is significantly populated in this case. This band only consists of one level, thus canonical relaxation behavior cannot be expected (since the lowest pair of bands consist of only 12 levels in total, the emergence of any quasiequilibrium state cannot be expected; large fluctuations of the reduced state of the central system remain).

Figure 6.2 shows the equilibrium temperatures for several different realizations of these models (dashed lines). Almost all systems of the ring-star class follow the canonical curve closely, at least for large temperatures. Again, the large width of the distributions for small temperatures is expected due to the small number of levels involved.

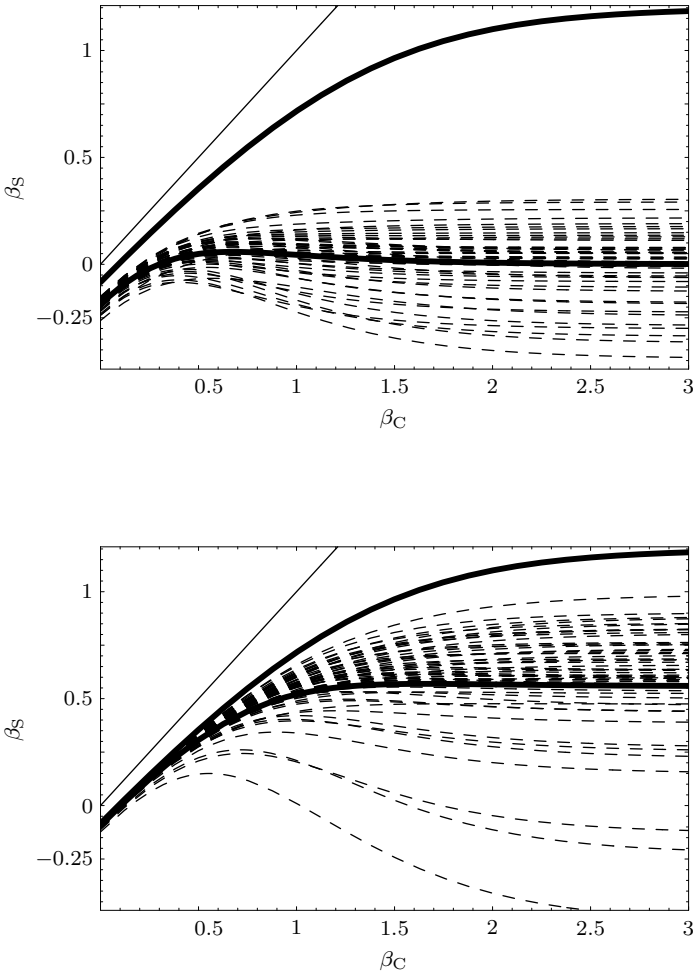

Figure 6.2: Dashed lines: equilibrium temperatures of several realizations of the spin-star (top figure) and the ring-star (bottom figure) model classes. Thick lines: Class average (lower) and canonical equilibrium (upper). The thin solid line indicates $\beta_S = \beta_C$. The deviation of the canonical equilibrium from the upper thick lines is due to finite size; see Sec. 2.3.2.

Part II.

Eigenvector Distribution

7. Energy Eigenvector Distribution

So far, several different types of environmental structures and different types of coupling between the central system and the environment had been considered. The relaxation behavior and, in particular, the quasiequilibrium state had been examined. It was shown that some environments lead to a relaxation towards canonical equilibrium in the sense of Sec. 2.2.3, but there are also environments, for which the equilibrium state is significantly "noncanonical."

Here, a method will be presented to calculate the equilibrium state of a TLS coupled to an environment with an arbitrary degeneracy structure. The environment is taken to be in a thermal state prior to the interaction with the central system, which should typically lead to thermal relaxation of the central system; see Sec. 2.3.

7.1. The Thermal Equilibrium State

Consider an environment consisting of several bands with energies $E_k = \delta k$ and degeneracies g_k weakly coupled to a central TLS. In general, superpositions of the local spin states $|0\rangle_{\mathrm{S}}$ and $|1\rangle_{\mathrm{S}}$ will decohere quickly. Therefore, the relaxation of both states can be treated separately.

The initial thermal state of the environment reads

$$\hat{\rho}_{\mathrm{C}} = \frac{1}{Z}\sum_k \mathrm{e}^{-\beta E_k}\hat{1}_k, \quad Z = \sum_k g_k \mathrm{e}^{-\beta E_k}, \tag{7.1}$$

where $\hat{1}_k$ denotes the projector onto band k. The possible initial states for the total system then are

$$\hat{\rho}^0(0) = |0\rangle\langle 0|_{\mathrm{S}} \otimes \hat{\rho}_{\mathrm{C}} \quad \text{and} \quad \hat{\rho}^1(0) = |1\rangle\langle 1|_{\mathrm{S}} \otimes \hat{\rho}_{\mathrm{C}}. \tag{7.2}$$

Introducing the operators $\hat{\kappa}_k^m(0) = |m\rangle\langle m|_{\mathrm{S}} \otimes \frac{\hat{1}_k}{g_k}$ to simplify the notation $(m = 0, 1)$, the total initial state can be written as

$$\hat{\rho}^m(0) = \frac{1}{Z}\sum_k g_k\, \mathrm{e}^{-\beta E_k}\hat{\kappa}_k^m(0). \tag{7.3}$$

If this state is subject to canonical or thermal relaxation, the equilibrium state of the central system according to Sec. 2.3 will be

$$\hat{\rho}_{\mathrm{can}} = \frac{1}{Z}\sum_k g_k \mathrm{e}^{-\beta E_k}\left(a_k^m \left|0\right\rangle\!\left\langle 0\right| + b_k^m \left|1\right\rangle\!\left\langle 1\right|\right), \tag{2.16'}$$

with the inversion

$$\langle\hat{\sigma}_z\rangle_{\mathrm{can}}^m = \frac{1}{Z}\sum_k g_k \mathrm{e}^{-\beta E_k}(b_k^m - a_k^m),$$

where

$$a_k^m = \frac{g_{k+m}}{g_{k-1+m}+g_{k+m}}, \quad b_k^m = \frac{g_{k-1+m}}{g_{g-1+m}+g_{k+m}}.$$

The index $k+m$ will be called the *total excitation* of the system in the following, since k is the number of the excited environmental band and $m = 0, 1$ is the "number of excitations" within the central system.

7.2. Energy Eigenstates

If the system, however, is not subject to canonical relaxation, we have to use a different approach to get the equilibrium state for the central system. Since the systems of interest are typically large, the central state will be close to its equilibrium state for almost all times. To get the equilibrium state we can therefore simply average the state of the system over all times. This is conveniently done in its energy eigenbasis. If the energy splitting δ within the environment and the Zeeman splitting of the TLS are in resonance and the coupling is weak, the total system will preserve the band structure of the environment. Only transitions between the states $\left|0\right\rangle_{\mathrm{S}} \otimes \left|k,\ell\right\rangle_{\mathrm{C}}$ and $\left|1\right\rangle_{\mathrm{S}} \otimes \left|k-1,\ell'\right\rangle_{\mathrm{C}}$ are possible in this case, similarly to the situation discussed in Sec. 2.2.1. There is only little mixing of states with different total excitation.

By virtue of this band structure, the total excitation of each energy eigenstate of the total system $\left|\varepsilon\right\rangle$ is (almost) sharply defined. The energy eigenstates with total excitation $k+0$ can be written in the form

$$\left|\varepsilon_k\right\rangle \approx \alpha_\varepsilon^k \left|0,\chi_\varepsilon^k\right\rangle + \beta_\varepsilon^k \left|1,\eta_\varepsilon^k\right\rangle, \tag{7.4}$$

where $\left|\chi_\varepsilon^k\right\rangle$ is a state in band k and $\left|\eta_\varepsilon^k\right\rangle$ is a state in band $k-1$ of the environment. Both $\left|\chi_\varepsilon^k\right\rangle$ and $\left|\eta_\varepsilon^k\right\rangle$ are taken to be normalized. For a given

total excitation k there are $g_k + g_{k-1}$ different $|\varepsilon_k\rangle$, since they form a complete basis within the given subspace. In the following, ε_k will be used as a discrete index numbering these states, as well as the energy eigenvalue corresponding to $|\varepsilon_k\rangle$. For notational convenience, ε is used instead of ε_k occasionally.

7.3. The Time Averaged State

In terms of the energy eigenbasis $\{|\varepsilon_{k+m}\rangle\}$ within the respective subspace, the operators $\hat{\kappa}_k^m(0)$ that are part of the total state operator (7.3) read (here $\varepsilon = \varepsilon_{k+m}$)

$$\hat{\kappa}_k^m(0) = \sum_{\varepsilon,\varepsilon'} \kappa_{k,\varepsilon\varepsilon'}^m \, |\varepsilon_{k+m}\rangle\langle\varepsilon'_{k+m}|$$

with $\kappa_{k,\varepsilon\varepsilon'}^m = \langle\varepsilon_{k+m}|\,\hat{\kappa}_k^m\,|\varepsilon'_{k+m}\rangle$. If the state $\hat{\kappa}_k^m$ is subject to Schrödinger dynamics, after the time t it is given by[1]

$$\hat{\kappa}_k^m(t) = \sum_{\varepsilon,\varepsilon'} \kappa_{k,\varepsilon\varepsilon'}^m \, \mathrm{e}^{\mathrm{i}(\varepsilon'-\varepsilon)t} \, |\varepsilon_{k+m}\rangle\langle\varepsilon'_{k+m}| \,.$$

These are the only time dependent terms of (7.3). Averaging over the exponential yields

$$\lim_{\tau\to\infty} \frac{1}{\tau} \int_{-\tau/2}^{\tau/2} \mathrm{d}t \, \mathrm{e}^{\mathrm{i}(\varepsilon-\varepsilon')t} = \delta_{\varepsilon,\varepsilon'}. \tag{7.5}$$

Thus, if the total system is nondegenerate—*i.e.*, if all energy eigenvalues are different—the time average over $\hat{\kappa}_k^m(t)$ is readily available,

$$\overline{\hat{\kappa}_k^m} = \sum_{\varepsilon} \kappa_{k,\varepsilon\varepsilon}^m \, |\varepsilon_{k+m}\rangle\langle\varepsilon_{k+m}| \,. \tag{7.6}$$

If there are degeneracies in the total system, Hilbert space consists of several invariant subspaces due to some symmetry of the Hamiltonian. By finding an irreducible representation for the Hamiltonian and treating each subspace separately, this method of averaging can still be applied.

[1] ε and ε' in the exponent denote the respective energy eigenvalues.

For the coefficients of the state (7.6) we find, using Eq. (7.4)

$$\kappa^0_{k,\varepsilon\varepsilon} = |\alpha^k_\varepsilon|^2/g_k, \quad \kappa^1_{k,\varepsilon\varepsilon} = |\beta^{k+1}_\varepsilon|^2/g_k.$$

Since we are only interested in the equilibrium state of the central system, we trace over the environmental degrees of freedom,

$$\begin{aligned}(\hat{\kappa}^m_k)_{\mathrm{eq}} = \mathrm{Tr}_{\mathrm{C}}(\overline{\hat{\kappa}^m_k}) &= \sum_\varepsilon \kappa^m_{k,\varepsilon\varepsilon}\,\mathrm{Tr}_{\mathrm{C}}\big(|\varepsilon_{k+m}\rangle\langle\varepsilon_{k+m}|\big) \\ &= \sum_\varepsilon \kappa^m_{k,\varepsilon\varepsilon}\Big(|\alpha^{k+m}_\varepsilon|^2\,|0\rangle\langle 0| + |\beta^{k+m}_\varepsilon|^2\,|1\rangle\langle 1|\Big).\end{aligned}$$

Summing over all bands of the environment, we arrive at the equilibrium states for the central system,

$$\hat{\rho}^0_{\mathrm{eq}} = \frac{1}{Z}\sum_k g_k \mathrm{e}^{-\beta E_k} \sum_{\varepsilon_k} \frac{|\alpha^k_\varepsilon|^2}{g_k}\Big(|\alpha^k_\varepsilon|^2\,|0\rangle\langle 0| + |\beta^k_\varepsilon|^2\,|1\rangle\langle 1|\Big), \tag{7.7a}$$

$$\hat{\rho}^1_{\mathrm{eq}} = \frac{1}{Z}\sum_k g_k \mathrm{e}^{-\beta E_k} \sum_{\varepsilon_{k+1}} \frac{|\beta^{k+1}_\varepsilon|^2}{g_k}\Big(|\alpha^{k+1}_\varepsilon|^2\,|0\rangle\langle 0| + |\beta^{k+1}_\varepsilon|^2\,|1\rangle\langle 1|\Big). \tag{7.7b}$$

These states are dependent, in general, on the initial state, in strong contrast to thermal equilibrium.

7.4. Inversion of the Equilibrium State

For many systems, the term $g_k \mathrm{e}^{-\beta E_k}$ is narrowly peaked around one $k_{\max}$, as discussed in Sec. 2.3.3. Therefore, very often only a few k will contribute strongly to the sums and for many practical cases all other values of k can be neglected. In the following calculations we will drop the sum over k. If needed, this sum can easily be applied to the final result.

For a single band, the inversion of the equilibrium states (7.7) is given by

$$\langle\bar{\sigma}_z\rangle^m_k = \mathrm{Tr}(\hat{\kappa}^m_k\hat{\sigma}_z), \tag{7.8a}$$

$$\langle\bar{\sigma}_z\rangle^0_k = \sum_{\varepsilon_k} \frac{|\alpha^k_\varepsilon|^2}{g_k}\big(|\beta^k_\varepsilon|^2 - |\alpha^k_\varepsilon|^2\big), \tag{7.8b}$$

$$\langle\bar{\sigma}_z\rangle^1_k = \sum_{\varepsilon_{k+1}} \frac{|\beta^{k+1}_\varepsilon|^2}{g_k}\big(|\beta^{k+1}_\varepsilon|^2 - |\alpha^{k+1}_\varepsilon|^2\big). \tag{7.8c}$$

These equations will now be brought into a new form. We start with $\langle\hat{\sigma}_z\rangle_k^1$. For simplicity, all band and excitation indices will be dropped; *i.e.*, $\alpha_\varepsilon = \alpha_\varepsilon^{k+1}$, $\beta_\varepsilon = \beta_\varepsilon^{k+1}$, $|\varepsilon\rangle = |\varepsilon_{k+1}\rangle$, $g = g_k$, and $g' = g_{k+1}$.

The term

$$\boxed{\lambda_\varepsilon = |\beta_\varepsilon|^2 - |\alpha_\varepsilon|^2} \tag{7.9}$$

is the inversion of the respective energy eigenstate $|\varepsilon\rangle$.[2] Since $|\alpha_\varepsilon|^2 + |\beta_\varepsilon|^2 = 1$, we can rewrite the equilibrium or time-averaged inversion of the central system completely in terms of the λ_ε's,

$$\langle\bar{\sigma}_z\rangle = \frac{1}{2g}\left(\sum_\varepsilon \lambda_\varepsilon + \sum_\varepsilon \lambda_\varepsilon^2\right). \tag{7.10}$$

The first sum can be expressed in terms of g and g' only,

$$\boxed{\sum_\varepsilon \lambda_\varepsilon = g - g',} \tag{7.11}$$

which is proven in Appendix C. Rewriting the second sum in terms of the variance $\Delta\lambda_\varepsilon^2$ of the distribution of the λ_ε's for a given Hamiltonian (see Appendix D) yields (now again fully indexed)

$$\boxed{\langle\bar{\sigma}_z\rangle_k^1 = \langle\hat{\sigma}_z\rangle_{k,\mathrm{can}}^1 + \frac{g_k + g_{k+1}}{2g_k}\,\Delta\lambda_{\varepsilon,k+1}^2.} \tag{7.12a}$$

A similar result is obtained, if the central system initially was in its ground state,

$$\boxed{\langle\bar{\sigma}_z\rangle_k^0 = \langle\hat{\sigma}_z\rangle_{k,\mathrm{can}}^0 - \frac{g_{k-1} + g_k}{2g_k}\Delta\lambda_{\varepsilon,k}^2.} \tag{7.12b}$$

We see that, as long as the variance of the λ_ε distribution for a given Hamiltonian of the total system is finite, there are always deviations of the time-averaged or equilibrium state from the canonical equilibrium. If the central system starts in its excited state, the reached inversion is always larger then the canonical one. If the central system starts in its ground state, the reached inversion is always smaller. After summing up over all

[2] If the band index is included, this quantity will be denoted by $\lambda_{\varepsilon,k+1}$.

bands this leads to a violation of thermal contact equilibrium. The temperature the TLS approaches during relaxation differs from the temperature of the environment. For a finite environment, $\Delta\lambda_\varepsilon^2$ is always finite. So there will always be deviations.

However, not only does the quasiequilibrium state for a general system differ from what we would expect, if the system relaxed canonically (or thermally), it is also dependent on the initial state of the central system, while a system relaxing thermally does not show such a dependence.

8. Energy Eigenvector Distributions of Different Abstract Model Systems

In the last chapter a method to determine the equilibrium state of a TLS coupled to a generally gapped environment was introduced. In this chapter the λ_ε distributions of several model systems will be discussed. Only environments with two bands will be considered, environments that naturally have more than two bands will be reduced to two bands. This can be done because the behavior of the total system can be obtained by simply summing up over all bands. In many cases, however, this is not even necessary since only few bands dominate the behavior of the small system as seen in Sec. 2.3.3.

Instead of denoting the degeneracies of both bands by an index as in g_k, simply g and g' will be used for the degeneracies of the lower and higher environmental band, respectively. The bands themselves will be denoted by k and k', respectively. As discussed in Sec. 2.2.1, only the subspace of Hilbert space spanned by the cross states

$$\left\{|0;k',b\rangle\,,|1;k,a\rangle\right\} \quad (1<a<g, \quad 1<b<g'). \tag{2.10'}$$

will be considered as these are the only relevant states for the dynamics of the central system. Typically, $g > g'$.

8.1. Random Hamiltonian

Again, the most general model system possible is the one without any structure within the environment or in the coupling between system proper and environment. The interaction Hamiltonian will be taken from the Gaussian unitary ensemble (GUE; see Chapter 3).

At first we will consider system and environment to be in resonance. In this case, $\hat{H}_\mathrm{S} + \hat{H}_\mathrm{C} \propto \hat{1}$ and can therefore be neglected. The only relevant part of the Hamiltonian is a random Hermitian matrix of dimension $g+g'$. For this setup, the complete probability density $P(\lambda)$ can be calculated

analytically for the whole ensemble for arbitrary system size. Therefore, both finite systems and the thermodynamic limit can be examined in detail.

8.1.1. Probability Density of the Eigenvector Inversion

Using the basis (2.10'), the state of the total system has the form

$$|\psi\rangle = \sum_{b=1}^{g'} \psi_{0b} \, |0\rangle \otimes |k', b\rangle + \sum_{a=1}^{g} \psi_{1a} \, |1\rangle \otimes |k, a\rangle \, .$$

For simplicity we introduce a single index n to label the amplitudes instead of the double index $0m$ or $1m$. n runs from 1 to the dimension of the considered subspace, $d = g + g'$. In this notation, the reduced state of the central TLS becomes

$$\hat{\rho}_{\mathrm{S}} = \mathrm{Tr}_{\mathrm{C}} \, |\psi\rangle\langle\psi| = \sum_{n=1}^{g'} |\psi_n|^2 \, |0\rangle\langle 0| + \sum_{n=g'+1}^{g'+g} |\psi_n|^2 \, |1\rangle\langle 1| \, .$$

We are interested in the distribution of the local inversion of the energy eigenstates. Since the inversion is determined by the population of each level, we will derive the distribution for the population of the ground state,

$$p_0 = \sum_{n=1}^{g'} |\psi_n|^2 .$$

According to Sec. 3.2 the amplitudes are now split into their real and imaginary parts, $\psi_n = x_k + \mathrm{i} x_{k+1}$. $1 \leq k \leq 2g'$ and $2g' + 1 \leq k \leq 2d$ correspond to $|0\rangle\langle 0|$ and $|1\rangle\langle 1|$, respectively. In this notation, $p_0 = \sum_{k=1}^{2g'} x_k^2$.

According to (3.5), the joint probability density of the first $2g'$ amplitudes x_k for the eigenvectors of random matrices from the GUE is

$$P_{\mathrm{a}}(x_1, \ldots, x_{2g'}) = \pi^{-g'} \, \frac{\Gamma(d)}{\Gamma(d - g')} \left(1 - \sum_{k=1}^{2g'} x_k^2 \right)^{d-g'-1} .$$

The desired probability density for the population p_0 of the ground state is then given by

$$P_{\mathrm{p}}(p_0) = \int \mathrm{d}^{2g'} x \, P_{\mathrm{a}}(x_1, \ldots, x_{2g'}) \, \delta\left(p_0 - \sum_{k=0}^{2g'} x_k^2 \right), \tag{8.1}$$

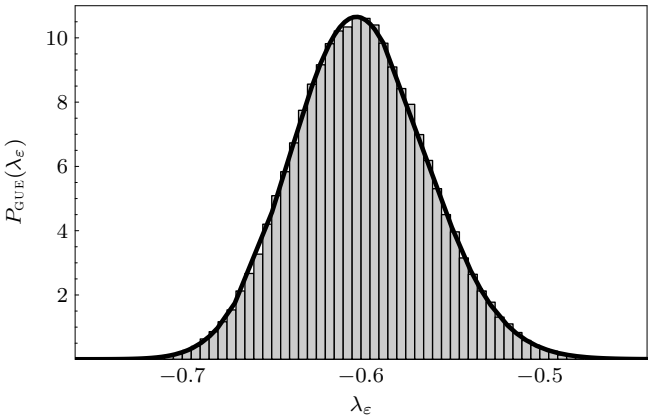

Figure 8.1: λ_ε distribution for random Hermitian matrices taken from the GUE. The solid line shows the normalized probability density (8.3) for $g = 91$ and $g' = 364$. The histogram was obtained from the eigenvectors of 400 different random matrices.

integrating over the volume of the hypersphere in $2g'$ dimensions. The integral is carried out in Appendix E and yields

$$P_{\mathrm{p}}(p_0) = \frac{\Gamma(d)}{\Gamma(d-g')\Gamma(g')} p_0^{g'-1}(1-p_0)^{d-g'-1}. \tag{8.2}$$

This can be transformed into the probability density for the inversion using $\lambda_\varepsilon = 1 - 2p_0$. We finally arrive at the desired distribution function (using $d = g + g'$)

$$\boxed{P_{\mathrm{GUE}}(\lambda_\varepsilon) = \frac{1}{2^{g+g'-1}} \frac{\Gamma(g+g')}{\Gamma(g)\Gamma(g')} (1-\lambda_\varepsilon)^{g'-1}(1+\lambda_\varepsilon)^{g-1}.} \tag{8.3}$$

We want to stress that this is not the distribution of the λ_ε-values for a single Hamiltonian but the probability density for these values for the whole Gaussian unitary ensemble. The λ_ε distribution of any single Hamiltonian can deviate strongly from (8.3), of course.

The distribution (8.3) is shown as the solid line in Fig. 8.1 for $g = 91$ and $g' = 364$. To obtain the histogram, 400 different random matrices were generated and diagonalized, so $400 \times (91 + 364) = 182000$ values were used. The analytical and the numerical results agree nicely.

8.1.2. Deviation from Canonical Relaxation and the Thermodynamic Limit

The probability density (8.3) is narrowly peaked around its mean value

$$\bar{\lambda}_\varepsilon = \int_{-1}^{1} \mathrm{d}\lambda_\varepsilon \, \lambda_\varepsilon P_{\mathrm{GUE}}(\lambda_\varepsilon) = \frac{g - g'}{g + g'} = \langle \hat{\sigma}_z \rangle_{\mathrm{can}}$$

which can be obtained exactly. This mean value is expected, as it is just the general result for the average of all λ_ε's of one Hamiltonian by virtue of (7.11).

The deviation of the equilibrium state is mainly given by the variance of the λ_ε distribution. The variance of the probability density (8.3) can also be calculated exactly and is given by

$$\Delta\lambda_\varepsilon^2 = \int_{-1}^{1} \mathrm{d}\lambda_\varepsilon \, (\lambda_\varepsilon^2 - \bar{\lambda}^2) \, P_{\mathrm{GUE}}(\lambda_\varepsilon) = 4\frac{gg'}{d^2(d+1)} \tag{8.4}$$

with $d = g + g'$. Since this is finite, the reached equilibrium state will typically deviate from the canonical equilibrium for finite environments.

For large systems (for constant ratio g/g'), however, one obtains

$$\boxed{\lim_{d\to\infty} \Delta\lambda_\varepsilon^2 = \lim_{d\to\infty} \langle \bar{\sigma}_z \rangle - \langle \hat{\sigma}_z \rangle_{\mathrm{can}} = 0.} \tag{8.5}$$

So for large systems the deviations should decrease. In the thermodynamic limit, the quasiequilibrium reached equals the canonical equilibrium which is just the expectation for completely disordered systems.

8.1.3. Sample Eigenvector Distributions

The histograms in figure 8.2 show the λ_ε distributions of four different random Hamiltonians. The system sizes for each Hamiltonian were taken differently but all with the ratio g/g' used in Fig. 8.1. Each Hamiltonian is a typical representative of its ensemble. The average value of λ_ε is $\langle \hat{\sigma}_z \rangle_{\mathrm{can}} = 0.6$ for each Hamiltonian due to the equal g/g'-ratio. However, since the Hamiltonians differ in size, the variance of the distribution varies.

Table 8.1 shows the expected and actual values of $\Delta\lambda_\varepsilon^2$ for each system as well as the expected and actual value of $|\langle \bar{\sigma}_z \rangle - \langle \hat{\sigma}_z \rangle_{\mathrm{can}}|$ (denoted as "deviation"). For the smaller systems, the actual λ_ε distributions differ from the expected distribution. But even for a very small system with only $g +$

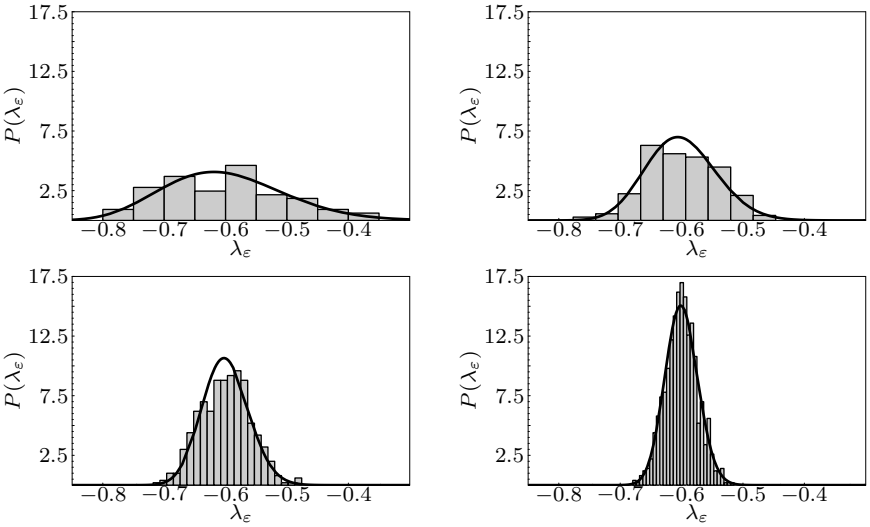

Figure 8.2: λ_ε distributions for four different random Hamiltonians with equal g/g' but with different size (histograms). The solid lines represent the respective functions $P_{\text{GUE}}(\lambda_\varepsilon)$ from (8.3). Top left: $g = 13$ and $g' = 52$; top right: $g = 39$ and $g' = 156$; bottom left: $g = 91$ and $g' = 364$; bottom right: $g = 182$ and $g' = 728$. For clarity, the same scaling was used in each graph.

$g' = 65$ levels, a peak around $\langle\hat{\sigma}_z\rangle_{\text{can}}$ can be seen for most Hamiltonians. As the system grows larger, the actual distributions approximate the expected distributions more closely. For $g+g' = 910$ only few deviations can be seen for the sample Hamiltonian.

The deviations from canonical equilibrium cannot be observed directly (simply by looking at the time evolution of $\langle\hat{\sigma}_z\rangle$) since the fluctuations in the quasiequilibrium are significantly larger than $|\langle\bar{\sigma}_z\rangle - \langle\hat{\sigma}_z\rangle_{\text{can}}|$ for all these systems.

To see how many Hamiltonians deviate from the expectations and how strongly these deviations are, Fig. 8.3 shows the distributions of the variance $\Delta\lambda_\varepsilon^2$ for two different system sizes. A general analytical expression does not exist (*i.e.*, is not an elementary function) for the probability density function $P_{\text{var}}(\Delta\lambda_\varepsilon^2)$. Therefore, for each diagram 2000 Hamiltonians

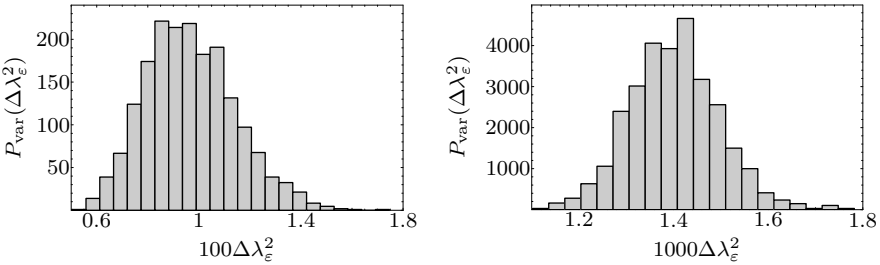

Figure 8.3: Distributions of $\Delta\lambda_\varepsilon^2$ for different system sizes. Left: $g = 13$ and $g' = 52$; right: $g = 91$ and $g' = 364$. The histograms were obtained from 2000 different random Hamiltonians. Note the different scalings of the abscissa.

were randomly chosen and their respective values of $\Delta\lambda_\varepsilon^2$ were calculated.

One can see that for $g+g' = 65$ levels only, there are a significant number of Hamiltonians deviating from the mean value; however, the distribution is still quite narrowly peaked already. The standard deviation is 1.77×10^{-3} and the relative deviation is 0.183. For $g+g' = 455$ levels the distributions becomes even narrower. Fewer Hamiltonians deviate strongly from the mean value. The standard deviation is 9.47×10^{-5}, the relative deviation is only 6.76×10^{-2}.

Thus, without further knowledge of the properties of the system, canonical relaxation becomes increasingly "typical" for larger systems: The mean time averaged state for random matrices from the GUE approaches the canonical averaged state with increasing system size and the number of Hamiltonians deviating strongly from this mean value decreases.

Table 8.1: Expected and actual λ_ε variance as well as expected and actual deviation of the equilibrium state to the canonical state for the Hamiltonians from Fig. 8.2.

g/g'	13/52	39/156	91/364	182/728
expected $\Delta\lambda_\varepsilon^2$	0.00970	0.00327	0.00140	0.000703
actual $\Delta\lambda_\varepsilon^2$	0.00957	0.00323	0.00164	0.000683
exp. deviation	0.0242	0.00816	0.00351	0.00176
act. deviation	0.0238	0.00808	0.00411	0.00171

8.2. Random Interaction with Degenerate Bands

The completely random Hamiltonian in Sec. 8.1 did not only introduce interactions between system proper and environment, it also changed the environmental spectrum. The original structure of the system (degenerate environmental bands) is destroyed. Now a model system will be discussed that retains the original structure of both the central spin and the environment.

8.2.1. Hamiltonian Matrix

The most general model to achieve this is to choose the interaction part V of the Hamiltonian matrix (2.11) to be random. The resulting Hamiltonian in the subspace (2.10') then has the form

$$\hat{H} = \left(\begin{array}{cc|cc} -\Delta & & & \\ & \ddots & & V^\dagger \\ & & -\Delta & \\ \hline & & \Delta & \\ & V & & \ddots \\ & & & \Delta \end{array}\right), \tag{8.6}$$

where $\Delta = (\delta_S - \delta_C)/2$ is half the detuning between the central system and the environment. The upper left block corresponds to the ground state of the TLS and is therefore of dimension g'; the lower right block, corresponding to the excited level, is of dimension g. These blocks are purely diagonal. For $\Delta \neq 0$, system and environment are off resonance and the full relaxation to the canonical equilibrium state is prohibited by energy conservation. So only $\Delta = 0$ will be considered. We assume that the degeneracy increases with energy, therefore we take $g' > g$.

The off-diagonal part V (a $g \times g'$-matrix) corresponds to energy exchange coupling. It is chosen randomly with normalized Gaussian distributions for the real and imaginary parts of the matrix elements.

8.2.2. Eigenvector Distribution

It can be seen that $\hat{H}$ is of rank $2g$ for $\Delta = 0$: Since the entries are random, all g row vectors of V are linearly independent, in general. However,

only g of the g' column vectors can be linearly independent, since V is not quadratic. Therefore, only $2g$ of the row and column vectors of $\hat{H}_{\text{int}}$ are independent and its rank then is $2g$.

The rank of a matrix is connected with the dimension of its null space,

$$\operatorname{rank} \hat{H} + \dim(\operatorname{null} \hat{H}) = d,$$

where d is the dimension of the matrix, here $d = g + g'$. We arrive at the dimension of the null space,

$$\dim(\operatorname{null} \hat{H}) = g' - g.$$

Thus, $\hat{H}$ has the $(g' - g)$-times degenerate eigenvalue 0. Due to the randomness of the matrix, there are no more degenerate eigenvalues.

The system of homogeneous linear equations to determine the null space of $\hat{H}$ splits into two sets, one with g' equations for g variables and another one with g equations for g' variables. Since the first set is overdetermined, the corresponding entries of all vectors within the null space must vanish. These vectors thus have the form

$$\boldsymbol{u} = \big(u_1, \ldots, u_{g'}, \underbrace{0, \ldots, 0}_{g \text{ zeros}}\big)^t. \tag{8.7}$$

The first g' entries correspond to the ground state of the central spin and the last g entries correspond to its excited state. Therefore, all these vectors are completely in the local ground state. In the notation (7.4) they read

$$|\varepsilon\rangle = |0, \chi_\varepsilon\rangle\,.$$

Therefore, $\alpha_\varepsilon = 1$, leading to $\lambda_\varepsilon = -1$.

The complete subspace corresponding to the local ground state is g'-dimensional. Of that, a $(g' - g)$-dimensional subspace is given by the null space, so g "ground-state dimensions" remain for vectors outside the null space. Since another g dimensions correspond to the excited state, the average local inversion of the all remaining $2g$ energy eigenvectors has to be $\lambda_\varepsilon = 0$.

The average value of all λ_ε's is again given by

$$\frac{(g' - g) \cdot (-1) + 2g \cdot 0}{g + g'} = \frac{g - g'}{g + g'},$$

as expected from Appendix C.

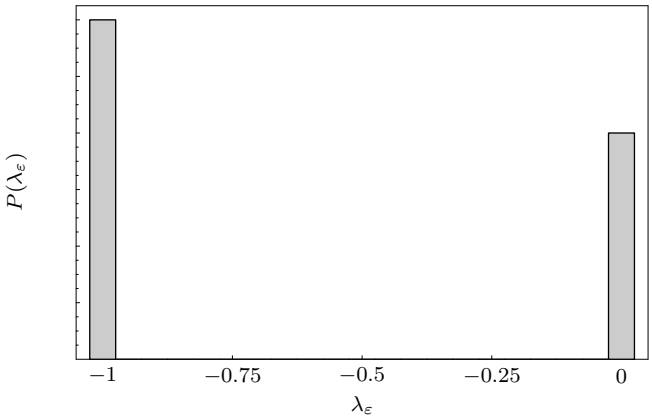

Figure 8.4: λ_ε distribution for random interaction and degenerate bands. The two bars represent δ peaks of different strength. For an explanation of the height see the text. $g = 91$ and $g' = 364$.

From numerical studies it was found that the eigenvectors outside the null space are not only distributed around their mean value, but that $\lambda_\varepsilon = 0$ exactly for all of them. This result could not be proven so far. The corresponding probability density consists of two δ peaks at $\lambda_\varepsilon = -1$ and $\lambda_\varepsilon = 0$,

$$P_\lambda(\lambda_\varepsilon) = \frac{g' - g}{g' + g}\delta(\lambda_\varepsilon + 1) + \frac{2g}{g' + g}\delta(\lambda_\varepsilon). \tag{8.8}$$

Figure 8.4 shows this distribution schematically for $g = 91$ and $g' = 364$. In strong contrast to the distribution for a completely random Hamiltonian, this one is not single peaked. It's variance

$$\boxed{\Delta\lambda_\varepsilon^2 = \frac{2g(g' - g)}{(g + g')^2}} \tag{8.9}$$

is considerably larger than (8.4). For the given system size, $\Delta\lambda_\varepsilon^2 = 6/25 = 0.24$ as opposed to $\Delta\lambda_\varepsilon^2 \approx 0.0014$. Stronger deviations from canonical equilibrium can be expected. In fact, this deviation is exactly given by

$$\langle\bar{\sigma}_z\rangle - \langle\hat{\sigma}_z\rangle_{\text{can}} = -\langle\hat{\sigma}_z\rangle_{\text{can}}\,,$$

which is nicely demonstrated in Fig. 8.5. Note that this is the time evolution of a pure state for the total system.

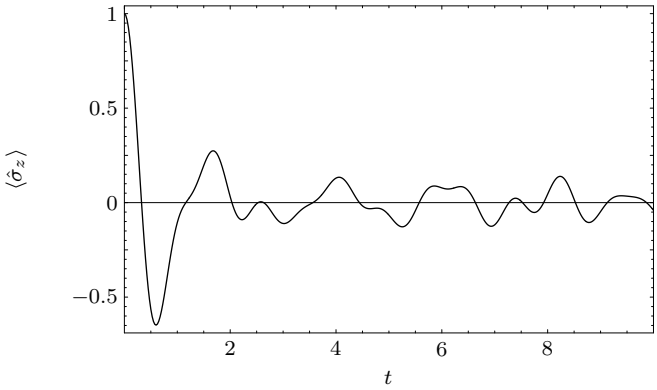

Figure 8.5: Inversion of the central spin with the initial state $|1;k,a\rangle$ for random interaction and degenerate environmental bands ($g = 91$ and $g' = 364$). The canonical equilibrium state for the given parameters would be at $\langle\hat{\sigma}_z\rangle = -0.6$.

Another major difference to a random Hamiltonian is the thermodynamic limit. While for the latter $\langle\bar{\sigma}_z\rangle$ approaches the canonical equilibrium value for large systems, here $\langle\bar{\sigma}_z\rangle$ is independent of the system size! Going to large environments will not change the relaxation and equilibrium behavior other than reducing the amplitude of the fluctuations. Even in the thermodynamic limit the canonical equilibrium state is never reached.

One has to be careful with the form of the λ_ε distribution for this type of matrices since they are highly degenerate. The averaging method used in (7.5) is valid only for nondegenerate systems and not all initial states can be expected to obey the results obtained from naively applying (7.12). However, Fig. 8.5 shows that those results are applicable for some special initial states.

8.2.3. Finite Detuning

By applying the Hamiltonian matrix (8.6) to the vectors (8.7) it is readily seen that all eigenvectors to the eigenvalue 0 in the resonant case are eigenvectors to the eigenvalue $-\Delta$ for finite detuning. For $\Delta > 0$, $\hat{H}$ thus has the $(g'-g)$-times degenerate eigenvalue $-\Delta$ and, therefore, $g'-g$ eigenvectors with $\lambda_\varepsilon = -1$. The peak of the λ_ε distribution at $\lambda_\varepsilon = 0$ is broadened

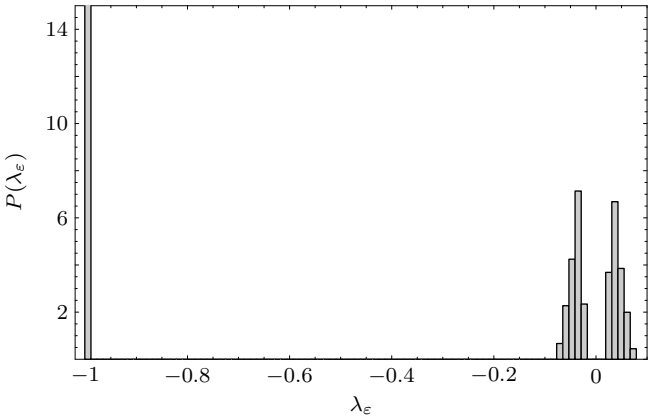

Figure 8.6: λ_ε distribution for random interaction and a small detuning between the central spin and the environment. The leftmost bar represents a δ peak. $g = 91$ and $g' = 364$. The histogram was obtained from the eigenvectors of 100 different random Hamiltonians.

and split into two parts and the variance of the distribution is increased. This is expected since now energy conservation additionally suppresses relaxation to canonical equilibrium.

Figure 8.6 shows the probability distribution for $\Delta = 1$, $g = 91$, and $g' = 364$. This is a small value for the detuning since it leads to eigenvalues of the diagonal part of 1 and -1, while the largest eigenvalues of the off-diagonal part are of modulus around 40 for matrices of this size. The histogram is actually slightly misleading, since for any value of λ_ε in the vicinity of 0 there is another value of $-\lambda_\varepsilon$, so the distribution is symmetrical about 0 (apart from the δ peak at $\lambda_\varepsilon = -1$). The variance of this distribution is $\Delta\lambda_\varepsilon^2 \approx 0.2407$ which is slightly more than $\Delta\lambda_\varepsilon = 0.24$ for $\Delta = 0$. The variance increases further if the detuning is increased.

8.3. Nondegenerate Bands

The situation discussed in Sec. 8.2 can be extended by adding some more structure to the environment by introducing a small spacing between the levels of each environmental band. We consider equidistant levels and

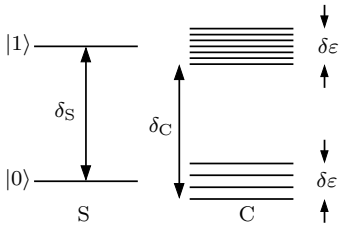

Figure 8.7: A TLS in contact with an environment consisting of two "bands" with equidistant level spacing. Both bands have the same width $\delta\varepsilon$; the lower band consists of g levels, the upper band of g' levels.

equal bandwidths $\delta\varepsilon$ for both bands. The very lowest (and very highest) levels of each band in the environment are in resonance with the central system. This situation is depicted schematically in Fig. 8.7 ($\delta_S = \delta_C$ will be considered in the following). The Hamiltonian in the subspace (2.10') has the form

$$\hat{H} = \left(\begin{array}{c|c} \begin{array}{ccc} 0 & & \\ & \frac{\delta\varepsilon}{(g'-1)} & \\ & & \ddots \\ & & \delta\varepsilon \end{array} & V^\dagger \\ \hline V & \begin{array}{ccc} 0 & & \\ & \frac{\delta\varepsilon}{(g-1)} & \\ & & \ddots \\ & & \delta\varepsilon \end{array} \end{array}\right) \tag{8.10}$$

with a random off-diagonal part V as in Sec. 8.2. This system is nondegenerate in general, so the caveat of Sec. 8.2.2 does not apply and the averaging (7.5) is always valid.

In a thermal state, the population of the levels within one band would decrease with increasing energy. However, if the band width $\delta\varepsilon$ is sufficiently small compared to the band splitting δ_C, the variation of the population is small and can be neglected as a good approximation. In this case, the results from chapter 7 can be applied.

When introducing a level splitting small compared to the interaction strength, the peaks in Fig. 8.4 become broader; especially the peak at $\lambda_\varepsilon =$

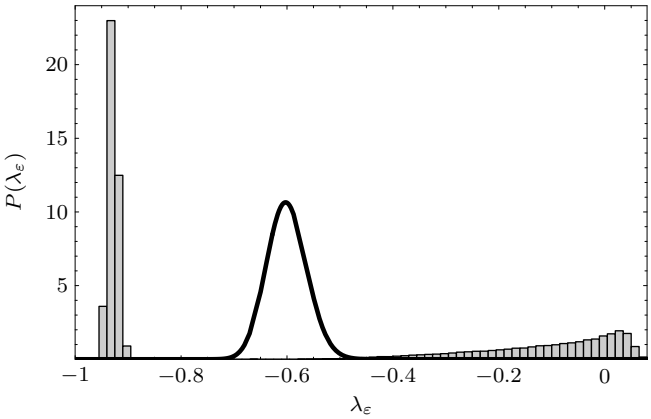

Figure 8.8: λ_ε distribution for random interaction and equidistant level spacing within each band, small compared to the interaction strength. $g = 91$ and $g' = 364$. The histogram was obtained from the eigenvectors of 400 different random Hamiltonians. The solid line shows the distribution for the completely random matrices.

0 becomes considerably flatter and is stretched towards negative λ_ε. The variance of the distribution becomes smaller. Figure 8.8 shows the λ_ε distribution compared with the distribution for random matrices from the GUE. The variance of this distribution is $\Delta\lambda_\varepsilon^2 \approx 0.19$, which is considerably less than $\Delta\lambda_\varepsilon^2 = 0.24$ for exactly degenerate bands. The notion of smaller and larger level splittings will be made more concrete later.

When the level splitting is increased, the two peaks in Fig. 8.8 "move" together to form a single peak close to the average value of $(g-g')/(g+g')$ for the distribution. This peak is of comparable height and width as the peak for the random matrices from the GUE; see Fig. 8.9. This leads to a further decrease in the width of the distribution. A long tail towards higher values of λ_ε prevails; therefore the variance is still considerably larger. For the distribution shown, $\Delta\lambda_\varepsilon^2 \approx 0.022$ (for matrices from the GUE with the same size, $\Delta\lambda_\varepsilon \approx 0.0014$). The level splitting in Fig. 8.9 is approximately 6.8 times wider than in Fig. 8.8.

Figure 8.10 shows the time evolution of a pure total state for the system from Fig. 8.9. Relaxation towards the canonical equilibrium can indeed be

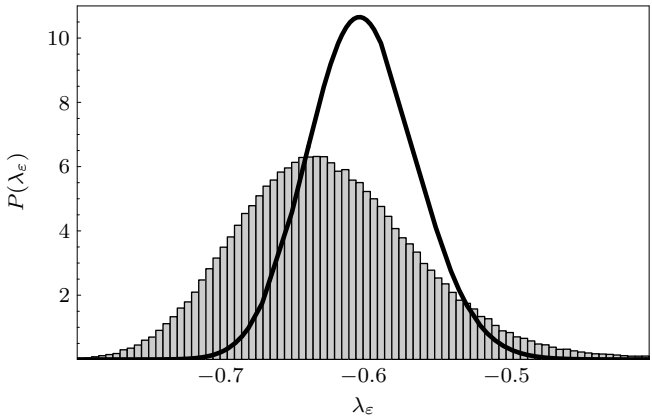

Figure 8.9: λ_ε distribution for random interaction and equidistant level spacing within each band, larger than in Fig. 8.8. $g = 91$ and $g' = 364$. The histogram was obtained from the eigenvectors of 400 different random Hamiltonians. The solid line shows the distribution for the completely random matrices.

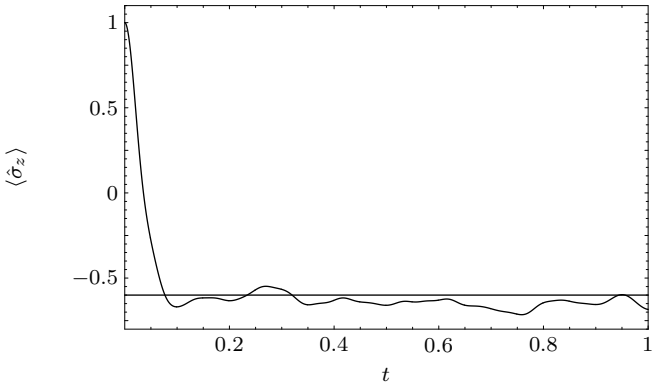

Figure 8.10: Inversion of the central spin with initial state $|1; k, a\rangle$ for random interaction and level splitting within the environment corresponding to Fig. 8.9 ($g = 91$ and $g' = 364$). The horizontal black line at $\langle\hat{\sigma}_z\rangle = -0.6$ represents the canonical equilibrium inversion.

observed. One has to be careful when calculating the time evolution for pure states for these systems, though. If the initial state of the environment is close to a border of a band, relaxation to the canonical state is suppressed, since not enough states in the other band are available due to energy conservation. This caveat applies, however, only to very few levels of the environment. With a thermal initial state, summing over all possible pure initial states, the system relaxes exactly as predicted in Chapter 7.

By introducing an additional structure in the environmental spectrum, the most general system with a random, energy exchanging interaction changes its behavior from nonthermal to thermal relaxation. This transition is continuous. If it is possible to design a system with a Hamiltonian similar to (8.6) or (8.10), one may imagine to control the relaxation or equilibrium behavior of the central spin by controlling some environmental Hamiltonian parameters.

8.3.1. Thermodynamic Limit

An analytical expression for the probability density for the system with random interaction and level spacing within the environment has not been found so far. Therefore, the thermodynamic limit is not readily available by a direct limit process. One can, however, calculate the λ_ε distributions for different system sizes numerically and hope to find a trend as the system size increases.

Figure 8.11 shows the variance of the lambda distributions for two different level splittings within the environment (left: smaller, right: larger). Since the strength of the interaction part of the Hamiltonian effectively increases with system size,[1] the bandwidths are increased accordingly to keep the relative strengths of both parts equal to get comparable results for different system sizes. The ratio g/g' is always kept constant with $g' = 4g$.

In the top row, $\Delta\lambda_\varepsilon^2$ is seen to decrease with system size. However, the curves do not seem to approach zero but some finite asymptotic value. For the bottom row, the guessed asymptotic values have been subtracted from the values of $\Delta\lambda_\varepsilon$ and the result was plotted with a logarithmic scale on the ordinate. Both curves show a somewhat linear decrease, at least for larger system sizes. This indicates that $\Delta\lambda_\varepsilon^2$ decreases with some inverse power of the system size, approaching a finite value as $g + g' \to \infty$. These

[1] The notion of the strength of different parts of the Hamiltonian will be defined in Chapter 10. A precise explanation of how the bandwidth has to be increased to maintain equal relative strength is given in Sec. 10.2.4.

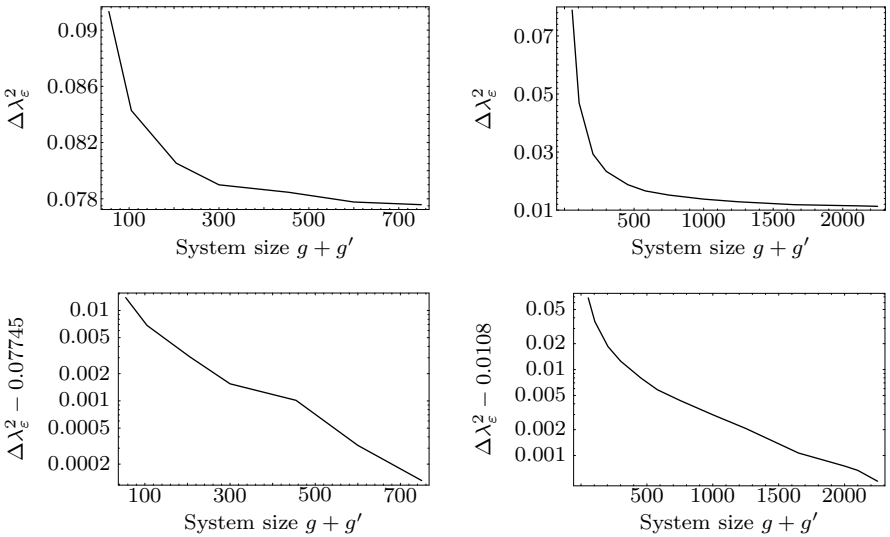

Figure 8.11: Variance of the λ_ε distribution for two different values of the environmental bandwidth; left: small bandwidth, right: large bandwidth. Top: linear plot, bottom: logarithmic plots with shifted values of $\Delta\lambda_\varepsilon^2$ (see text).

results are not exact, of course, and no precise statement for the thermodynamic limit can be made, but still there is a strong indication that some of the nonthermal behavior is retained even for very large systems. This is emphasized by the fact that the canonical average is surely never reached for exactly degenerate bands even in the thermodynamic limit.

8.4. Random Environmental Levels

If the energies $\epsilon_\ell^{(k)}$ from the matrix (2.11) are taken randomly instead of choosing an equidistant spacing as in the last section, the situation doesn't change qualitatively. In this case, the bandwidth can be increased simply by multiplying the diagonal of the Hamiltonian by a scaling factor (for vanishing detuning Δ). As in Sec. 8.3, the δ peaks in Fig. 8.4 are broadened and, when the bandwidths are increased sufficiently, merge to form a single peak close to the mean value $(g - g')/(g + g')$.

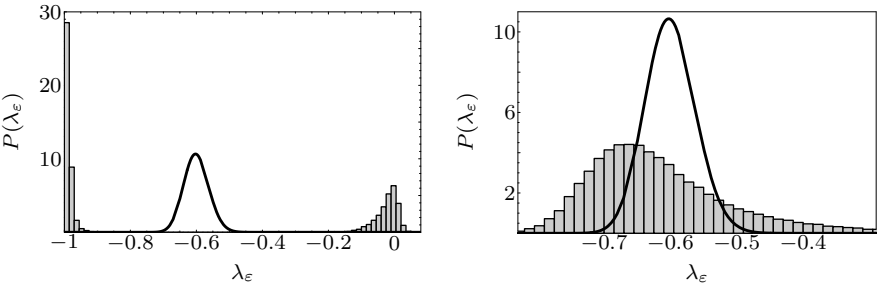

Figure 8.12: λ_ε distribution for random interaction and random diagonal part. $g = 91$ and $g' = 364$. Left: small bandwidth, right: larger bandwidth. The histograms were obtained from the eigenvectors of 100 different random Hamiltonians. The solid lines show the distribution for the completely random matrices.

Figure 8.12 shows the λ_ε distributions for small and large bandwidth (smaller and larger prefactor). The diagonal elements were chosen from a normalized Gaussian distribution. The prefactors for the diagonal part are 4 for small and 40 for big bandwidth. The variances of the distributions are $\Delta\lambda_\varepsilon^2 = 0.22$ and $\Delta\lambda_\varepsilon^2 = 0.027$ for smaller and larger bandwidth, respectively.

Note that this situation is different from choosing a completely random matrix from the GUE. If the diagonal blocks of a GUE matrix are diagonalized separately, the diagonal entries would be distributed as a semicircle rather than as a Gaussian (see Eq. (3.7)).

9. Energy Eigenvector Distributions of Spin Systems

In the previous chapter abstract models were discussed, looking at the (quasi)equilibrium state after relaxation from a nonequilibrium situation. Now, some more concrete systems will be considered, namely the spin systems already discussed in Chapter 4. These spin systems show some similarities with the systems discussed in Chapter 8, both in the structure of the Hamiltonian and in their local quasiequilibrium states.

9.1. Spin-Star Configuration

As before, central and environmental spins are taken to be in resonance. If there is no mutual interaction between the outer spins, the dynamics are determined by the interaction Hamiltonian

$$\hat{H}_{\mathrm{int}} = \sum_{\nu=1}^{N} \sum_{i,j=1}^{3} \gamma_{ij}^{\nu}\, \hat{\sigma}_i \otimes \hat{\sigma}_j^{\nu}. \tag{4.2}$$

The situation is schematically depicted in Fig. 4.2. The form of the Hamiltonian matrix in the subspace

$$\left\{ |0; k', b\rangle\,, |1; k, a\rangle \right\} \quad (1 \le a \le g, \quad 1 \le b \le g') \tag{2.10'}$$

is calculated in appendix F. This Hamiltonian is similar to the one with random interaction and some finite environmental bandwidth. In contrast to the situation discussed in Sections 8.3 and 8.4, the off-diagonal block V is only sparsely populated. In general, these systems have no symmetry and are nondegenerate, therefore the method from Chapter 7 can be applied directly. The probability distribution functions could not be calculated analytically. As before, the λ_ε distributions are obtained from diagonalizing a number of random representation of this class of systems.

Figure 9.1 shows the λ_ε distribution for the class. The probability density indeed shows some similarities to the distribution for the systems with

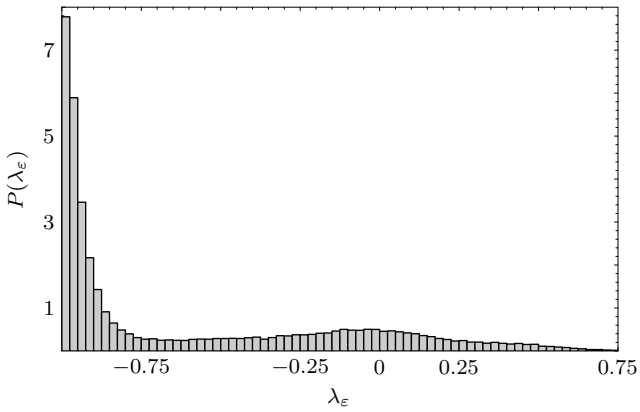

Figure 9.1: λ_ε distribution for the spin-star configuration ($N = 14$, $k = 2$, $g_2 = 91$, and $g_3 = 364$). The histogram was obtained from 100 different random realizations of the model.

completely random interaction and some finite environmental bandwidth: There is a large peak at $\lambda_\varepsilon = -1$ and a much smaller and broader peak at $\lambda_\varepsilon = 0$. This corresponds to the fact that the local canonical equilibrium state is typically not reached, as shown dynamically in Fig. 4.3. The variance of this distribution is $\Delta\lambda_\varepsilon^2 = 0.22$, which is not considerably smaller than the variance for vanishing diagonal elements.

For distributions of this type one can readily understand why initial states of the type $|1; k, a\rangle$ do not relax towards canonical equilibrium: All the energy eigenvectors forming the peak at $\lambda_\varepsilon \approx -1$ have the form

$$|\varepsilon\rangle \approx |0\rangle_{\mathrm{S}} \otimes |\chi\rangle_{\mathrm{C}} \,.$$

These states have only very little overlap with the initial state and thus do not contribute to the dynamics. The time averaged inversion for the initially pure total state $|\psi_0\rangle$ is

$$\langle \bar{\sigma}_z \rangle = \sum_\varepsilon |\psi_\varepsilon|^2 \lambda_\varepsilon$$

with $\psi_\varepsilon = \langle \varepsilon | \psi_0 \rangle$. Since the mean value of all λ_ε's is $\langle \hat{\sigma}_z \rangle_{\mathrm{can}} = (g - g')/(g + g')$ (see Appendix C), the average value of the contributing energy eigenstates must be larger than that. Therefore, also $\langle \bar{\sigma}_z \rangle$ must be larger

than $\langle\hat{\sigma}_z\rangle_{\mathrm{can}}$. This way, also the increased fluctuations can be understood: Fewer energy eigenstates and, therefore, a smaller number of different (incommensurate) frequencies take part in the dynamics, leading to larger average deviations from the mean value (see also Appendix H).

9.2. Ring-Star Configuration

Now next neighbor coupling between the environmental spins is added; the situation is schematically depicted in Fig. 4.4, the additional Hamiltonian is given by (4.4). Most types of spin-spin interactions within the environment lead to off-diagonal entries in the diagonal blocks of the Hamiltonian matrix (2.11). Since they are local to the environment they don't have matrix elements between different states of the central system, thus leaving the interaction block V invariant.

The diagonal blocks can be diagonalized separately,

$$\begin{pmatrix} U_1^\dagger & 0 \\ 0 & U_2^\dagger \end{pmatrix} \begin{pmatrix} D_1 & V^\dagger \\ V & D_2 \end{pmatrix} \begin{pmatrix} U_1 & 0 \\ 0 & U_2 \end{pmatrix} = \begin{pmatrix} U_1^\dagger D_1 U_2^\dagger & U_1^\dagger V^\dagger U_2 \\ U_2^\dagger V U_1 & U_2^\dagger D_2 U_2 \end{pmatrix} = \begin{pmatrix} D_1' & W^\dagger \\ W & D_2' \end{pmatrix},$$

with a new interaction block W, diagonal matrices D_j', and appropriate unitary matrices U_j. Apart from changing the interaction (but not changing its strength; see Chapter 10), this usually leads to an increased bandwidth and to a situation similar to the one discussed in Sections 8.3 and 8.4.

The λ_ε distribution for this class of systems is indeed similar to those for random interaction and finite bandwidth, as seen in Fig. 9.2. The two "peaks" have merged to one close to $\langle\hat{\sigma}_z\rangle_{\mathrm{can}}$. The variance is $\Delta\lambda_\varepsilon^2 \approx 0.0295$, considerably smaller than for the spin-ring configuration. As before, a long tail towards larger values of λ_ε prevails. Also similar to the abstract models, there is a continuous transition from a considerably nonthermal situation to one that is almost thermal. This transition was already observed by examining the relaxation dynamics in Sec. 4.3. Figure 9.3 visualizes this transition for the λ_ε distributions from the front (no intra-environmental interaction) to the back (relatively strong intra-environmental interaction).

These results were obtained for the XY next-neighbor coupling within the environment already discussed in Sec. 4.3, but the distributions for many different types of coupling are similar.

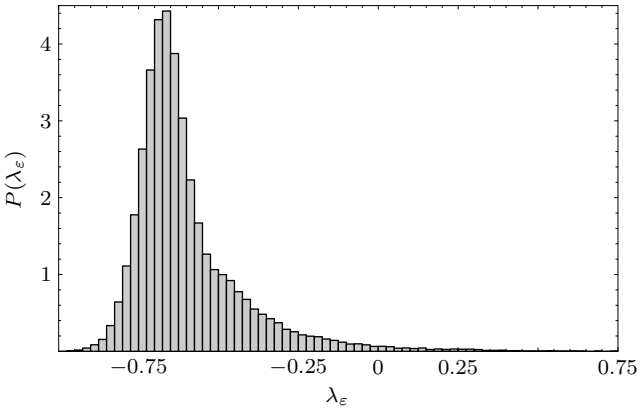

Figure 9.2: λ_ε distribution for the ring-star configuration ($N = 14$, $k = 2$, $g_2 = 91$, and $g_3 = 364$). The histogram was obtained from 100 different random realizations of the model.

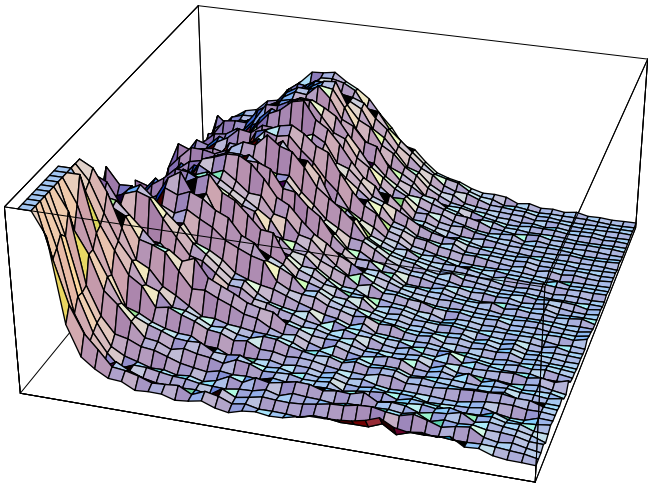

Figure 9.3: Visualization of the transition from a strongly nonthermal situation for the spin-star configuration (front) to a approximately thermal situation for a ring-star with relatively strong next neighbor coupling (back, $J = 3/2$). At the left $\lambda_\varepsilon = -1$; at the right $\lambda_\varepsilon = 0.4$.

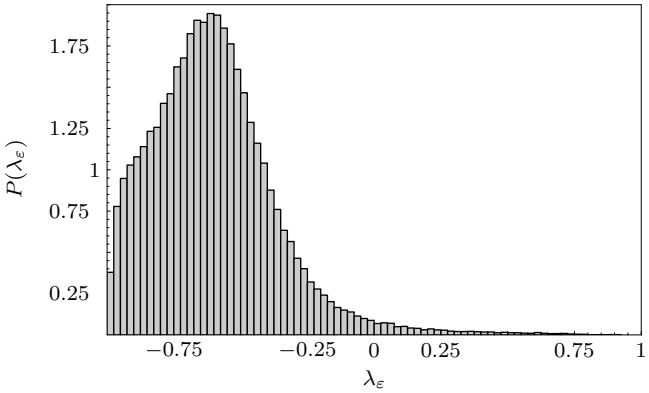

Figure 9.4: λ_ε distribution for the spin-star configuration with inhomogeneous Zeeman splittings of the environmental spins ($N = 14$, $k = 2$, $g_2 = 91$, and $g_3 = 364$). See the text for the spreading of the Zeeman splittings. The histogram was obtained from 100 different random realizations of the model.

9.3. Inhomogeneous Zeeman Splitting

Instead of adding interaction within the environment, the bandwidth can also be increased by introducing a different Zeeman splitting for each environmental spin. Again, the situation becomes similar to the ones discussed in Sections 8.3 and 8.4. The distribution in Fig. 9.4 shows a peak around the mean value $\bar{\lambda}_\varepsilon$, although broader than in the previous cases. Here, the Zeeman splittings were homogeneously distributed within a certain range. The smallest splitting was 0.3 % smaller than resonance, the largest 0.3 % larger. A continuous transition from Fig. 9.1 to Fig. 9.4 can be observed by increasing this range from zero.

9.4. Heisenberg Spin Chain

In Sec. 4.4 it was shown that the first spin of a Heisenberg spin chain relaxes canonically from a pure total product state. Therefore, the corresponding λ_ε distribution can be expected to have a similar structure as the ones for inhomogeneous Zeeman splitting or stronger intra-environmental

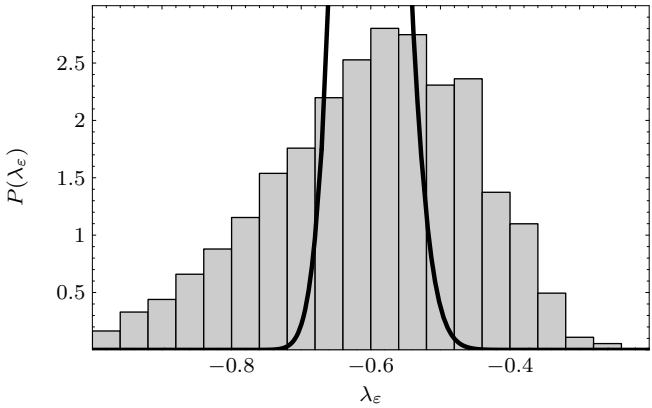

Figure 9.5: λ_ε distribution for the first spin of the Heisenberg spin chain ($N = 14$, $k = 2$, $g_2 = 91$, and $g_3 = 364$). The solid line shows the distribution for the completely random matrices.

interaction. It should be singly peaked around $\langle\hat{\sigma}_z\rangle_{\text{can}} = -0.6$. Actually, the Heisenberg spin chain, where all spins are coupled equally to their next neighbors, has strong intra-environmental coupling. The main difference to the ring-star configuration is the absence of interactions between the "central" spin and most of the environmental spins.

The λ_ε distribution indeed has the expected structure, as shown by Fig. 9.5. The distribution is in fact even narrower than the one discussed in Sections 9.2 and 9.3. Its variance is $\Delta\lambda_\varepsilon^2 \approx 0.0204$ which is still far away from the distribution for the completely random matrices from the GUE, as is also evident from Fig. 9.5.

Part III.

Model Classification

10. Spectral Width

In the previous chapters it was shown that for many systems there is a continuous transition from a situation far from canonical to an almost canonical relaxation, depending on the environmental spectrum. In all models, the local quasiequilibrium state approaches the canonical state when the width of the environmental bands is increased. In this chapter this width will be related to the variance of the λ_ε distributions for the various models. Also, the notion of the *strength of an Hamiltonian*, used at several point throughout the text, will be defined.

In Sec. 10.1 the quantity to compare different Hamiltonian models will be introduced. In Sections 10.2 and 10.3 this quantity will be calculated for the models discussed in Chapters 8 and 9. Finally, in Sec. 10.4, the quantity will be brought into relation with the widths of the λ_ε distributions.

10.1. Relative Spectral Width

In order to relate different types of spectra or different types of models, the Hamiltonian matrix (in the considered subspace) is split into its respective diagonal and off-diagonal parts. The off-diagonal part $\hat{H}_{\text{off}}$—V and $V^\dagger$ of (2.11)—describes the interaction between the central system and its environment, while the diagonal part $\hat{H}_{\text{diag}}$ describes the environmental spectrum alone, if system and environment are in resonance. This diagonal part may also comprise some parts of the interaction Hamiltonian between system and environment. The diagonal part is usually taken to be traceless (exceptions to traceless diagonal parts will be explained below; the off-diagonal part is traceless by construction).

The quantity that will be used to compare different spectra will be the ratio of the quadratic mean value of the eigenvalues of these two parts,

$$R_{\text{s}} = \sqrt{\frac{\text{Tr}(\hat{H}^2_{\text{diag}})}{\text{Tr}(\hat{H}^2_{\text{off}})}}. \tag{10.1}$$

This quantity will be called the relative strength or relative spectral width of both parts.

The quadratic mean value of the eigenvalues $\{m_k\}$ of an operator $\hat{M}$ acting on a Hilbert space of dimension d,

$$W_\mathrm{s} = \sqrt{\frac{1}{d}\sum_k m_k^2} = \sqrt{\frac{1}{d}\,\mathrm{Tr}(\hat{M}^2)},$$

is a measure of the width of the spectrum of this matrix. If the matrix is traceless, the sum of all eigenvalues vanishes and $\sqrt{\mathrm{Tr}(\hat{M}^2)/d}$ is the standard deviation of the spectrum (*i.e.*, its "width"). The width of the spectrum of a Hamiltonian acting on a system can be regarded as the "strength" of this Hamiltonian, when comparing different Hamiltonians. In this sense R_s measures the relative strength of the two parts of this system.

To compare different classes of systems, the distributions and ensemble averages of W_s and R_s for each class can be compared. If the diagonal and off-diagonal parts of the Hamiltonians of one class are statistically independent, the ensemble average of R_s is readily available from the ensemble averages of W_s,

$$\bar{R}_\mathrm{s} = \sqrt{\frac{E(\mathrm{Tr}\,\hat{H}_\mathrm{diag}^2)}{E(\mathrm{Tr}\,\hat{H}_\mathrm{off}^2)}}.$$

10.2. Spectral Widths of Different Systems

For some parts ($\hat{H}_\mathrm{diag}$, $\hat{H}_\mathrm{off}$) of the model system classes discussed in Chapters 8 and 9, the probability densities of the spectral width can be calculated explicitely. For simplicity, the factor $1/\sqrt{d}$ will be omitted as this factor cancels when calculating the relative strength. Only the probability distributions of the squares of the spectral width will be presented,

$$W_2 := W_\mathrm{s}^2 d = \mathrm{Tr}(\hat{M}^2).$$

The probability distribution of W_s follows from a simple transformation of the variable.

10.2.1. Random Interaction

At first, the average spectral width for the Hamiltonian (8.6) with $\Delta = 0$ will be calculated—*i.e.*, for the interaction part of the abstract random models. Since V has $2gg'$ entries (real and imaginary parts of gg' matrix elements), the spectral width is a sum of the squares of $4gg'$ random variables. However, only $2gg'$ of those are independent. If the independent variables are denoted by $\{x_1, \ldots, x_{2gg'}\}$, we get

$$W_2 = 2\tilde{W} = 2\sum_{k=1}^{2gg'} x_k^2.$$

Since the x_n's are determined by a normalized Gaussian distribution, $\tilde{W}$ is distributed as χ^2 with $2gg'$ degrees of freedom (see Appendix I). The probability density for W_2 for the random off-diagonal (ro) blocks is then given by

$$P_{\mathrm{ro}}(W_2) = \frac{1}{2^{2gg'}\Gamma(gg')} W_2^{gg'-1} \mathrm{e}^{-W_2/4}.$$

Its expectation value grows quadratically with the size of the system,

$$\boxed{E_{\mathrm{ro}}(W_2) = 4gg'.} \tag{10.2}$$

10.2.2. Diagonal Blocks of the GUE Matrices

The completely random matrices can be separated into two diagonal and two off-diagonal blocks. Both diagonal blocks (GUE,d) are again random Hermitian matrices distributed as the GUE, the upper left block is a $g' \times g'$ random matrix, the lower right block is a $g \times g$ random matrix.

Although the expectation value of the trace of these matrices vanishes (being a sum over $(0, \sqrt{2})$-Gaussian distributed random variables), the trace of every single one does not vanish (apart from a set of matrices with vanishing measure). In order to meet the criteria of being traceless, a multiple of the identity matrix has to be subtracted,

$$\hat{H}' = \hat{H} - \frac{\mathrm{Tr}\,\hat{H}}{d}\hat{1},$$

with the dimension d of Hilbert space. However, the standard deviation of $\mathrm{Tr}\,\hat{H}$ grows only with $\sqrt{d}$, so the additional term decreases on average with increasing system size, it will therefore be neglected.

The real and imaginary parts of the matrix elements are Gaussian distributed, on the diagonal with the standard deviation $\sqrt{2}$, all other elements with standard deviation 1. There are $d = g+g'$ diagonal elements (denoted by x_k) and $n_\mathrm{o} = 2(g^2+g'^2-(g+g'))$ off-diagonal elements (denoted by y_k), only one half of the latter are independent. The spectral width is the sum over the squares of all these elements,

$$W_2 = \sum_{k=1}^{d} x_k^2 + 2\sum_{k=1}^{n_\mathrm{o}/2} y_k^2 = \sum_{k=1}^{d} x_k^2 + \sum_{k=1}^{n_\mathrm{o}/2} (\sqrt{2}y_k)^2.$$

In the second sum, $\sqrt{2}y_k$ are $(0,\sqrt{2})$-Gaussian distributed random variables, so W_2 is a sum of $d + n_\mathrm{o}/2 = g^2 + g'^2$ random variables with standard deviation $\sqrt{2}$. Its probability density reads (see Appendix I)

$$P_{\mathrm{GUE,d}}(W_2) = \frac{1}{2^n \Gamma(n/2)} W_2^{n/2-1} \mathrm{e}^{W_2/4}, \quad n = g^2 + g'^2$$

with an expectation value of

$$\boxed{E_{\mathrm{GUE,d}}(W_2) = 2(g^2 + g'^2).} \tag{10.3}$$

Just like (10.2), this expectation value grows quadratically with the system size. In both cases, the standard deviation (which is only of little importance here) grows only linearly with the system size.

10.2.3. Random Diagonal

If the diagonal of the Hamiltonian is populated simply by random numbers with a normalized Gaussian distribution as in Sec. 8.4 (random diagonal, rd), W_2 is given by the sum of the squares of $g + g'$ random numbers and is therefore distributed as χ^2 with $g + g'$ degrees of freedom (again, the Hamiltonian is not made traceless explicitely). The expectation value is

$$\boxed{E_{\mathrm{rd}}(W_2) = g + g',} \tag{10.4}$$

scaling linearly with the system size.

10.2.4. Equidistant Environmental Spectrum

Since the diagonal elements of the Hamiltonian (8.10) are fixed rather than random numbers, the respective spectral width can be calculated exactly instead of giving an ensemble average. In contrast to the random diagonal blocks discussed in the previous section, here it is important to make the Hamiltonian traceless, since the trace of (8.10) grows linearly with the system size.

The spectral width of the Hamiltonian

$$\hat{H} = \hat{H}_\mathrm{t} - \frac{\mathrm{Tr}\,\hat{H}_\mathrm{t}}{d}\hat{1},$$
$$\hat{H}_\mathrm{t} = \mathrm{diag}\left(0, \frac{\delta\varepsilon}{(g'-1)}, \ldots, \delta\varepsilon, 0, \frac{\delta\varepsilon}{(g-1)}, \ldots, \delta\varepsilon\right)$$

is given by

$$\boxed{W_2 = \left(\frac{g(2g-1)}{6(g-1)} + \frac{g'(2g'-1)}{6(g'-1)} - \frac{g+g'}{4}\right)\delta\varepsilon^2.} \tag{10.5}$$

This result is not particularly intuitive. However, for large g and g', W_2 grows linearly with the system size,

$$\boxed{W_2 \xrightarrow[g,g'\gg 1]{} \frac{g+g'}{12}\,\delta\varepsilon^2} \tag{10.6}$$

(for the "intermediate" values of g and g' used for the examples throughout this text, the approximation $(g+g')/12 + 1/3$ fits slightly better).

This linear scaling is the reason for increasing the bandwidth in Sec. 8.3.1 with increasing system size. Since the spectral width (or strength) of the off-diagonal part grows quadratically with the system size, the diagonal part becomes weaker in relation as the system grows. In the limit of the system size going to infinity, the behavior of these systems (random interaction, equidistant environmental level spacing) would approach the behavior of exactly degenerate environmental bands, should the bandwidth be kept constant. To maintain equal relative strength, the bandwidth has to be increased with the size of the system.

10.2.5. Diagonal Part of the Spin-Star Configuration

As shown in Appendix F, the diagonal elements of the spin-star Hamiltonian (ssd) for N environmental spins are linear combinations of all N pa-

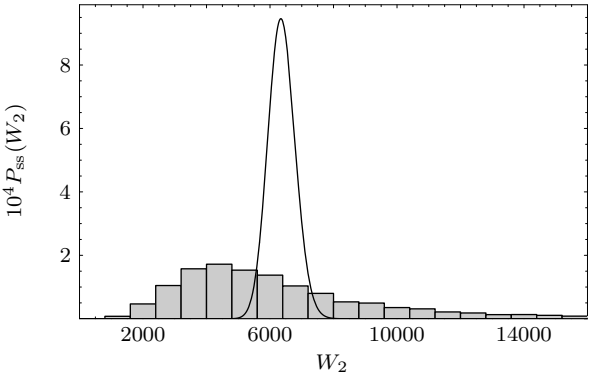

Figure 10.1: W_2 distribution of the diagonal part of the spin-star configuration (histogram). The histogram was obtained from 5000 random realizations of the model. The solid line shows the χ^2 distribution for $g + g'$ degrees of freedom with a standard deviation of $\sqrt{N}$.

rameters γ_{33}^{ν} with coefficients $+1$ and -1. Therefore, each diagonal element is normally distributed with the standard deviation $\sqrt{N}$. The expectation value of the square of each diagonal element therefore is N; see Appendix I and Eq. (I.1) for $n = 1$. The expectation value for the sum of the squares of all $g + g'$ diagonal elements then amounts to

$$\boxed{E_{\rm ssd}(W_2) = N(g + g') = N\binom{N+1}{k+1}} \tag{10.7}$$

which grows as a power of N for fixed k.

The complete probability density is not as readily available as in the previous sections. The trace is not a sum of $g + g'$ independent random variables, since each of these variables is a linear combinations of the same N random variables. Therefore, the probability distribution for W_2 is not simply given by a χ^2 distribution with $g + g'$ degrees of freedom. Figure 10.1 compares the actual distribution for W_2 with the corresponding χ^2 distribution.

So far, the trace of $\hat{H}_{\rm int,d}$ (the diagonal part of the spin-star interaction) was neglected. As for the random models before, the expectation value of

this trace vanishes. The standard deviation, however, is given by

$$\sigma(\mathrm{Tr}\,\hat{H}_{\mathrm{int,d}}) = \sqrt{N} f_{N,k}$$

according to Eq. (F.2). This standard deviation grows strongly with N. In particular, the standard deviation of the factor $\mathrm{Tr}(\hat{H}_{\mathrm{int,d}})/d$ grows as $\sqrt{N}$ for large N ($\mathrm{Tr}(\hat{H}_{\mathrm{int,d}})/d$ is normally distributed with a standard deviation of $\sqrt{N}$ for N large). There are many spin-star interaction Hamiltonians with a large trace which cannot be neglected when calculating the respective spectral width. If the Hamiltonian is rewritten as

$$\hat{H}' = \hat{H}_{\mathrm{int,d}} - \frac{\mathrm{Tr}\,\hat{H}_{\mathrm{int,d}}}{d}\hat{1},$$

with $d = g + g'$, the spectral width becomes

$$\mathrm{Tr}(\hat{H}'^2) = \mathrm{Tr}(\hat{H}^2_{\mathrm{int,d}}) - \frac{1}{d}(\mathrm{Tr}\,\hat{H}_{\mathrm{int,d}})^2.$$

For large N, the expectation value of the second part approaches $N(g + g')$ for constant band index k. But this is just the expectation value of $\mathrm{Tr}(\hat{H}^2_{\mathrm{int,d}})$; see Eq. (10.7). So, in the limit of large system size, the spectral width vanishes on average,

$$\boxed{E_{\mathrm{ssd}}(W_2) \xrightarrow[N\to\infty]{} 0.} \tag{10.8}$$

Since W_2 is positive for each Hamiltonian, every W_2 has to vanish individually.

However, the approximation $\mathrm{Tr}(\hat{H}_{\mathrm{int,d}})/d \approx \sqrt{N}$ is valid only for values of N considerably larger than are available for numerical analysis, as $\mathrm{Tr}(\hat{H}_{\mathrm{int,d}})/d - \sqrt{N}$ converges only very slowly towards zero, namely as $12/\sqrt{N}$. For the system sizes used in the examples throughout this text ($N = 14$), $(\mathrm{Tr}\,\hat{H}_{\mathrm{int,d}})^2/d$ is considerably smaller than $\mathrm{Tr}(\hat{H}^2_{\mathrm{int,d}})$. Nevertheless, it cannot be neglected in general.

10.2.6. Interaction Part of the Spin-Star Configuration

As shown in Appendix F, there are $2N\binom{N-1}{k}$ complex off-diagonal elements in the spin-star Hamiltonian (sso) for N particles, N of which are different. The spectral width therefore consists of a sum of the squares

of $4N\binom{N-1}{k}$ random variables distributed as a Gaussian with standard deviation $\sqrt{2}$, $2N$ of which are different. As in Sec. 10.2.1 and 10.2.2, the independent variables will be denoted by x_ℓ and the spectral width becomes

$$W_2 = 2\binom{N-1}{k}\sum_{\ell=1}^{2N} x_\ell^2 = \sum_{\ell=1}^{2N}\left(\sqrt{2\binom{N-1}{k}}\,x_\ell\right)^2 .$$

This is the sum of the squares of normally distributed variables with standard deviation $2\sqrt{\binom{N-1}{k}}$. Therefore, W_2 is distributed according to a properly scaled χ^2 distribution. Its expectation value is

$$\boxed{E_{\mathrm{sso}}(W_2) = 8N\binom{N-1}{k}} \tag{10.9}$$

growing as a power of N for fixed k.

10.2.7. Spin-Ring Interaction

As discussed in Appendix G, the spin-ring interaction $\hat{H}_{\mathrm{CC}}$ within the environments used in Sections 4.3 and 9.2 has no matrix elements in the off-diagonal blocks, so it only changes the environmental spectrum, not the spin-environment interaction (this is expected, of course). The number of matrix elements in the diagonal blocks is given by Eq. (G.1), all matrix elements are equal to J. $\hat{H}_{\mathrm{CC}}$ is obviously traceless, so no adjustments have to be made.

Each entry of $\hat{H}_{\mathrm{CC}}$ contributes J^2 to the squared spectral width, so

$$\boxed{W_2 = 2J^2N\binom{N-1}{k},} \tag{10.10}$$

growing with the same power of N as (10.9).

10.3. Relative Spectral Widths

After having calculated the spectral widths of different model systems, the ensemble averages of the relative spectral widths of several system classes considered in Chapters 8 and 9 will now be presented briefly.

Gaussian Unitary Ensemble
From Eqs. (10.2) and (10.3) follows the ensemble average of R_s for the GUE,

$$\bar{R}_{\mathrm{s,GUE}} = \sqrt{\frac{g^2 + g'^2}{2gg'}}, \tag{10.11}$$

which does not depend on the absolute system size $d = g + g'$.

Random Interaction, Equidistant Bands
From Eqs. (10.2) and (10.6) the ensemble average for sufficient system size reads

$$\bar{R}_\mathrm{s} = \sqrt{\frac{g + g'}{48gg'}}\,\delta\varepsilon. \tag{10.12}$$

For constant bandwidth $\delta\varepsilon$ this decreases with increasing system size.

Ring-Star Interaction
If the system is large enough, the strength of the diagonal part of the spin-star Hamiltonian vanishes. In this case the ensemble average of the ring-star class is given by Eqs. (10.9) and (10.10),

$$\bar{R}_\mathrm{s} = J/2, \tag{10.13}$$

which neither depends on the system size nor on the ratio g/g'.

10.4. Spectral Width and Eigenvector Distributions

The relative spectral width will now be brought into relation with the variance of the λ_ε distributions of these models. In Chapters 8 and 9 it was shown that by introducing some complexity for the environmental spectrum, a continuous transition from a noncanonical to an almost canonical situation could be observed. In all cases, the spectral width of the diagonal blocks of the Hamiltonian was increased from zero (for the abstract models) or from a relatively small value (for the spin systems) to some larger value in order to see the transition. Particularly, the relative spectral width R_s was increased (an overall factor only scales the unit of time).

One may wonder how the "optimal" values (with respect to canonical relaxation) of R_s for different systems are related and how these values are

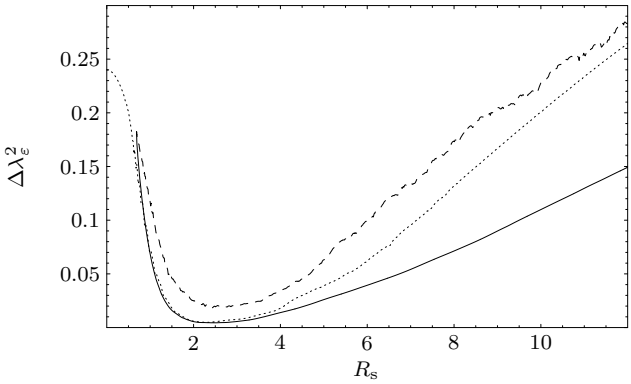

Figure 10.2: Variance of the λ_ε distribution over the relative strength of the diagonal and off-diagonal blocks of the Hamiltonian. Solid line: ring-star with random S-C coupling; dashed line: spin-star, inhomogeneous Zeeman splitting, random S-C coupling; dotted line: spin-star, inhomogeneous Zeeman splitting, XY coupling between S and each spin in C.

related to the average relative spectral width of the GUE matrices (10.11), which only depends on g/g'. For the following examples the degeneracies used were again $g = 91$ and $g' = 364$, so

$$\bar{R}_{\mathrm{s,GUE}} \approx 1.46.$$

The solid line in Fig. 10.2 shows the variation of $\Delta\lambda_\varepsilon^2$ with R_s for one random realization of the spin-star interaction (4.2). The environmental spins form a ring as discussed in Sections 4.3 and 9.2. The intra-environmental coupling strength J is increased from zero. The curve doesn't start at $R_\mathrm{s} = 0$ for $J = 0$, since the diagonal blocks of the spin-star interaction Hamiltonian itself have a finite spectral width; see Sec. 10.2.5. As J is increased, R_s increases and $\Delta\lambda_\varepsilon^2$ decreases, as previously observed. The curve has a minimum at $R_\mathrm{s} \approx 2.5$ with $\Delta\lambda_\varepsilon \approx 4.43 \times 10^{-3}$.

The two other curves in Fig. 10.2 (for a random spin-star and for an XY spin-star, both with an inhomogeneous Zeeman splitting within the environment; see Sec. 9.3) show a similar behavior: both curves have a minimum around $R_\mathrm{s} = 2$. The precise value of $\Delta\lambda_\varepsilon^2$, however, differs for these systems.

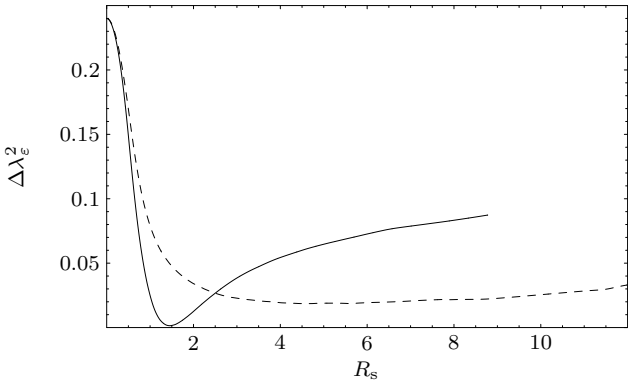

Figure 10.3: Variance of the λ_ε distribution over the relative strength of the diagonal and off-diagonal blocks of the Hamiltonian. Solid line: One random realization of the GUE with scaled diagonal blocks (see text); dashed line: random interaction with equidistant level spacing.

The precise values for the minima are

$$\begin{aligned} &\text{random spin star:} \quad R_{\mathrm{s,min}} \approx 2.43, \quad \Delta\lambda^2_{\varepsilon,\mathrm{min}} \approx 1.84 \times 10^{-2}, \\ &XY \text{ spin star:} \qquad R_{\mathrm{s,min}} \approx 2.34, \quad \Delta\lambda^2_{\varepsilon,\mathrm{min}} \approx 4.88 \times 10^{-3}. \end{aligned}$$

For both the solid and the dashed curve the same spin-star interaction Hamiltonian was used. The dotted curve starts at $R_\mathrm{s} = 0$: If the central spin is coupled to all environmental spins via an Heisenberg XY interaction, the diagonal blocks vanish.

Similar results hold for other types of systems. The dashed curve in Fig. 10.3 shows $\Delta\lambda_\varepsilon^2$ for the systems discussed in Sec. 8.3, random interaction with equidistant level spacing. This level spacing was increased from zero to some finite value. In contrast to the spin systems, the minimum here is considerably broader (the curve increases again to the right of the diagram) with $R_{\mathrm{s,min}} \approx 4.56$. The solid curve was obtained from one matrix taken randomly from the Gaussian unitary ensemble, a scaling factor was applied to the diagonal blocks. The sharp minimum is located at the point of no scaling with $R_\mathrm{s} \approx 1.44$ (close to the ensemble average).

For the three spin system examples, the optimal value of R_s with respect to canonical relaxation is similar for all considered spin systems. This is not

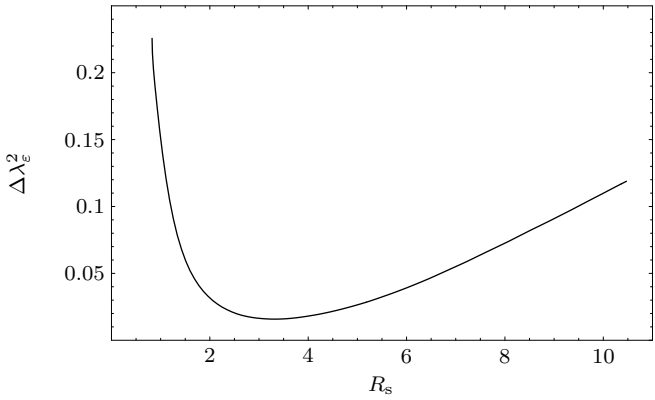

Figure 10.4: Variance of the λ_ε distribution over the relative strength of the diagonal and off-diagonal blocks of the Hamiltonian. Averaged over 50 different random realization of the ring-star model, corresponding to the solid line in Fig. 10.2.

true, however, for all systems. The precise value of R_s for the minimal value of $\Delta\lambda_\varepsilon^2$ typically varies from system to system. Nevertheless, all minimal values are close to the ensemble average of the relative spectral width of the GUE matrices. So, R_s can give, at least, an estimate, whether canonical relaxation can be expected at all. This can be useful, since R_s typically is easier to calculate than $\Delta\lambda_\varepsilon^2$. To calculate $\Delta\lambda_\varepsilon^2$, the Hamiltonian has to be diagonalized partially, while R_s usually is readily available. Even its probability distribution for whole ensembles of systems can often be calculated, as shown in Sec. 10.2.

For completeness, Fig. 10.4 shows the mean $\Delta\lambda_\varepsilon^2$ for several different random realizations of the spin-ring class. As expected, the form of the curve is similar to the solid line in Fig. 10.2. The minimum is at $R_\mathrm{s} \approx 3.34$ with $\Delta\lambda_\varepsilon^2 \approx 1.58 \times 10^{-2}$.

10.5. Discussion

The ensemble average of the relative spectral width of the GUE matrices (10.11) does not depend on the absolute system size $d = g + g'$. For all considered models, the optimal value with respect to canonical relaxation

was close to or at least of the order of magnitude of $\bar{R}_{\mathrm{s,GUE}}$. One can expect that this is the case for all types and sizes of systems. By calculating the relative spectral width it should therefore be possible to get some estimate of the equilibrium state of any system.

For some of the discussed systems, the spectral widths of the diagonal and the off-diagonal blocks scale differently with system size. In particular, for the spin-star Hamiltonian the expectation value of the diagonal part vanishes for large systems, while the expectation value of the off-diagonal part grows with system size. So, as N grows one can expect the deviations from canonical behavior to increase! In contrast, the spectral width of the XY next-neighbor interaction grows with the same power as the off-diagonal part of the spin-star Hamiltonian; so the same value of J should provide canonical behavior for a many (all?) system sizes.

Even though no distinct relation between the relative spectral width and the width of the λ_ε distributions seems to exist, R_{s} can still be used to give an estimate for the behavior of large systems not accessible by numerical methods.

11. Towards Higher Dimensional Central Systems

One can try to generalize the method presented in Chapter 7 to central systems of higher dimension. An arbitrary state of a n dimensional system with diagonal state operator is described by $n-1$ independent parameters rather than only one parameter for a TLS. The deviation from canonical equilibrium will then likely be described by more than one parameter.

The energy eigenstates of central system will be denoted by

$$\{|0\rangle\langle 0|, |1\rangle\langle 1|, \ldots, |n-1\rangle\langle n-1|\},$$

from low to high energy.

11.1. Basis in Liouville Space

The general state operator of an n level system is described by n^2-1 independent real parameters [6]. A basis in Liouville space for all possible state operators should therefore consist of $s = n^2 - 1$ linearly independent operators $\hat{\omega}_k$ (in addition, the identity operator is needed to get proper normalization). It is convenient to require that these basis operators fulfill an orthogonality relation,

$$\mathrm{Tr}(\hat{\omega}_j \hat{\omega}_k) = 2\delta_{jk}.$$

There are, of course, infinitely many possible orthogonal bases in Liouville space. Since the state operator is Hermitian, it is useful to choose $\hat{\omega}_k$ to be Hermitian, too. Often the generating operators of the $SU(n)$ Lie algebra are used, fulfilling the commutator relations

$$[\hat{\omega}_i, \hat{\omega}_j] = 2\mathrm{i} \sum_{k=1}^{s} f_{ijk} \hat{\omega}_k,$$

with structure constants f_{ijk}. The Pauli operators introduced in Sec. 2.1 are generators of $SU(2)$.

Since only diagonal states will be discussed in the following, only those $SU(n)$ generators involving diagonal elements will be needed. These are

$$\hat{w}_\ell = -\sqrt{\frac{2}{\ell(\ell+1)}}\left(|0\rangle\langle 0| + \cdots + |\ell\rangle\langle\ell| - \ell\,|\ell+1\rangle\langle\ell+1|\right), \tag{11.1}$$

where $1 \leq \ell \leq n-1$. The Pauli operator $\hat{\sigma}_z$ is the only operator of this type for $n = 2$.

11.2. Thermal Equilibrium of Three-Level Systems

Now a system with $n = 3$ levels will be considered. The generalization of the discussion in Sec. 2.2 leads to the canonical equilibrium state

$$\hat{\rho}_{\text{can}} = \frac{1}{g_0 + g_1 + g_2}\left(g_2\,|0\rangle\langle 0| + g_1\,|1\rangle\langle 1| + g_0\,|2\rangle\langle 2|\right)$$

if the system is coupled to an environment of three bands with respective degeneracies g_0, g_1, and g_3 and a total energy of $E = 2\delta$ (δ being the energy splitting of both system and environment). If the environment initially is in a thermal state with inverse temperature β and the central system initially is in the state $|m\rangle\langle m|$ ($m = 0, 1, 2$), this leads to a thermal equilibrium state of

$$\hat{\rho}_{\text{eq}} = \frac{1}{Z}\sum_k g_k \mathrm{e}^{-\beta E_k}\left(a_k^m\,|0\rangle\langle 0| + b_k^m\,|1\rangle\langle 1| + c_k^m\,|2\rangle\langle 2|\right)$$

with

$$a_k^m = \frac{g_{k+m}}{\sum_{\ell=k-2}^{k} g_{\ell+m}},\quad b_k^m = \frac{g_{k-1+m}}{\sum_{\ell=k-2}^{k} g_{\ell+m}},\quad c_k^m = \frac{g_{k-2+m}}{\sum_{\ell=k-2}^{k} g_{\ell+m}}.$$

11.3. General Equilibrium of Three-Level Systems

As a generalization of Eq. (7.4), the energy eigenstates of the total system with total excitation k can be written in the form

$$|\varepsilon_k\rangle \approx \alpha_\varepsilon^k\,|0, \chi_\varepsilon^k\rangle + \beta_\varepsilon^k\,|1, \eta_\varepsilon^k\rangle + \gamma_\varepsilon^k\,|2, \zeta_\varepsilon^k\rangle\,. \tag{11.2}$$

For simplicity, only the initial state $|2\rangle$ of the central system is considerd in the following, band and excitation indices will be dropped. Again, operators $\hat{\kappa} = |2\rangle\langle 2| \otimes \frac{\hat{1}}{g}$ can be introduced, expanded by the energy eigenstates, and averaged over time. Tracing out the environmental degrees of freedom finally yields

$$\hat{\kappa}_{\mathrm{eq}} = \sum_{\varepsilon} \kappa_{\varepsilon\varepsilon} \Big(|\alpha_\varepsilon|^2 \, |0\rangle\langle 0| + |\beta_\varepsilon|^2 \, |1\rangle\langle 1| + |\gamma_\varepsilon|^2 \, |2\rangle\langle 2| \Big), \tag{11.3}$$

where

$$\kappa_{\varepsilon\varepsilon} = |\gamma_\varepsilon|^2 / g.$$

Now the operators

$$\begin{aligned} \hat{w}_1 &= -\,|0\rangle\langle 0| + |1\rangle\langle 1|\,, \\ \hat{w}_2 &= \big(-\,|0\rangle\langle 0| - |1\rangle\langle 1| + 2\,|2\rangle\langle 2|\big)/\sqrt{3} \end{aligned}$$

are used to characterize this state. Using generalized eigenvector inversions,

$$\begin{aligned} \lambda_{\varepsilon,1} &= \mathrm{Tr}(\hat{w}_1 \, |\varepsilon\rangle\langle\varepsilon|) = |\beta_\varepsilon|^2 - |\alpha_\varepsilon|^2, \\ \lambda_{\varepsilon,2} &= \mathrm{Tr}(\hat{w}_2 \, |\varepsilon\rangle\langle\varepsilon|) = \big(2|\gamma_\varepsilon|^2 - |\beta_\varepsilon|^2 - |\alpha_\varepsilon|^2\big)/\sqrt{3}, \end{aligned}$$

the generalized inversions of state (11.3) are given by

$$\begin{aligned} \langle \hat{w}_1 \rangle &= \frac{1}{3g} \sum_{\varepsilon} \big(1 + \sqrt{3}\lambda_{\varepsilon,2}\big)\lambda_{\varepsilon,1}, \\ \langle \hat{w}_2 \rangle &= \frac{1}{\sqrt{3}g} \sum_{\varepsilon} \big(1 + \sqrt{3}\lambda_{\varepsilon,2}\big)\lambda_{\varepsilon,2}. \end{aligned}$$

The mixed term $\lambda_{\varepsilon,1}\lambda_{\varepsilon,2}$ indicates that not only the individual probability distributions of both generalized eigenvector inversions, but also their joint probability distribution are needed to calculate the deviation of the quasiequilibrium from the canonical state.

No linear transformation exists that decouples $\lambda_{\varepsilon,1}$ and $\lambda_{\varepsilon,2}$ in these equations. This means that any other basis of Liouville space would lead to a similar result. The need to calculate joint probability distributions makes this method considerably more complicated for higher dimensional systems.

12. Conclusion and Outlook

We examined the equilibrium properties of two-level systems coupled to large but finite environments. The environments consisted mainly of an array of two-level systems with and without mutual interaction. The system was taken to be closed and subject only to unitary Schrödinger dynamics. No approximations were made in order to solve the systems.

It was shown by numerically calculating the time evolution that the quasiequilibrium state of the central system after relaxation from a nonequilibrium state (like a product state) deviates from canonical or thermal relaxation for many of the considered systems. Usually, the state reached depends on the initial state and, therefore, violates contact equilibrium. In particular, the class of systems with no interaction within the environment—the spin-star model class—showed strongly noncanonical behavior. When the structure of the system was changed by introducing interaction between the environmental spins—the ring-star configuration—, the quasiequilibrium state approached the canonical state for increasing coupling strength. A continuous transition from a situation far from canonical behavior towards canonical behavior could be observed. If it is possible to tune these intra-environmental interactions, one might tune the effective equilibrium state of the central system. One can imagine that this could be a novel way to drive quantum thermodynamic processes.

The quasiequilibrium state of the central system can be calculated without simulating the time evolution of the whole system. It is readily available by averaging the state over all times. This averaging procedure is conveniently done in the energy eigenbasis and is directly applicable for nondegenerate spectra; if the spectrum is degenerate, an irreducible representation of the Hamiltonian has to be found first. It was shown that the local quasiequilibrium state depends only on the distribution of the local inversions λ_ε of the energy eigenvectors; more precisely, only on the variance $\Delta\lambda_\varepsilon^2$ of this distribution. This variance can never vanish for any finite system; therefore, there are always deviations from the canonical equilibrium. It was shown that the mean value of all λ_ε's for a single Hamiltonian is given by the canonical equilibrium inversion.

The λ_ε distributions of several abstract model systems were considered in detail. All these systems had in common that the interaction between system and environment was modeled randomly. For complete random matrices, taken from the Gaussian unitary ensemble, the λ_ε distribution and the ensemble average of the variance could be calculated exactly. The distribution is narrowly peaked around its mean value. The variance decreases linearly with the size of the system. In the thermodynamic limit the deviation from canonical equilibrium vanishes.

If the environmental "bands" are exactly degenerate, though, the local quasiequilibrium state deviates significantly from the canonical state. This deviation is independent of the system size and is also present in the thermodynamic limit. The λ_ε distribution consists of two δ peaks. By introducing a finite level splitting within each environmental band, the peaks are broadened and move towards each other; the variance decreases. For this class of systems, the thermodynamic limit could not be calculated analytically. Numerical studies, however, indicate that the deviation from canonical equilibrium remains finite as the system size approaches infinity. If the level splitting is sufficiently large, the distribution becomes single peaked and has some similarity with the distribution for the GUE matrices, although with a larger variance.

Similar results were obtained for the spin-ring and the ring-star model classes. The spin-ring configuration somewhat resembles a random interaction with a small but finite level splitting. The λ_ε distribution has two peaks (one of them very broad) and a large variance. As the interaction strength between the environmental spins is increased, the distribution becomes narrower and single peaked, similar to the random system with finite level splitting. A similar behavior is observed if the Zeeman splitting of the environmental spins is made slightly inhomogeneous.

The calculation of the λ_ε distribution requires the partial diagonalization of the Hamiltonian, which may be hard to accomplish for large systems. So far it was seen that the behavior is approximately canonical if the local Hamiltonian of the environment (the diagonal blocks of the total Hamiltonian) had a certain finite width of its spectrum. This width was compared to the width of the interaction spectrum. It was seen that there exists a certain value of the ratio of these two spectral widths for which $\Delta\lambda_\varepsilon^2$ was minimal. This value of the relative spectral width varies from system to system, but is always of the same order of magnitude as for the GUE matrices. Therefore, it is not possible to predict the quasiequilibrium state from the relative spectral width alone. However, the relative spectral width

can indicate whether canonical behavior can be expected at all for a given system. This may be of importance since the width of a spectrum can be calculated without (partially) diagonalizing the Hamiltonian.

No "physical" explanation for the observed deviations from canonical equilibrium was been found. One may speculate that for those systems with an insufficient spectral width of the environment, the environment or bath correlation function does not relax quickly enough. Therefore, a non-markovian behavior can be expected and a Born-Markov master equation for the central system is supposed to fail.

By changing the environmental spectrum one may exert a thermal control on the "working gas" of a quantum thermodynamic process—the central system considered—in addition to a mechanical control (directly changing the spectrum of the central system). If both thermal and mechanical control were implemented by appropriate time dependent parameters of the Hamiltonian, a thermodynamic process would be completely parameterized. In this way one could possibly implement a cyclic process not by using several baths at different temperatures, but by changing the *action* of a single environment.

The generalization of the λ_ε distributions to higher dimensional central systems poses some problems: The state (and also the deviation from the canonical or thermal state) of a system with more than two levels is characterized by more than one parameter. So far it is not clear yet, whether these parameters can be found in a way that the deviation form canonical equilibrium is as readily available from distributions for generalized inversions.

Appendix

A. Proof of (2.17)

The following identity is needed to proof (2.17):

$$\begin{aligned}\sum_{k=0}^{n} k\binom{n}{k}a^k &= \sum_{k=1}^{n}\frac{n!}{(k-1)!(n-k)!}a^k = n\sum_{k=1}^{n}\frac{(n-1)!}{(k-1)!(n-k)!}\\ &= n\sum_{k=1}^{n}\binom{n-1}{k-1}a^k = na\sum_{k=0}^{n-1}\binom{n-1}{k}a^k\end{aligned}$$

$$\sum_{k=0}^{n} k\binom{n}{k}a^k = na(1+a)^{n-1}. \tag{A.1}$$

Now (2.17) can be proven:

$$\begin{aligned}&Z^{-1}\sum_{k=0}^{n}\frac{k+1}{n+1}\binom{n}{k}\mathrm{e}^{-\beta\delta k}\\ &= \frac{1}{(n+1)Z}\Bigg(\underbrace{\sum_{k} k\binom{n}{k}\mathrm{e}^{-\beta\delta k}}_{(A.1)} + \underbrace{\sum_{k}\binom{n}{k}\mathrm{e}^{-\beta\delta k}}_{Z}\Bigg)\\ &= \frac{1}{(n+1)Z}\Big(n\mathrm{e}^{-\beta\delta}\big(1+\mathrm{e}^{-\beta\delta}\big)^{n-1}+Z\Big)\\ &= \frac{1}{(n+1)Z}\Big(n\frac{\mathrm{e}^{-\beta\delta}}{1+\mathrm{e}^{-\beta\delta}}\underbrace{\big(1+e^{-\beta\delta}\big)^{n}}_{Z}+Z\Big).\end{aligned}$$

B. Properties of the $|\chi_\varepsilon^k\rangle$ and $|\eta_\varepsilon^k\rangle$

These vectors were defined by

$$|\varepsilon_k\rangle \approx \alpha_\varepsilon^k\,|0,\chi_\varepsilon^k\rangle + \beta_\varepsilon^k\,|1,\eta_\varepsilon^k\rangle\,. \tag{7.4}$$

with $|\alpha_\varepsilon^k|^2 + |\beta_\varepsilon^k|^2 = 1$. From Eqs. (7.7) it can be seen that

$$\sum_{\varepsilon_k}|\alpha_\varepsilon^k|^2 = g_k \quad \text{and} \quad \sum_{\varepsilon_k}|\beta_\varepsilon^k|^2 = g_{k-1}.$$

Orthogonality

The $|\chi_\varepsilon^k\rangle$'s and $|\eta_\varepsilon^k\rangle$'s lie almost completely within bands k and $k-1$ of the environment, respectively; therefore, $\langle\chi_\varepsilon^k|\eta_\varepsilon^k\rangle \approx 0$. The form (7.4) thus is a Schmidt decomposition of $|\varepsilon_k\rangle$.

Completeness

There are $g_{k-1} + g_k$ energy eigenvectors $|\varepsilon_k\rangle$ in the subspace with total excitation k; thus there are also this many $|\chi_\varepsilon^k\rangle$'s and $|\eta_\varepsilon^k\rangle$'s. They are overcomplete. However, there are generalized completeness relations:

$$\sum_{\varepsilon_k}|\alpha_\varepsilon^k|^2\,|\chi_\varepsilon^k\rangle\langle\chi_\varepsilon^k| = \hat{1}_k, \qquad \sum_{\varepsilon_k}|\beta_\varepsilon^k|^2\,|\eta_\varepsilon^k\rangle\langle\eta_\varepsilon^k| = \hat{1}_{k-1}.$$

This can be readily seen from

$$\begin{aligned}\sum_{\varepsilon_k}|\varepsilon_k\rangle\langle\varepsilon_k| = \hat{1}_k^{(\mathrm{S+C})} &= |0\rangle\langle 0|_{\mathrm{S}} \otimes \hat{1}_k + |1\rangle\langle 1|_{\mathrm{C}} \otimes \hat{1}_{k-1} \\ &= \sum_{\varepsilon_k}\Big(|\alpha_\varepsilon^k|^2\,|0,\chi_\varepsilon^k\rangle\langle 0,\chi_\varepsilon^k| + |\beta_\varepsilon^k|^2\,|1,\eta_\varepsilon^k\rangle\langle 1,\eta_\varepsilon^k| \\ &\qquad + \alpha_\varepsilon^k(\beta_\varepsilon^k)^*\,|0,\chi_\varepsilon^k\rangle\langle 1,\eta_\varepsilon^k| + \text{h.c.}\Big).\end{aligned}$$

It further follows that

$$\sum_{\varepsilon_k}\alpha_\varepsilon^k(\beta_\varepsilon^k)^*\,|0,\chi_\varepsilon^k\rangle\langle 1,\eta_\varepsilon^k| = 0.$$

C. Proof of (7.11)

Here it is shown that $\sum_\varepsilon \lambda_\varepsilon = g - g'$.

$$\begin{aligned}\sum_\varepsilon \lambda_\varepsilon &= \sum_\varepsilon \mathrm{Tr_S}\big\{\hat\sigma_z^{\mathrm S}\,\mathrm{Tr_C}\,|\varepsilon\rangle\langle\varepsilon|\big\}\\ &= \sum_\varepsilon \mathrm{Tr}\big\{(\hat\sigma_z^{\mathrm S}\otimes\hat 1^{\mathrm C})\,|\varepsilon\rangle\langle\varepsilon|\big\} = \mathrm{Tr}\big\{(\hat\sigma_z^{\mathrm S}\otimes\hat 1^{\mathrm C})\big\},\end{aligned}$$

the last equality follows from the fact that the energy eigenvectors form a complete orthonormal basis in Hilbert space. If we now use the basis $\{|0,\ell'\rangle, |1,\ell\rangle\}$ to calculate the trace (ℓ and ℓ' denote the levels in band k and $k' = k+1$, respectively), we see that the g kets $|1,\ell\rangle$ yield 1's, while the g' kets $|0,\ell'\rangle$ yield -1's and the total trace equals $g - g'$.

It follows that the mean value of all λ_ε's for one Hamiltonian is given by

$$\bar\lambda_\varepsilon = \frac{g-g'}{g+g'} = \langle\hat\sigma_z\rangle_{\mathrm{can}}\,.$$

D. Derivation of (7.12a)

At first, the second sum in (7.10) will be rewritten using the mean value $\bar\lambda$ of all λ_ε's within one band. This mean value is $\bar\lambda = (g-g')/(g+g') = \langle\hat\sigma_z\rangle_{\mathrm{can}}$ by virtue of Eq. (7.11).

$$\begin{aligned}\sum_\varepsilon \lambda_\varepsilon^2 &= \sum_\varepsilon\Big[(\lambda_\varepsilon-\bar\lambda)^2 + 2\lambda_\varepsilon\bar\lambda - \bar\lambda^2\Big]\\ &= \underbrace{\sum_\varepsilon(\lambda_\varepsilon-\bar\lambda)^2}_{(g+g')\Delta\lambda_\varepsilon^2} + 2\bar\lambda\underbrace{\sum_\varepsilon\lambda_\varepsilon}_{g-g'} - \bar\lambda^2\underbrace{\sum_\varepsilon 1}_{g+g'}\\ &= (g+g')\Delta\lambda_\varepsilon^2 + \frac{(g-g')^2}{g+g'}\end{aligned}$$

This result is now inserted into (7.10), arriving at

$$\langle\bar\sigma_z\rangle = \frac{1}{2g}\left((g-g') + \frac{(g-g')^2}{g+g'} + (g+g')\Delta\lambda_\varepsilon^2\right).$$

The first two summands can be further simplified to $2g\,\langle\hat{\sigma}_z\rangle_{\mathrm{can}}$, so we finally get

$$\langle\bar{\sigma}_z\rangle = \langle\hat{\sigma}_z\rangle_{\mathrm{can}} + \frac{g+g'}{2g}\Delta\lambda_\varepsilon^2. \tag{7.12a'}$$

E. Integration of (8.1)

For simplicity we write $g = g'$ and $p = p_0$.

The integral is conveniently carried out in $2g$-dimensional polar coordinates, since $P_{\mathrm{a}}(\{x_k\})$ is symmetrical with respect to rotation and the integration is carried out over the bulk of the unit sphere in $2g$ dimensions. The angular part of the integration simply yields the surface area of the $2g$-dimensional hypersphere, $S_n = 2\pi^g/\Gamma(g)$. Using $r = \sum_{k=1}^{2g} x_k^2$ and dropping the normalization constant, the integral (8.1) therefore becomes

$$\begin{aligned}&\int \mathrm{d}^{2g}x \left(1 - \sum_{k=1}^{2g} x_k^2\right)^{d-g-1} \delta\left(p - \sum_{k=0}^{2g} x_k^2\right)\\ &\quad = S_{2g}\int_0^1 \mathrm{d}r\, r^{2g-1}(1-r^2)^{d-g-1}\,\delta(p-r^2).\end{aligned}$$

Substituting $u = r^2$,

$$\frac{S_{2g}}{2}\int_0^1 \mathrm{d}u\, u^{g-1}(1-u)^{d-g-1}\,\delta(p-u) = \frac{\pi^g}{\Gamma(g)}p^{g-1}(1-p)^{d-g-1}.$$

With proper normalization we arrive at (8.2).

F. Form of the Spin-Star Interaction Matrix

The form of the spin-star interaction Hamiltonian

$$\hat{H}_{\mathrm{int}} = \sum_{\nu=1}^{N}\sum_{i,j=1}^{3} \gamma_{ij}^{\nu}\,\hat{\sigma}_i \otimes \hat{\sigma}_j^{\nu} \tag{4.2}$$

in the subspace of Hilbert space spanned by the states

$$\left\{|0;k',b\rangle\,,|1;k,a\rangle\right\} \quad (1 \le a \le g, \quad 1 \le b \le g') \tag{2.10'}$$

will be calculated here. The Pauli operators of the central spin will be denoted by $\hat{\sigma}_j$ $(j = x, y, z)$, the Pauli operators of the ν^{th} environmental spins by $\hat{\sigma}_j^\nu$.

The total magnetization of the central and environmental spins is fixed in this subspace, so only those terms of $\hat{H}_{\text{int}}$ conserving the total magnetization will contribute. $\hat{\sigma}_z \otimes \hat{\sigma}_j^\nu$ with $j = x, y$ never conserve the magnetization and can therefore be dropped while $\hat{\sigma}_z \otimes \hat{\sigma}_z^\nu$ fully conserves the magnetization. From the other terms we get

$$\begin{aligned}
\hat{\sigma}_x \otimes \hat{\sigma}_x^\nu &= \hat{\sigma}_+\hat{\sigma}_-^\nu + \hat{\sigma}_-\hat{\sigma}_+^\nu + \cancel{\hat{\sigma}_+\hat{\sigma}_+^\nu + \hat{\sigma}_-\hat{\sigma}_-^\nu},\\
\hat{\sigma}_y \otimes \hat{\sigma}_y^\nu &= \hat{\sigma}_+\hat{\sigma}_-^\nu + \hat{\sigma}_-\hat{\sigma}_+^\nu - \cancel{\hat{\sigma}_+\hat{\sigma}_+^\nu - \hat{\sigma}_-\hat{\sigma}_-^\nu},\\
\hat{\sigma}_x \otimes \hat{\sigma}_y^\nu &= \mathrm{i}(\hat{\sigma}_+\hat{\sigma}_-^\nu - \hat{\sigma}_-\hat{\sigma}_+^\nu + \cancel{\hat{\sigma}_-\hat{\sigma}_-^\nu - \hat{\sigma}_+\hat{\sigma}_+^\nu}),\\
\hat{\sigma}_y \otimes \hat{\sigma}_x^\nu &= \mathrm{i}(\hat{\sigma}_-\hat{\sigma}_+^\nu - \hat{\sigma}_+\hat{\sigma}_-^\nu + \cancel{\hat{\sigma}_-\hat{\sigma}_-^\nu - \hat{\sigma}_+\hat{\sigma}_+^\nu}).
\end{aligned}$$

The canceled terms don't conserve the total magnetization. Putting all remaining terms together for one environmental spin ν, the interaction in the considered subspace has the form

$$\begin{aligned}
&\sum_{i,j} \gamma_{ij}^\nu \hat{\sigma}_i \hat{\sigma}_j^\nu = \\
&\qquad = \gamma_{33}^\nu \hat{\sigma}_z \hat{\sigma}_z^\nu + \Big\{ \big[(\gamma_{11}^\nu + \gamma_{22}^\nu) + \mathrm{i}(\gamma_{12}^\nu - \gamma_{21}^\nu)\big] \hat{\sigma}_+ \hat{\sigma}_-^\nu + \text{H.c.} \Big\}. \qquad \text{(F.1)}
\end{aligned}$$

When summing up over all particles, the total interaction Hamiltonian has the form (2.11). The diagonal parts consist of linear combinations of the γ_{33}^ν's (with coefficients of $+1$ and -1) while the off-diagonal parts are sparsely populated by linear combinations of γ_{11}^ν, γ_{22}^ν, γ_{21}^ν, and γ_{12}^ν.

The trace of $\hat{H}_{\text{int}}$ within the subspace of interest is readily calculated: For each parameter γ_{33}^ν, there are $\binom{N-1}{k}$ factors -1 and $\binom{N-1}{k+1}$ factors $+1$ for the ground state of the central spin, as well as $\binom{N-1}{k-1}$ factors $+1$ and $\binom{N+1}{k}$ factors -1 for the excited state of the central system. Therefore we get

$$\begin{aligned}
\operatorname{Tr} \hat{H}_{\text{int}} &= f_{N,k} \sum_{\nu=1}^{N} \gamma_{33}^\nu,\\
f_{N,k} &= \binom{N-1}{k+1} + \binom{N-1}{k-1} - 2\binom{N-1}{k}. \qquad \text{(F.2)}
\end{aligned}$$

Since the parameters γ_{33}^ν are distributed as a normalized Gaussian, the sum is normally distributed with the standard distribution $\sqrt{N}$ and $\operatorname{Tr} \hat{H}_{\text{int}}$ is

normally distributed with the standard deviation $f_{N,k}\sqrt{N}$ which grows strongly with N. Of particular interest is the limit

$$\lim_{N\to\infty} \frac{f_{N,k}}{\binom{N}{k} + \binom{N}{k+1}} = 1 > 0.$$

The denominator is the Hilbert space dimension of the considered subspace 4.2.

There are $2\binom{N-1}{k}$ nonvanishing off-diagonal elements, two for each pair of states

$$|0\rangle_{\mathrm{S}} \otimes |1, \boldsymbol{v}^t\rangle_{\mathrm{C}}\,, \quad |1\rangle_{\mathrm{S}} \otimes |0, \boldsymbol{v}^t\rangle_{\mathrm{C}}\,,$$

where $\boldsymbol{v}^t$ is an row vector of dimension $N-1$, containing k ones and $N-1-k$ zeros. All matrix elements corresponding to one particle are equal. The real and imaginary parts of the off-diagonal elements are normally distributed with a standard deviation of $\sqrt{2}$ since each is a sum of two variables distributed as a normalized Gaussian.

G. Form of the Spin-Ring Interaction Matrix

The number of nonvanishing matrix elements of the spin-ring Hamiltonian for the environment,

$$\hat{H}_{\mathrm{CC}} = \frac{J}{2} \sum_{\nu=1}^{N} \big(\hat{\sigma}_x^{\nu} \otimes \hat{\sigma}_x^{\nu+1} + \hat{\sigma}_y^{\nu} \otimes \hat{\sigma}_y^{\nu+1}\big), \tag{4.4}$$

is needed to calculate its spectral width in Sec. 10.2.7. $\hat{H}_{\mathrm{CC}}$ can be rewritten in terms of the transition operators,

$$\hat{H}_{\mathrm{CC}} = J \sum_{\nu=1}^{N} \big(\hat{\sigma}_+^{\nu} \hat{\sigma}_-^{\nu+1} + \mathrm{H.c.}\big).$$

Consider only $\nu = 1$ at first. The terms for the first pair of particles only has matrix elements between

$$|0\rangle_{\mathrm{S}} \otimes |1, 0, \boldsymbol{v}^t\rangle\,, \quad |0\rangle_{\mathrm{S}} \otimes |0, 1, \boldsymbol{v}^t\rangle\,, \quad \text{as well as between}$$
$$|1\rangle_{\mathrm{S}} \otimes |1, 0, \boldsymbol{u}^t\rangle\,, \quad |1\rangle_{\mathrm{S}} \otimes |0, 1, \boldsymbol{u}^t\rangle\,.$$

$\boldsymbol{v}^t$ and $\boldsymbol{u}^t$ are $(N-2)$-dimensional row vectors or 0's and 1's. $\boldsymbol{v}^t$ contains k ones while $\boldsymbol{u}^t$ contains $k-1$ ones. Since there are two matrix elements for each pair of states and N particle pairs, $\hat{H}_{\mathrm{CC}}$ has

$$2N\left[\binom{N-2}{k}+\binom{N-2}{k-1}\right]=2N\binom{N-1}{k} \tag{G.1}$$

nonvanishing matrix elements, all equal to J.

H. Estimate of the Involved Hilbert Space

Often it is important to have a quick estimate of the expected fluctuations around the time averaged state in quasiequilibrium for a given initial state $|\psi_0\rangle$. The average size of these fluctuations depend on the number of (incommensurate) frequencies determining the dynamics and these depend in turn on the number of energy eigenvectors $|\varepsilon\rangle$ or the "size" or "dimensionality" of Hilbert space involved. A quick estimate can be obtained from the sum of the overlaps between the energy eigenstates and the initial state,

$$F=\sum_{\varepsilon}|\langle\varepsilon|\psi_0\rangle|.$$

The minimal value of this sum is 1 if $|\psi_0\rangle$ equal to an energy eigenstate and its maximal value is the square root of the Hilbert space dimension, $\sqrt{d}$, if the initial state is equally constituted by all energy eigenstates: $\langle\varepsilon|\psi_0\rangle = d^{-1/2}$ for all $|\varepsilon\rangle$. If F is of the order of 1, large fluctuations are expected, as F increases, the fluctuations decrease.

I. Chi-Squared Distribution

If $\{x_1,\ldots,x_n\}$ are n independent random variables with a normalized Gaussian distribution, then the distribution of

$$v=\sum_{k=1}^{n}x_k^2$$

is called χ^2 distribution with n degrees of freedom [36]. Its probability density is given by

$$P_{\chi^2}(v)=\frac{1}{2^{n/2}\Gamma(n/2)}v^{n/2-1}\mathrm{e}^{-v/2}$$

for $v > 0$ (zero otherwise). The expectation value and variance are

$$E(v) = \int_0^\infty v P_{\chi^2}(v)\,\mathrm{d}v = n, \quad \sigma^2(v) = E(v^2) - E(v)^2 = 2n.$$

The expectation value grows linearly with the number of summands while the standard distribution only grows with the square root of this number.

If the x_n's are distributed according to a Gaussian with standard deviation σ, the probability density is given by

$$P_{\chi^2,\sigma}(v) = \frac{1}{\sigma^2} P_{\chi^2}\Big(\frac{x}{\sigma^2}\Big). \tag{I.1}$$

Deutsche Zusammenfassung

Die Kontrolle und Manipulation kleiner Quantensysteme hat sich in den letzten Jahren zu einem wichtigen Forschungsgebiet entwickelt. Man denke dabei nur an die Versuche, Systeme zur Quanteninformationsverarbeitung zu entwickeln. Allerdings ist kein System in der Realität vollständig isoliert. Immer ist eine große, unkontrollierbare Umgebung angekoppelt, die zu Dekohärenz und Dissipation im zu kontrollierenden System führt. Es relaxiert in einen stationären Zustand oder Gleichgewichtszustand, der in der Regel einige thermodynamische Eigenschaften wie Temperatur und Entropie besitzt. Das Verständnis sowohl des Relaxationsprozesses als auch des stationären Zustands ist wichtig für die Kontrolle des Systems.

In dieser Arbeit wird der Gleichgewichtszustand von Zweiniveausystemen (TLS) untersucht, die zumeist an eine Umgebung aus Spin-1/2-Systemen gekoppelt sind. Das besondere Augenmerk liegt dabei auf dem Einfluss von Wechselwirkungen innerhalb der Umgebung und auf Abweichungen vom thermischen Gleichgewicht.

Thermische Eigenschaften von Zweiniveausystemen

Grundlegende Begriffe und Definitionen

Jedem Zustand eines TLS, der diagonal in der Energieeigenbasis ist, lässt sich eine Temperatur gemäß

$$\beta = \frac{1}{k_\mathrm{B} T} = \frac{1}{\delta} \ln \frac{\rho_{00}}{\rho_{11}}$$

zuordnen. ρ_{00} ist dabei die Besetzung des Grundzustands und ρ_{11} die Besetzung des angeregten Zustands. Häufig wird die Inversion

$$I = \langle \hat{\sigma}_z \rangle = \mathrm{Tr}(\hat{\rho}\,\hat{\sigma}_z) = \rho_{11} - \rho_{00} = -\tanh(\beta\delta/2)$$

statt der Temperatur zur Charakterisierung des Zustandes verwendet.

Ist das TLS schwach an eine größere Umgebung angekoppelt, kann der Hamiltonoperator des Gesamtsystems als Summe der lokalen Hamiltonoperatoren $\hat{H}_{\mathrm{S}}$ des Zentralsystems (des TLS) und $\hat{H}_{\mathrm{C}}$ der Umgebung sowie der Wechselwirkung $\hat{H}_{\mathrm{int}}$ dargestellt werden,

$$\hat{H} = \hat{H}_{\mathrm{S}} + \hat{H}_{\mathrm{C}} + \hat{H}_{\mathrm{int}}.$$

Wenn das Spektrum der Umgebung aus zwei hochgradig entarteten Energieniveaus oder Bändern besteht und die Energieaufspaltungen in System und Umgebung identisch sind (siehe Abb. 2.1), ist die Zeitentwicklung des Zentralsystems nur in dem Unterraum des Hilbertraums von Interesse, der von den Zuständen

$$\left\{ |0;1,b\rangle\,, |1;0,a\rangle \right\} \quad (1 \le a \le g_0, \quad 1 \le b \le g_1). \tag{Z1}$$

aufgespannt wird (g_0 und g_1 sind die Entartungsgrade der beiden Umgebungsbänder).

Kanonisches und thermisches Gleichgewicht

Für nahezu alle Zustände im Unterraum (Z1) hat der reduzierte Zustand des zentralen TLS die Form

$$\hat{\rho}_{\mathrm{can}} = \frac{1}{g_0 + g_1} \left(g_1 \, |0\rangle\langle 0| + g_0 \, |1\rangle\langle 1| \right) \tag{Z2}$$

und besitzt die Inversion

$$\langle \hat{\sigma}_z \rangle_{\mathrm{can}} = \frac{g_0 - g_1}{g_0 + g_1}.$$

Dieser Zustand wird kanonischer Gleichgewichtszustand genannt, der Teil des Hilbertraums des Gesamtsystems, in dem die Zustände diese Eigenschaft besitzen, dominierende Region. Startet das Gesamtsystem in einem Nichtgleichgewichtszustand, so wird es im Laufe der Zeitentwicklung typischerweise die dominierende Region erreichen und diese dann nahezu nie mehr verlassen. Daher erwartet man den Zustand (Z2) als stationären Zustand des Zentralsystems nach einer „kanonischen“ Relaxation.

Besteht die Umgebung aus vielen Bändern und befindet sie sich anfangs in einem thermischen Zustand mit der inversen Temperatur β,

$$\hat{\rho}_{\mathrm{C}} = \frac{1}{Z} \, \mathrm{e}^{-\beta \hat{H}_{\mathrm{C}}} = \frac{1}{Z} \sum_k \mathrm{e}^{-\beta E_k} \sum_{\ell=1}^{g_k} |k,\ell\rangle\langle k,\ell|_{\mathrm{C}}\,, \quad Z = \sum_k g_k \mathrm{e}^{-\beta E_k},$$

so führt eine kanonische Relaxation für die einzelnen Bänder meistens zu thermischer Relaxation insgesamt: Die (inverse) Temperatur des Zentralsystems nach der Relaxation ist gegeben durch die (inverse) Temperatur β der Umgebung (Kontaktgleichgewicht). Das gilt insbesondere, wenn der Faktor $g_k \mathrm{e}^{-\beta E_k}$ ein scharfes Maximum besitzt, was für viele Umgebungen gegeben ist.

Energieeigenvektor-Verteilung

Es soll der Gleichgewichtszustand des Zentralsystems im Unterraum (Z1) berechnet werden, ausgehend vom unkorrelierten Anfangszustand

$$\hat{\rho}(0) = |1\rangle\langle 1|_{\mathrm{S}} \otimes \hat{\rho}_{\mathrm{C}}, \quad \hat{\rho}_{\mathrm{C}} = \frac{1}{Z} \sum_k \mathrm{e}^{-\beta E_k} \hat{1}_k,$$

sowie die Abweichung vom kanonischen Gleichgewicht. $\hat{1}_k$ ist der Projektor auf den Unterraum eines Bandes, $\hat{\rho}_{\mathrm{C}}$ ist somit ein thermischer Zustand. Da sich der Zustand während der Zeitentwicklung für fast alle Zeiten in der Nähe des Gleichgewichts befindet, kann er durch Mittelung über alle Zeiten bestimmt werden. Diese Mittelung wird direkt in der Energieeigenbasis durchgeführt, sofern das Gesamtsystem keine Entartungen aufweist. Andernfalls muss zunächst eine irreduzible Darstellung für den Hamiltonoperator gefunden und danach invariante Unterräume getrennt voneinander betrachtet werden. Die Energieeigenvektoren im Unterraum (Z1) haben aufgrund der Struktur des Systems die Form

$$|\varepsilon_k\rangle \approx \alpha_\varepsilon^k \, |0, \chi_\varepsilon^k\rangle + \beta_\varepsilon^k \, |1, \eta_\varepsilon^k\rangle \, .$$

k ist dabei die gesamte „Anregung“ in Zentralsystem und Umgebung.

Die lokale Inversion des Zentralsystems im zeitgemittelten Zustand für ein benachbartes Paar Bänder lautet (unter Vernachlässigung der Anregungsindizes)

$$\langle \bar{\sigma}_z \rangle = \sum_\varepsilon \frac{|\beta_\varepsilon^2|}{g} \big(|\beta_\varepsilon|^2 - |\alpha_\varepsilon|^2 \big);$$

die tatsächliche Inversion erhält man durch Summation über alle Bänder. Dabei ist

$$\lambda_\varepsilon = |\beta_\varepsilon|^2 - |\alpha_\varepsilon|^2$$

die lokale Inversion eines Energieeigenzustandes. Führt man die Varianz $\Delta\lambda_\varepsilon^2$ der Verteilung aller λ_ε eines Hamiltonoperators ein, so kann man die zeitgemittelte Inversion schreiben als

$$\langle\bar{\sigma}_z\rangle = \langle\hat{\sigma}_z\rangle_{\mathrm{can}} + \frac{g+g'}{2g}\,\Delta\lambda_\varepsilon^2.$$

g und g' bezeichnen dabei die Entartungen des unteren und oberen Umgebungsbandes. Im Wesentlichen ist die Abweichung vom kanonischen Gleichgewicht also gegeben durch die Breite der λ_ε-Verteilung. Da diese Breite bei endlichen Systemen immer endlich ist, tritt immer eine Abweichung auf. Wenn das Zentralsystem im Grundzustand startet, erhält man ein ähnliches Ergebnis.

Eigenvektor-Verteilungen verschiedener Systeme

Gaußsches unitäres Ensemble

Für das Gaußsche unitäre Ensemble (GUE) kann man die Wahrscheinlichkeitsdichte für die λ_ε analytisch berechnen. Die Verteilung ist schmal um ihren Mittelwert $(g-g')/(g+g')$ gepeakt. Ihre Varianz ist gegeben durch $(d=g+g')$

$$\Delta\lambda_\varepsilon^2 = 4\frac{gg'}{d^2(d+1)}.$$

Die Varianz und damit die Abweichung vom kanonischen Gleichgewicht verschwindet wie $1/d$ für große Systeme, im thermischen Grenzfall relaxieren Systeme, die durch vollständig zufällige Hamiltonoperatoren beschrieben werden, also tatsächlich kanonisch. Praktisch ist $\Delta\lambda_\varepsilon^2$ schon bei kleinen Werten von d so klein, dass Abweichungen nicht oder nur schwierig zu beobachten sind.

Zufällige Wechselwirkung

Wird nur die Wechselwirkung zwischen System und Umgebung zufällig gewählt (und sind die Bänder der Umgebung echt entartet), so erhält man eine bimodale Verteilung bestehend aus zwei δ-Distributionen mit einer großen Varianz. Der erreichte quasistationäre Zustand weicht deutlich vom

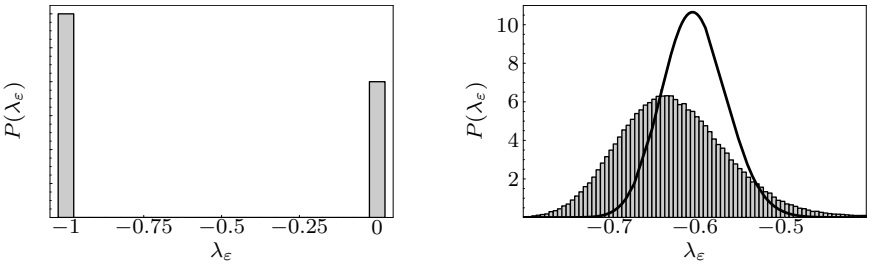

Abbildung 12.1: λ_ε-Verteilungen für ein System mit zufälliger Wechselwirkung. Links: entartete Bänder, rechts: aufgespaltene Bänder. $g = 91$ und $g' = 364$. Die durchgezogene Linie zeigt die Verteilung für das GUE.

kanonischen Zustand ab. Werden die Bänder der Umgebung leicht aufgespalten, so werden die beiden Peaks breiter und verschmelzen schließlich, bei ausreichend großer Aufspaltung. In diesem Fall ähnelt die λ_ε-Verteilung derjenigen für das GUE.

Abb. 12.1 zeigt die Verteilungen für entartete und aufgespaltene Bänder. Variiert man die Aufspaltung, so erhält man einen kontinuierlichen Übergang zwischen beiden Fällen. Betrachtet man die Zeitentwicklung, so beobachtet man tatsächlich deutliche Abweichungen vom kanonischen Verhalten im ersten und fast kanonisches Verhalten im zweiten Fall.

Spinsysteme

Die Umgebung wird nun ihrerseits durch Spin-1/2-Systeme modelliert, wobei alle Spins der Umgebung mit dem Zentralspin in Resonanz sein sollen. Wenn das zentrale TLS an alle Umgebungsspins gekoppelt ist, so lautet der allgemeinste Hamiltonoperator der Wechselwirkung

$$\hat{H}_{\text{int}} = \sum_{\nu=1}^{N} \sum_{i,j=1}^{3} \gamma_{ij}^{\nu}\, \hat{\sigma}_i \otimes \hat{\sigma}_j^{\nu}.$$

Zunächst sollen die Umgebungsspins untereinander nicht gekoppelt sein (Spin-Stern-Konfiguration). In diesem Fall ist die Struktur des Hamiltonoperators ähnlich zu dem mit komplett zufälliger Wechselwirkung und leicht aufgespaltenen Bändern. Werden die Koeffizienten zufällig gewählt,

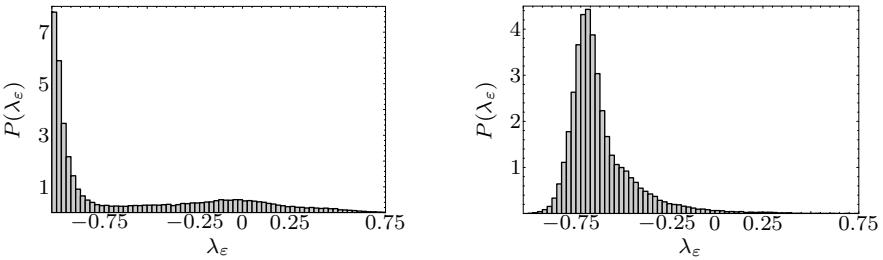

Abbildung 12.2: λ_ε-Verteilungen für Spinumgebungen. Links: Spin-Stern-Konfiguration, rechts: Ring-Stern-Konfiguration. $g = 91$ und $g' = 364$.

so ergibt sich tatsächlich eine breite, bimodale Verteilung mit einem sehr hohen Peak bei $\lambda_\varepsilon = -1$ und einem sehr flachen und breiten bei $\lambda_\varepsilon = 0$. Die meisten Vertreter dieser Systemklasse zeigen deutliche Abweichungen vom kanonischen Gleichgewichtszustand. Summiert man nun über alle Bänder der Umgebung auf, so führt das nichtkanonische Verhalten zu einer Verletzung des Kontaktgleichgewichts im stationären Zustand: Die Temperatur des Zentralsystems stimmt nicht mit der Temperatur der Umgebung überein.

Werden zusätzlich Wechselwirkungen zwischen den Umgebungsspins eingeführt, so verschmelzen die beiden Peaks zu einem und die Verteilung ähnelt wieder derjenigen für das GUE. Entsprechend geht die Abweichung vom kanonischen Verhalten zurück.

Abb. 12.2 zeigt die Verteilungen für die Spin-Stern-Konfiguration und die Ring-Stern-Konfiguration (periodische Nächstnachbar-Wechselwirkung in der Umgebung). Ebenso wie für das abstrakte zufällige Modell im letzten Abschnitt gibt es einen kontinuierlichen Übergang zwischen beiden Fällen. Wenn man die Wechselwirkung zwischen den Umgebungsspins steuern kann, kann die Breite der Verteilung eingestellt werden. Da der erreichte stationäre Zustand nur von dieser Breite abhängt, kann so die Wirkung der Umgebung als Bad teilweise gesteuert werden.

Abb. 12.3 (links) zeigt die Zeitentwicklung der Inversion des Zentralsystems für verschiedene Kopplungsstärken. Deutlich ist der Übergang von nichtkanonischem zu kanonischem Verhalten zu erkennen. Rechts ist die zeitgemittelte Inversion über der Kopplungsstärke dargestellt.

Ein entsprechendes Verhalten ist für viele konkrete Umgebungsmodel-

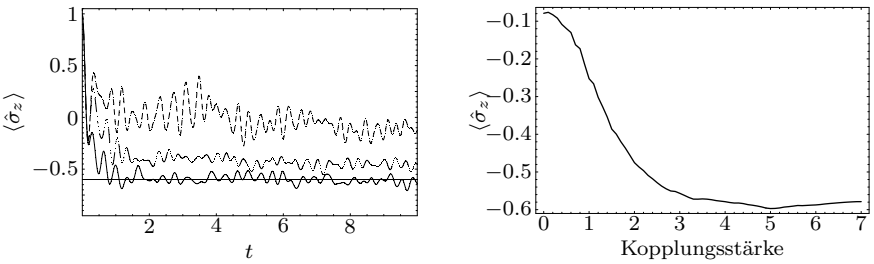

Abbildung 12.3: Links: Inversion des Zentralspins für verschiedene Kopplungsstärken in der Umgebung (oben: keine Kopplung, unten: starke Kopplung); die horizontale waagerechte Line zeigt die Inversion des kanonischen Gleichgewichtszustands. Rechts: Zeitgemittelte lokale Inversion für verschiedene Kopplungsstärken J.

le sichtbar, nicht nur für eine ringförmige Nächstnachbar-Wechselwirkung. Derartige kontinuierliche Übergänge sind typisch, wenn die Bänder der Umgebung aufgespalten werden. Außer durch das Einführen einer Wechselwirkung kann das beispielsweise auch dadurch erfolgen, dass die Zeeman-Aufspaltung der Umgebungsspins leicht variiert wird. Es müssen auch nicht notwendigerweise alle Umgebungsspins an den Zentralspin koppeln. Kanonisches Gleichgewicht kann auch beobachtet werden, wenn die „Umgebung“ die Form einer Heisenberg-Spinkette besitzt und nur ein Spin mit dem Zentralsystem wechselwirkt.

Relative spektrale Breite

Der Übergang von nichtkanonischem zu kanonischem Verhalten fand immer statt, wenn die „Stärke“ des Umgebungsspektrums vergrößert wurde. Ein Maß für diese Stärke ist die Breite des Spektrums. Die Varianz der Energieeigenwerte m_k eines Operators $\hat{M}$ auf einem Hilbertraum der Dimension d ist gegeben durch

$$W_\mathrm{s} = \sqrt{\frac{1}{d}\sum_k m_k^2} = \sqrt{\frac{1}{d}\,\mathrm{Tr}(\hat{M}^2)},$$

sofern die Spur von $\hat{M}$ verschwindet. Das Umbegungsspektrum ist gegeben durch die Diagonalblöcke der Hamiltonmatrix, die Wechselwirkung zwischen System und Umgebung durch ihre Nichtdiagonalblöcke. Von Interesse für die Relaxation und das Gleichgewicht ist nun die relative Breite des Umgebungsspektrums zum Wechselwirkungsspektrum,

$$R_{\mathrm{s}} = \sqrt{\frac{\mathrm{Tr}(\hat{H}^2_{\mathrm{diag}})}{\mathrm{Tr}(\hat{H}^2_{\mathrm{off}})}}, \tag{Z3}$$

da ein gemeinsamer Faktor beider Teile nur die Einheit der Zeit skaliert.

R_{s} kann für viele Systeme direkt berechnet werden. Für die behandelten Systemklassen kann das Ensemblemittel angegeben werden. Für das Ensemblemittel des Gaußschen unitären Ensembles erhält man beispielsweise

$$\bar{R}_{\mathrm{s,GUE}} = \sqrt{\frac{g^2 + g'^2}{2gg'}}.$$

Für diejenige „Stärke“ des Umgebungsspektrums, für das die Abweichung des Gleichgewichtszustandes eines Systems vom kanonischen Gleichgewicht minimal ist, ist die relative spektrale Breite bei allen betrachteten Systemen von der Größenordnung von $R_{\mathrm{s,GUE}}$. Abb. 12.4 zeigt die Varianz der λ_ε-Verteilung für verschiedene Systeme über der relativen spektralen Breite. Bei den meisten Systemen ist ein deutliches Minimum auszumachen.

Es existiert kein eindeutiger Zusammenhang zwischen dem Minimum der λ_ε-Varianz und der relativen spektralen Breite für alle Systeme. Da das Minimum jedoch immer in der Nähe des Wertes für GUE-Matrizen liegt, kann R_{s} als Indikator dafür dienen, ob kanonisches Verhalten erwartet werden kann, oder nicht. In manchen Fällen kann der Wert von R_{s} dabei helfen, das Verhalten einer Systemklasse im thermischen Gleichgewicht zu bestimmen, für die $\Delta\lambda^2_\varepsilon$ nicht explizit ausgerechnet werden kann. Beispielsweise geht der Ensemblemittelwert von W_{s} des Diagonalteils der Spin-Stern-Wechselwirkung gegen Null für große Systeme; folglich zeigt die Spin-Stern-Wechselwirkung allein (ohne Wechselwirkung in der Umgebung) auch im Grenzfall sehr großer Systeme kein kanonisches Verhalten.

Zusammenfassung

Das Gleichgewichtsverhalten eines Zweiniveausystems, das an eine größere Umgebung gekoppelt ist, hängt stark von der spektralen Struktur der

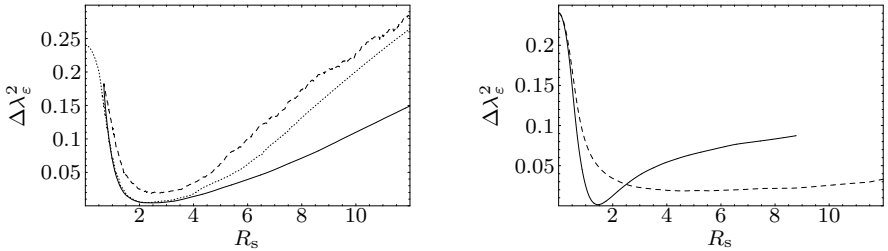

Abbildung 12.4: Varianz der λ_ε-Verteilung über der relativen spektralen Breite. Links: Ring-Stern mit zufälliger S-C-Kopplung (durchgezogen); Spin-Stern mit inhomogener Zeeman-Aufspaltung (gestrichelt); Spin-Stern mit XY-Kopplung und inhomogener Zeeman-Aufspaltung. Rechts: GUE-Matrix mit skalierten Diagonalblocks (durchgezogen); zufällige Wechselwirkung mit aufgespaltenen Bändern.

Umgebung ab. Für Umgebungen mit schmaler spektraler Breite weicht der stationäre Zustand nach einer Relaxationszeit deutlich vom kanonischen Gleichgewicht ab. Werden die Bänder der Umgebung zunehmend aufgespalten, so verringert sich die Abweichung, wobei für endliche Systeme der kanonische Zustand nie exakt erreicht werden kann. Dieses Verhalten wurde zurückgeführt auf die Verteilung der lokalen Inversionen der Energieeigenzustände des Gesamtsystems, namentlich auf die Varianz dieser Verteilung.

Insbesondere das Verhalten von Spinumgebungen wurde betrachtet. Es zeigte sich, dass das Gleichgewicht des Zentralsystems allein durch Umgebungsparameter gesteuert werden kann, beispielsweise durch die Wechselwirkungsstärke zwischen den Umgebungsspins. Man kann sich vorstellen, dass man durch kontrollierte Manipulation dieser Umgebungsparameter eine thermische Kontrolle auf das Zentralsystem ausüben kann. Eine einzige Umgebung kann dann möglicherweise als Bad mit unterschiedlicher effektiver Temperatur wirken.

Schließlich wurde mit der relativen spektralen Breite ein Maß präsentiert, mit dem man schnell abschätzen kann, ob kanonisches Verhalten zu erwarten ist, oder nicht. Im Gegensatz zu der Verteilung der Energieeigenzustände ist die relative spektrale Breite zumeist direkt berechenbar.

List of Symbols

$\hat{1}_k$	Projector on band k of the environment
$\langle\cdot\rangle$	Quantum mechanical expectation value
α_ε^k	Schmidt coefficient of $\lvert\varepsilon_k\rangle$
β	Inverse temperature, $1/k_\mathrm{B}T$
β_ε^k	Schmidt coefficient of $\lvert\varepsilon_k\rangle$
C	Environment
$\lvert\chi_\varepsilon^k\rangle$	Environmental state, Schmidt vector of $\lvert\varepsilon_k\rangle$
δ	Energy splitting
$\delta(x)$, δ_{ij}	Dirac distribution, Kronecker symbol
$\delta\varepsilon$	Environmental bandwidth
Δ	Half of the detuning between system and environment
E	Energy
$E(x)$	Expectation value of the random variable x
ε_k	Energy eigenvalue of the total system
$\lvert\varepsilon\rangle$	Energy eigenstate of the total system
$\lvert\varepsilon_k\rangle$	Energy eigenstate of the total system with total excitation k
$\lvert\eta_\varepsilon^k\rangle$	Environmental state, Schmidt vector of $\lvert\varepsilon_k\rangle$
g, g_k	Degeneracies of environmental bands
γ_{ij}^ν	Coefficient of the spin-star interaction
γ_ε^k	Schmidt coefficient of $\lvert\varepsilon_k\rangle$ for three-level central systems
$\Gamma(x)$	Gamma function
$\hbar$	Planck's constant, set equal to 1 throughout this text
$\hat{H}$	Hamilton operator
H.c.	Hermitian conjugate
$\hat{H}_\mathrm{C}$	Local Hamilton operator of the environment C
$\hat{H}_\mathrm{CC}$	Hamilton operator describing the mutual interaction between the spins of a spin environment
$\hat{H}_\mathrm{int}$	Hamilton operator describing the interaction between central system and environment

$\hat{H}_{\mathrm{S}}$	Local Hamilton operator of the central system S
I	Inversion, z component of the Bloch vector
J	Interaction strength within the environment
k_{B}	Boltzmann constant
λ_ε	Local inversion of an energy eigenstate
$\Delta\lambda_\varepsilon^2$	Variance of the λ_ε distribution of a single Hamiltonian or an ensemble of systems
N	Number of particles in the environment
P	Purity
$P(x)$	Probability density of the random variable x
$\hat{\rho}$	State operator, statistical operator
R_{s}	Relative spectral width of two Hamiltonians
S	Von Neuman entropy
σ	Standard deviation
$\hat{\sigma}_j$	Pauli operator
$\langle\bar{\sigma}_z\rangle$	Time averaged inversion
$\langle\hat{\sigma}_z\rangle_{\mathrm{can}}$	Inversion of the canonical equilibrium state
$\hat{\sigma}_j^\nu$	Pauli operator of the νth environmental particle
$\hat{\sigma}_\pm$	Transition operators
S_n	Surface area of the unit sphere in n dimensions, the n hypersphere
S	Central system
T	Temperature
V	Matrix populating the off-diagonal blocks of the Hamiltonian matrix, describing system-environment interaction
$\hat{\omega}_k$	Basis operator in $n \times n$ dimensional Liouville space
$\hat{w}_\ell$	Diagonal basis operator in $n \times n$ dimensional Liouville space
W_{s}	Spectral width of a Hamiltonian
W_2	$W_{\mathrm{s}}^2 d$
Z	Partition function
$\lvert\zeta_\varepsilon^k\rangle$	Environmental state, Schmidt vector of $\lvert\varepsilon_k\rangle$ for three-level central systems

References

[1] H.-P. Breuer and F. Petruccione: *The Theory of Open Quantum Systems.* Oxford, New York, 2002.

[2] D. Giulini, E. Joos, C. Kiefer, J. Kupsch, I.-O. Stamatescu, and H. D. Zeh: *Decoherence and the Appearence of a Classical World in Quantum Theory.* Springer, Berlin, 1996.

[3] R. Omnès: *General theory of the decoherence effect in quantum mechanics.* Phys. Rev. A **56**, 3383–3394, 1997.

[4] P. Blanchard, D. Giulini, E. Joos, C. Kiefer, and I.-O. Stamatescu (eds): *Decoherence: Theoretical, Experimental, and Conceptual Problems*, Bielefeld, 1998. Springer.

[5] U. Weiss: *Quantum Dissipative Systems.* World Scientific, Singapore, 1999.

[6] G. Mahler and V. A. Weberruß: *Quantum Networks.* Springer, Berlin, 1998.

[7] M. A. Nielsen and I. L. Chuang: *Quantum Computation and Quantum Information.* Cambridge University Press, Cambridge, 2000.

[8] F. Tonner and G. Mahler: *Autonomous quantum thermodynamic machines.* Phys. Rev. E **72**, 066118, 2005.

[9] R. P. Feynman and F. L. Vernon: *The Theory of a General Quantum System Interacting with a Linear Dissipative System.* Ann. Phys. **24**, 118–173, 1963.

[10] H. Bethe: *Eigenwerte und Eigenfunktionen der linearen Atomkette.* Z. Phys. **71**, 205–226, 1931.

[11] E. Lieb, T. Schultz, and D. Mattis: *Two Soluble Models of an Antiferromagnetic Chain.* Ann. Phys. **16**, 407–466, 1961.

[12] X. Wang: *Entanglement in the quantum Heisenberg XY model*. Phys. Rev. A **64**, 012313, 2001.

[13] X. Wang: *Thermal and ground-state entanglement in Heisenberg XX qubit rings*. Phys. Rev. A **66**, 034302, 2002.

[14] X. Wang, H. Li, Z. Sun, and Y.-Q. Li: *Entanglement in spin-one Heisenberg chains*. quant-ph/0501032, 2005.

[15] A. Hutton and S. Bose: *Mediated entanglement and correlations in a star network of interacting spins*. Phys. Rev. A **69**, 042312, 2004.

[16] A. Hutton and S. Bose: *Ground State Entanglement in a Combination of Star And Ring Geometries Of Interacting Spins*. quant-ph/0408077, 2004.

[17] T. J. Osborne and M. A. Nielsen: *Entanglement in a simple quantum phase transition*. Phys. Rev. A **66**, 0321101, 2002.

[18] A. Osterloh, L. Amico, G. Falci, and R. Fazio: *Scaling of entanglement close to a quantum phase transition*. Nature **416**, 608–610, 2002.

[19] N. V. Prokof'ev and P. C. E. Stamp: *Theory of the spin bath*. Rep. Prog. Phys. **63**, 669–726, 2000.

[20] M. Munowitz: *Coherence and NMR*. Wiley, New York, 1988.

[21] N. V. Prokof'ev and P. C. E. Stamp: *Low-Temperature Quantum Relaxation in a System of Magnetic Nanomolecules*. Phys. Rev. Lett. **80**, 5794–5797, 1998.

[22] M. Dube and P. C. E. Stamp: *Dynamics of a Pair of Interacting Spins Coupled to an Environmental Sea*. Int. J. Mod. Phys. B **12**, 1191–1245, 1998.

[23] H.-P. Breuer, D. Burgarth, and F. Petruccione: *Non-Markovian dynamics in a spin star system: Exact solution and approximation techniques*. Phys. Rev. B **70**, 045323, 2004.

[24] H. Schmidt and G. Mahler: *Control of local relaxation behavior in closed bipartite quantum systems*. Phys. Rev. E **72**, 016117, 2005.

[25] H. Schmidt and G. Mahler: *Nonthermal equilibrium states of closed bipartite systems*. Phys. Rev. E **75**, 061111, 2007.

[26] J. Gemmer, M. Michel, and G. Mahler: *Quantum Thermodynamics: The Emergence of Thermodynamical Behaviour within Composite Quantum Systems*. Springer, Berlin, 2004.

[27] J. Gemmer, A. Otte, and G. Mahler: *Quantum Approach to a Derivation of the Second Law of Thermodynamics*. Phys. Rev. Lett. **86**, 1927–1930, 2001.

[28] J. Gemmer and G. Mahler: *Distribution of local entropy in the Hilbert space of bi-partite quantum systems: origin of Jaynes' principle*. Eur. Phys. J. B **31**, 249–257, 2003.

[29] F. Haake: *Quantum Signatures of Chaos*. Springer, Berlin, 2001.

[30] M. L. Mehta: *Random Matrices*. Academic Press, Boston, 1990.

[31] P. Borowski, J. Gemmer, and G. Mahler: *Relaxation into equilibrium under pure Schrödinger dynamics*. Eur. Phys. J. B **35**, 255–259, 2003.

[32] B. Diu, C. Guthmann, D. Lederer, and B. Roulet: *Grundlagen der Statistischen Physik*. de Gruyter, Berlin, 1994.

[33] M. Stollsteimer and G. Mahler: *Suppression of arbitrary internal coupling in a quantum register*. Phys. Rev. A **64**, 052301, 2001.

[34] N. F. Ramsey: *Thermodynamics and Statistical Mechanics at Negative Absolute Temperatures*. Phys. Rev. **103**, 20–28, 1956.

[35] P. T. Landsberg: *Heat engines and heat pumps at positive and negative absolute temperatures*. J. Phys. A **10**, 1773–1780, 1977.

[36] I. N. Bronstein, K. A. Semendjaev, G. Musiol, and H. Mühlig: *Taschenbuch der Mathematik*. Harri Deutsch, Frankfurt, 1995.

Acknowledgments

The advice and support of several persons have significantly influenced this work. It is my pleasure to acknowledge their help.

First and foremost I would like to thank Prof. Dr. G. Mahler for supervising my work, for his constant interest, and for giving me direction and support over the last years.

I thank Prof. Dr. U. Seifert for kindly writing the second report on my dissertation.

I would like to thank Prof. Dr. G. Wunner for the technical equipment of the institute that made the numerical studies possible.

Many stimulating discussions with my present and former colleagues at the Intitut für Theoretische Physik 1 (Universität Stuttgart) made my time there enjoyable. I would like to thank Dr. Peter Borowski, Dr. Jochen Gemmer, Dr. Michael Hartmann, Markus Henrich, Thomas Jahnke, Alexander Kettler, Christos Kostoglou, Dr. Mathias Michel, Florian Rempp, Georg Reuther, Heiko Schröder, Dr. Marcus Stollsteimer, Jens Teifel, Dr. Friedemann Tonner, Pedro Vidal, Hendrik Weimer, and Mohamed Youssef for fruitful discussions about physics and other topics.

I am indebted to my friend Dr. phil. Peter Krug for proofreading part of the manuscript.

I am grateful for the financial support of the Landesstiftung Baden-Württemberg and of the Deutsche Forschungsgemeinschaft.

I would like to thank my parents for their extensive support during my studies.

Finally, I am deeply indebted to Sabrina for her moral support, her patience, her love, and for proofreading the manuscript.